May 1967

USCEE Report 202

UNIVERSITY OF SOUTHERN CALIFORNIA

SYNTHESIS AND IDENTIFICATION OF MATHE-MATICAL MODELS FOR THE DISCRETE CONTROL BEHAVIOR OF HUMAN OPERATORS

M. J. Merritt

ELECTRONIC SCIENCES LABORATORY

USCEE Report 202

Technical Report

SYNTHESIS AND IDENTIFICATION OF MATHEMATICAL MODELS FOR THE DISCRETE CONTROL BEHAVIOR OF HUMAN OPERATORS

M. J. Merritt

ELECTRICAL ENGINEERING DEPARTMENT
UNIVERSITY OF SOUTHERN CALIFORNIA
LOS ANGELES, CALIFORNIA

May 1967

This research was sponsored by the National Aeronautics and Space Administration under Grant No. NGR 05-018-022 of the Office of Advanced Research and Technology.

ABSTRACT

This report describes the synthesis and identification of mathematical models which characterize the discrete control behavior of human operators. This type of behavior occurs in control situations where the human operator must decide between a small number of alternatives, while generating continuous control actions at the same time. Models of this type have been proposed previously, however, systematic techniques for their synthesis and identification have been lacking. In this report a systematic treatment of discrete control actions is made possible by the introduction of two new elements which can be used to configure complete human operator models.

Two types of hybrid elements are presented. One accepts continuous inputs and produces binary outputs, while the other has continuous inputs and produces continuous outputs under the control of binary signals, Decisions to initiate an action, throw a switch, or select which switch out of a group of switches should be operated are described by a Multi-State Decision Element (MSDE). Decisions concerning the magnitude of a discrete control action, the length of a control interval, etc. are modeled by a Proportional Decision Element (PDE),

Procedures and digital computer programs for the complete identification of both types of elements are given.

The Multi-State Decision Element and the Proportional Decision Element are applied to the modeling of human operators performing compensatory tracking of gaussian random inputs. Two experiments were performed. The basic control task was the same in both cases. The controlled element resembled the pitch axis of an aircraft and was selected in such a manner that pulsatile control

actions were generated by the operators.

In the first experiment, the operator viewed a single compensatory oscilloscope display, which presented altitude error. A Multi-State Decision Element was used to model the operators decision to initiate a pulsatile control event. A Proportional Decision Element was used to model the operators decision as to the amplitude and width of the pulse event. The elements were completely identified and resulted in an asynchronous input dependent sampled data model of the human operator's control actions.

The second experiment was an extension of the first, in which the resemblance to an aircraft stick axis was enhanced by adding an attitude display presenting pitch angle. The operators control behavior consisted of pulsatile stick motions and eye motions between the widely separated attitude and error displays. A complete human operator model, describing both stick motion and eye motion was constructed using the two decision elements. The resultant model contains a deterministic input dependent decision element modeling the operators eye motions.

ACKNOWLEDGEMENT

The author wishes to express his most sincere gratitude to Professor George Bekey whose guidance, encouragement and sense of humor made this work possible. The efforts of Professors Robert McGhee and Walter Kyner are appreciated in the preparation of this manuscript.

This research was supported in part by the National Aeronautics and Space Administration under Contract No. NGR 05-018-022 from the Office of Advanced Research and Technology.

The author also wishes to thank his colleagues and friends who assisted in the preparation and execution of the experimental studies, with special thanks to Christopher Jacobs for service rendered as a test subject.

Many people were extremely helpful at various stages of the project and their help is gratefully acknowledged. Mr. Sam Shaar developed a new design for a low inertia side arm controller. Mr. Doyle Holland prepared the figures for the manuscript. Mrs. Francine Moore typed the manuscript and rendered invaluable assistance.

Last, and certainly not least, the author is grateful to his wife for her encouragement and understanding during periods w-hen it seemed that human operators really couldn't be modeled after all.

CONTENTS

ILLUSTRATIONS

CHAPTER I

INTRODUCTION AND BACKGROUND

1. 1 General Statement of The Problem

This report is concerned w-ith the mathematical representation of a particular class of input-output behavior exhibited by human operators in a control system. A block diagram of such a system is seen in Figure 1. 1.

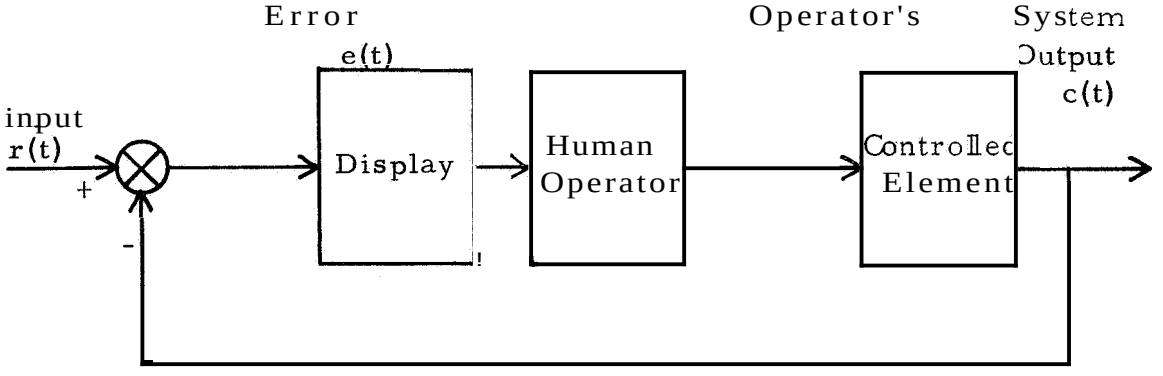

If the display device presents both the input, r(t), and the system output, c(t), to the operator, then the operator's task is known as pursuit tracking. If the operator observes the difference between these signals, e(t), then the operator performs compensatory tracking. In compensatory tracking the operator attempts to

reduce the error signal to zero. The mathematical models most commonly used to represent the human operator in a system such as Figure 1.1 are continuous describing functions, synthesized by linear, constant coefficient differential equations and time delay.

Continuous describing function models are suitable for a wide class of tracking situations. How-ever, they are not w-ell suited to the description of an important class of control reponses, defined as "discrete control behavior." Discrete control actions are responses w-hich are composed of a limited set of patterns, such as those show-n in Figure 1.2. The aircraft throttle position of Figure 1.2(a) may be synthesized from tw-o types of patterns: (a) ramps of slope k and duration t_r and (b) constant positon regions, of amplitude p_i and duration t_c. Each of the above patterns is characterized by a pair of numbers. In general, each pattern of a set comprising a discrete control action is characterized by an n-tuple of numbers. Two additional examples are given in Figure 1.2(b) and (c).

Discrete control actions of operators are not limited to manual manipulation of a control device, but include, for example, visual scanning between separated display devices, and mental decisions w-hich affect the process by w-hich the control actions are generated. Discrete control processes may occur simultaneously

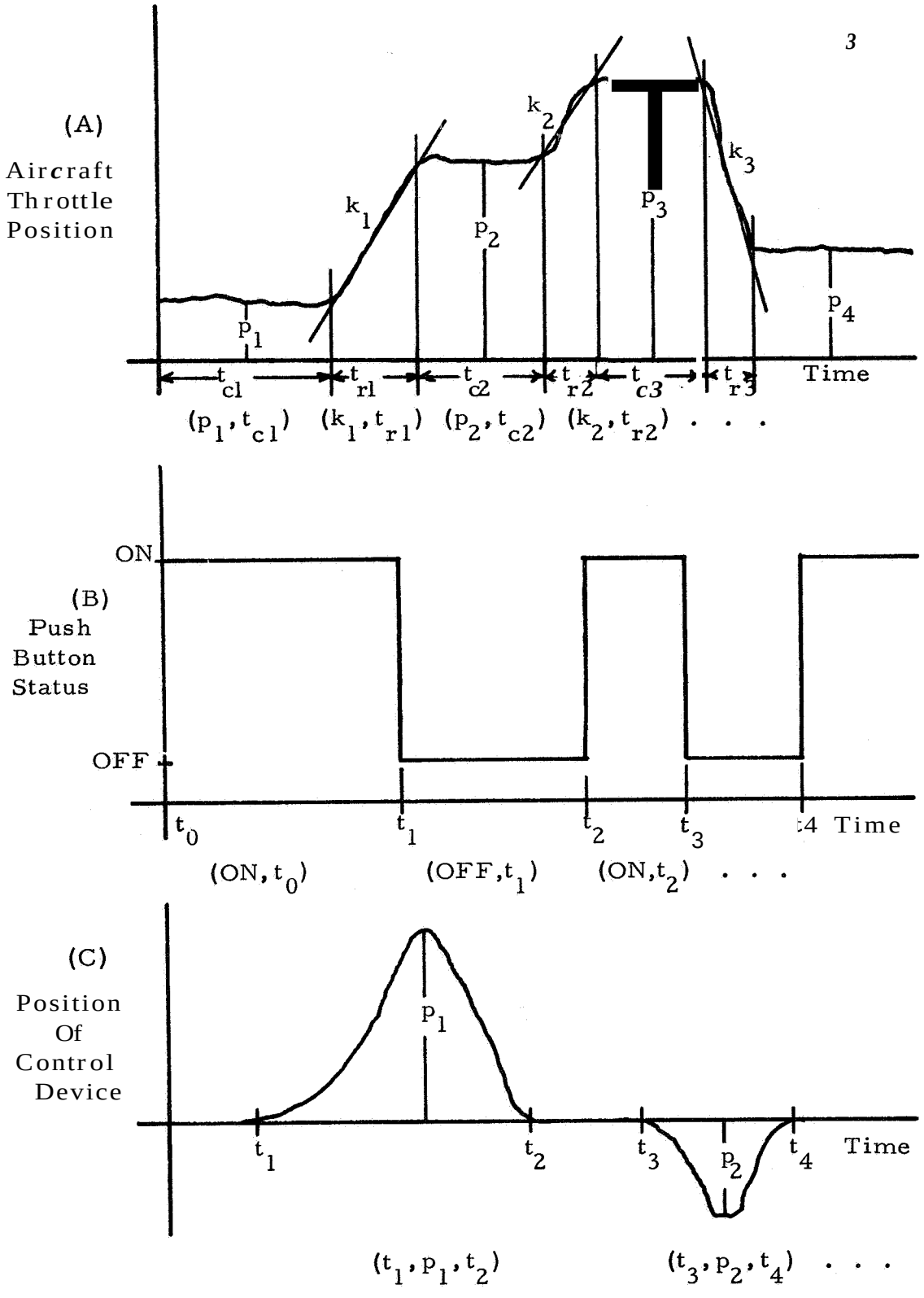

Figure 1.2 Examples of Discrete Human Operator Control Actions

with continuous control actions, or they may provide supervisory monitoring and modification of a continuous control action.

The major objective of this report is to present an analytical and experimental study of a new class of mathematical models for the discrete control behavior of human operators. These models are synthesized by two general purpose decision elements and their associated identification algorithms, While certain types of discrete control behavior have been presented previously, this research is the first to present general purpose elements which can be combined to model discrete control behavior, Complete identification procedures for the two elements are described. The purpose of this introductory chapter is to give a brief description of the background for the investigation, outline its major objectives, describe the limitations of the research program and present in detail the organization of the body of the report.

1.2 Background

The development of mathematical models for human operators began late in World War II when human trackers were widely used in target tracking for anti-aircraft guns and similar devices. The first engineering approaches to the problem were reported by Tustin [53] in England and Ragazzini [54] in the United States.

Both investigators utilized linear describing functions, thus allowing linear control system techniques to be applied to the analysis and synthesis of man-machine systems.

1,2. 1 Linear Describing Function Models

A linear describing function model consists of a constant coefficient differential equation and a time delay, selected such that the mean squared difference between the model output and the operator output is minimized, when both are forced with the same input. Most describing function models in the literature are obtained by using signals composed of sums of sinusoids which are approximately gaussian and random appearing. The parameters of describing function models are usually obtained by spectral analysis techniques.

Describing functions of the type just described were obtained by McRuer, Krendel, Graham, et al [21-5] for single axis compensatory tracking tasks. By systematically studying a variety of controlled elements, input bandwidths, controllers and displays, a general purpose describing function model was obtained. In addition, a set of rules were formulated to allow the model parameters to be selected according to the transfer function of the plant, bandwidth of the input signal and type of controller used. Describing function models for multi-axis tracking tasks are given by Bekey, et at [41] and McRuer and Graham [24].

Multiple linear regression techniques w-ere utilized by Wierwille [45] to identify describing function models, while Bekey and Meissinger[26] utilized gradient search parameter identification.

1.2.2 Intermittent Models

In appendix I of his dissertation, Bekey [3] presents substantial evidence for the existence of intermittent behavior in human operators. The physiology of the visual, cerebral and neuromuscular systems supports the hypothesis that human operators utilize inputs intermittently. It has been said that the pow-er spectrum of the difference between the output of a linear describing function model and the output of an intermittent operator w-ould contain easily recognized peaks. These peaks would be the result of periodicities caused by the sampling behavior of the operator. A careful study of the power spectrum of this difference by McRuer [25] revealed no significant periodicities. Following this, Biddle, et al [57] found that random perturbations of the periodic sampling interval caused the peaks in the power spectrum due to sampling to disappear.

Sampling human operator models offer many advantages over continuous models. These advantages are offset by the lack of suitable identification techniques, An input dependent sampling model of a human operator is synthesized in Chapter 5 below-. The

identification of the input dependent sampling behavior w-as possible only because the operator's output consisted of pulsatile control motions. The application of the discrete elements to continuous output human operator models remains to be carried out.

1.3 Discrete Control Behavior In Human Operators

Three examples of discrete control behavior were given in Figure 1.2. Numerous examples of discrete control behavior in human operators are available in the literature. The role played by models for this type of behavior may be illustrated by considering tw-o examples in detail.

Chalk [6] recorded the control actions of pilots performing instrument landings in a variable stability T-33 aircraft, A typical time history of elevator deflection, aileron deflection, rudder deflection and throttle oosition is seen in Figure 1.3. A typicalaircraft instrument panel is shown in Figure 1.4. In order to perform the desired landing maneuver satisfactorily, the pilot must scan betw-een a number of separated instruments, This is certainly discrete human operator behavior. The elevator deflection time history appears to be continuous, w-hile the aileron and rudder deflection time histories are quite pulsatile. The throttle position is

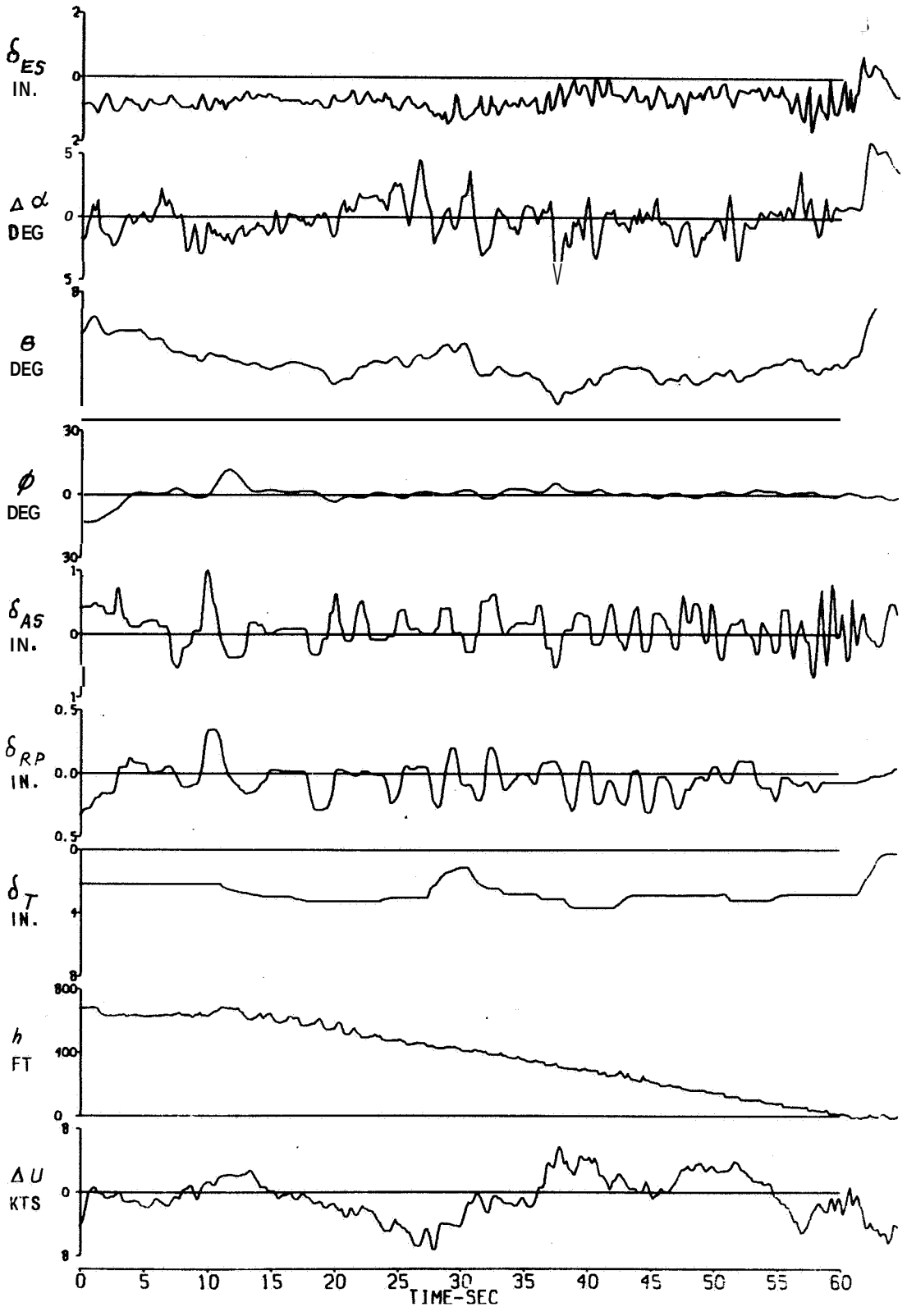

FIGURE 1.3 - Time Histories Of Landing Approaches In **A T-33** Aircraft (Chalk, 1966)

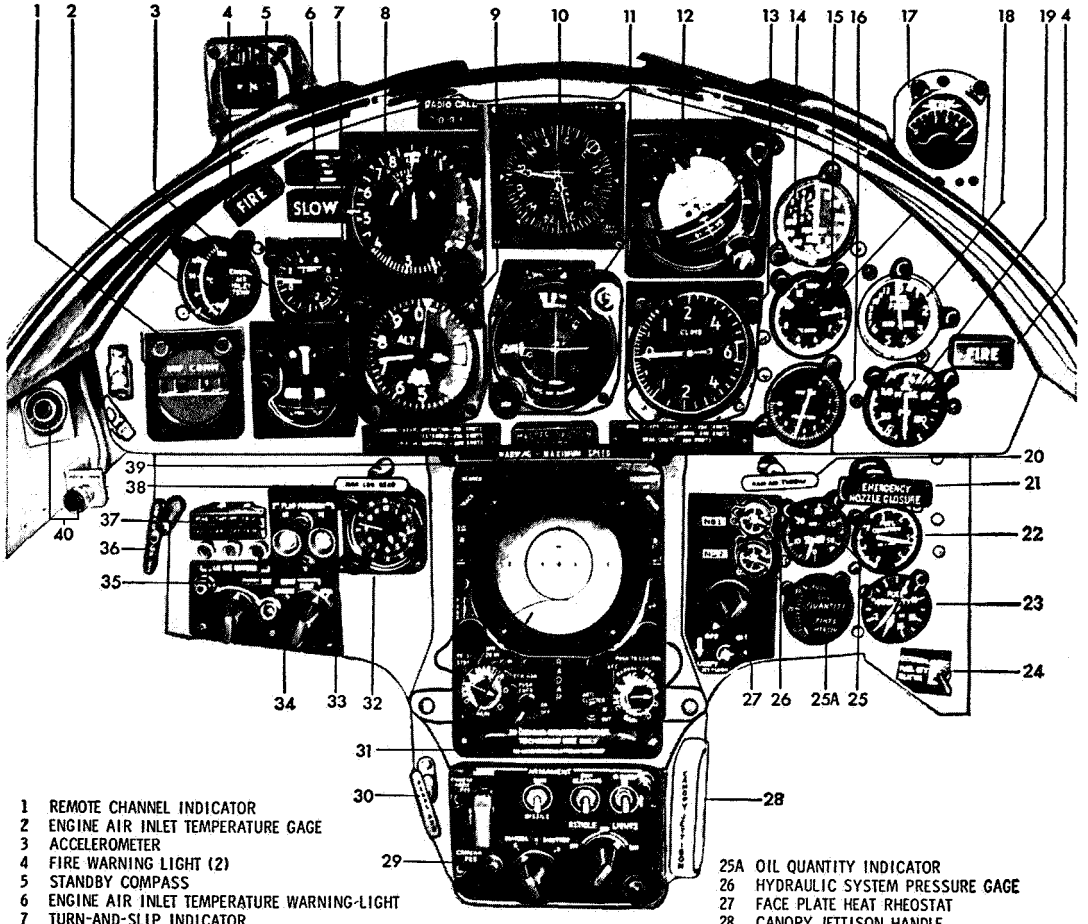

1 REMOTE CHANNEL INDICATOR
2 ENGINE AIR INLET TEMPERATURE GAGE
3 ACCELEROMETER
4 FIRE WARNING LIGHT (2)
5 STANDBY COMPASS
6 ENGINE AIR INLET TEMPERATURE WARNING-LIGHT
7 TURN-AND-SLIP INDICATOR
8 AIRSPEED AND MACH NUMBER INDICATOR
9 ALTIMETER
10 BEARING DISTANCE HEADING INDICATOR ID-526 BDHI
11 COURSE INDICATOR (ID-249)
12 ATTITUDE INDICATOR
13 VERTICAL VELOCITY INDICATOR
14 TACHOMETER
15 EXHAUST GAS TEMPERATURE GAGE
16 EXHAUST NOZZLE POSITION INDICATOR
17 AUTOMATIC PITCH CONTROL INDICATOR
18 FUEL FLOW INDICATOR
19 OIL PRESSURE GAGE
20 RAM AIR TURBINE EXTENSION HANDLE
21 EMERGENCY NOZZLE CLOSURE HANDLE
22 INTERNAL FUEL QUANTITY INDICATOR
23 EXTERNAL FUEL QUANTITY INDICATOR
24 EXTERNAL FUEL QUANTITY SELECTOR SWITCH
25 CABIN ALTIMETER
25A OIL QUANTITY INDICATOR
26 HYDRAULIC SYSTEM PRESSURE GAGE
27 FACE PLATE HEAT RHEOSTAT
28 CANOPY JETTISON HANDLE
29 ARMAMENT CONTROL PANEL
30 RUDDER PEDAL ADJUSTMENT HANDLE
31 RADAR SCOPE AND CONTROL PANEL
32 CLOCK
33 WING FLAP POSITION INDICATORS
34 GUNSIGHT CONTROL SWITCH
35 LANDING GEAR POSITION INDICATOR LIGHTS
36 DRAG CHUTE HANDLE
37 STABILIZER AND AILERON TAKEOFF TRIM INDICATOR LIGHTS
38 MANUAL LANDING GEAR RELEASE HANDLE
39 MASTER CAUTION LIGHT AND RESET BAR
40 ARRESTING HOOK RELEASE BUTTON AND ARRESTING HOOK DOWN WARNING LIGHT

FIGURE 1.4 -- AN AIRCRAFT INSTRUMENT PANEL

incremented or decremented at irregular intervals. The last three control actions may be described as discrete control actions,

A human operator model which is to reflect both the continuous elevator control and the discrete control of the aileron, rudder, throttle, and visual scanning mechanism would be complicated indeed. In the face of this complexity and lacking systematic techniques for the synthesis and identification of discrete models, two courses of action have been followed. Some investigators neglected the scanning behavior and assumed all of the inputs were utilized continuously, or neglected all but one input entirely. Other investigators, notably Senders [34], concentrated on the visual scanning behavior of operators, neglecting entirely any input-output behavior. In both cases satisfactory models for behavior of pilots performing instrument maneuvers were obtained. The models were, however, limited to representing only part of the operator's control actions.

As another example, consider the task of driving an automobile down a winding road. The driver has available not only the present input (the portion of road immediately ahead of the car) but a substantial part of the future input (the road ahead of the car). The availability of Preview information about the input signal makes this a more complex task to model than a standard tracking task. An

investigation was conducted by Wierwille [47] in order to obtain information about the way human operators control an automobile at high speed. A typical time history of steering wheel Position is found in Figure 1.5. The steering wheel position is strongly pulsatile and may be classed as discrete control behavior. The model selected by Wierw-ille, as best suited to the objectives of his study, was a linear describing function. The output of his model is also seen in Figure 1.5. The model clearly reflects the basic control actions of the onerator, but does not produce pulsatile control actions.

In the examnles above, the discrete control behavior has been neglected because, in part, generalized techniques for the synthesis and identification of discrete human onerator models w-ere not available, A number of investigations, in which discrete behavior was modeled, will be discussed in detail in the next chanter, In each case, the model develoned w-as annlicable only to the particular experimental situation.

1.4 Objectives Of The Study

The major objective of this study is the development of systematic techniques for the synthesis and identification of mathematical models for discrete human operator behavior. This

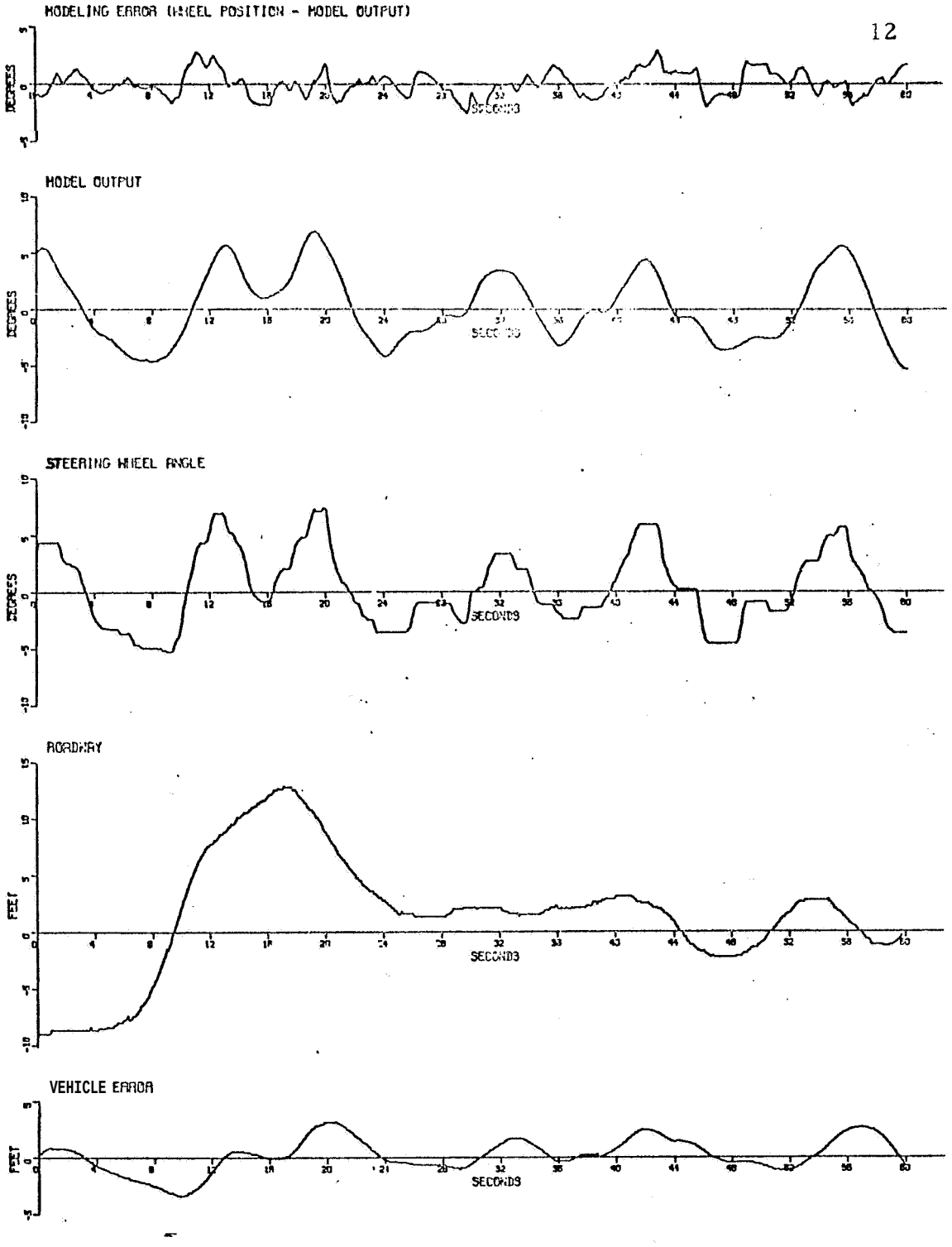

FIGURE 1.5 - Time Histories of High Speed Automobile Driving (Wierwille, et al, 1966)

objective can be restated in terms of more specific goals as follows:

a) Examine the literature on human onerator modeling and isolate the types of discrete control behavior observed.

b) Analyze the results of part (a) and determine specifications for general structure discrete model elements.

c) Formulate mathematical descriptions of the discrete model elements,

d) Develop identification procedures for the discrete elements

e) Perform experimental studies to evaluate the effectiveness and utility of the discrete elements,

f) On the basis of the experimental studies, propose extensions of the study.

The study proceeds from background to analytical investigation, and finally to experimental verification.

1.5 Limitations Of The Study

A number of restrictions apply to the broad abjectives stated above. The restrictions fall into two categories: those affecting the experiments and those affecting the mathematical models.

1, 5, 1 Restrictions On The Experiments

The experiments described below- were limited to compensatory tracking of single axis systems. Further, the dynamics of the controlled elements elicited pulsatile control actions from the operators.

The experiments w-ere based on results obtained from two subjects. These restrictions reflect on the experimental results and not on the two decision elements nresented. The intention of the experiments is to demonstrate the applicability of the decision elements to the modeling of discrete human operator behavior. The models obtained from the experiments are representative of one, well trained onerator and much work remains to establish the significance of the numerical results,

1,5. 2 Restrictions Of The Mathematical Models

The decision elements represented below are not primarily suited to the representation of continuous human onerator behavior.

Examples are taken from the literature in which discrete control actions effect the characteristics of an operator's continuous control behavior. The modeling of such behavior by discrete decision elements is described, but no attempts are made to synthesize complete human operator models.

1.6 Organization Of The Dissertation

The dissertation is organized into seven chapters, The present chapter has indicated the major objectives of the study, the restrictions nlaced on these objectives, and presented the background which motivated the study.

Chapter 2 considers the present status of discrete human operator models, Requirements and desirable features of elements which reflect the discrete control behavior of human operators are presented. Based on these, two decision elements, the Proportional Decision Element (PDE) and the Multi-State Decision Element (MSDE) are developed. Examples from the literature are considered in detail and the application of the decision elements to the synthesis of models is described,

Chapter 3 formalizes the verbal, block diagram descriptions of the PDE and MSDE developed in Chapter 2, by defining the input-output relationships mathematically.

Chapter 4 presents identification algorithms for the PDE and the MSDE. The algorithms are easily mechanized on general purpose digital computers and hybrid computers.

Chapter 5 describes the complete synthesis and identification of a model for a human operator performing compensatory single

axis tracking of gaussian random signals. The controlled element is such that the operator elects to generate oulsatile control actions. The resultant model contains an input monitoring decision element which controls sample and holds. The result is an input dependent sampling model for a human onerator.

Chapter 6 is an extension of the work of Chapter 5, The controlled element of Chapter 5 resembled an aircraft pitch axis. The input to the controlled element was elevator nosition and the output w-as altitude. **A** second disnlay was added presenting pitch angle, simulating an attitude display, The geometry of the task was selected to simulate a terrain avoidance problem. The controlled elements w-ere such that the operator again elected to produce pulsatile control actions. A complete human operator model w-as synthesized and identified. The model contains a deterministic visual scanning and signal processing system in addition to the pulse generation system.

Chapter 7 summarizes the results of the study and presents recommendations for future work.

1. 7 Applications Of The Dissertation

There are an increasing number of investigations described in the literature on human operator modeling which delve into the

detailed structure of human operators. Models are being studied which probe into the operator's ability to recognize plant changes and adapt to them. It is hoped that this dissertation will be a contribution to the scientific goal of furthering the understanding of human operator behavior by providing tools for the analysis of discrete human operator behavior. Further, this study is an example of a methodology for the development of mathematical models which may find increasing usefulness in the future.

CHAPTER 2

AN ANALYSIS AND REVIEW OF DISCRETE CONTROL BEHAVIOR IN HUMAN OPERATORS

2.1 Classes Of Discrete Control Behavior

The synthesis of mathematical models of human operators in closed loop control systems is based on the assumption that a causal relationship exists between the sensory stimuli available to the operator and the control actions which result from muscle flexures. The sensory stimuli are usually continuous functions of time. Some examples of discrete control actions were presented in the preceding chapter. These were pulsatile and incremental control actions and visual scanning between separate displays. A review of the literature on human operator modeling reveals three classes of discrete behavior in human operators:

1. Visual scanning between separated display devices.
2. Pulsatile or incremental control actions.
3. Detection and switching.

The ability of human operators to adapt to sudden changes in almost any portion of the control system is well known. The

adaptation to these sudden changes in environment requires the operator to detect the change and modify his control strategy accordingly.

2.2 Requirements For Models Of Discrete Control Behavior

From the descriptions given above, it is not clear what the output of a discrete control element should be. In the case of visual scanning the model must indicate which of the available displays is to be viewed and for how long. Alternatively the model can point to the next display to be viewed and produce an output when it is time to view another display. In both cases, the model must select between possible alternative decisions. This may be achieved if the model generates N binary signals on separate output lines, corresponding to N possible alternative decisions. Since only one alternative can be selected at a time, only one output at a time can be true. If the decisions are considered to be discrete operator states then this may be described as a multi-state decision. The inputs to the decision model are continuous functions of time and the output is a set of binary signals, only one of which can be true at a time. A multi-state decision process also occurs in the other classes of discrete control behavior. In generating a pulsatile or incremental control action the operator must decide when to start the control action and what polarity to make it. The detection of a sudden plant change is

similarly a multi-state decision. In the multiple display case, there are many possible alternative states. In the last two cases, only two output states are required, In the case of pulsatile control actions the operator must select a pulse amplitude and a pulse width. This may be viewed as a multi-state decision in w-hich the states represent quantized pulse amplitudes or widths. If the human operator is provided w-ith a continuous control device, the the number of quantization states required to adequately describe the output may become quite large. A more convenient approach is to consider the output of the decision model to be a number, the magnitude of w-hich determines the amplitude or width of the control action. Assume that some functional relationship exists betw-een the displayed signals and the pulse amplitude, for example. This may be modeled by sampling and holding the transient signals and then computing the pulse amplitude from the known functional relationship. This requires a control signal to operate the sample and hold device. The control signal is a binary, on-off signal and may be obtained from a multi-state process.

Thus far, two types of decision processes have been isolated. These are the multi-state decision and the function generation decision. The latter is called a decision as the output is a discrete quantity and not a continuous function of the inputs.

2. 3 Elements For Discrete Control Models

Tw-o general purpose elements can be constructed from these verbal descriptions.

2. 3. 1 Multi-State Decisions

Multi State decisions can be generated by adapting pattern recognition techniques [13]. A number of hypersurfaces are generated in the space formed by the linear combinations of the input signals. **A** threshold element determines the position of the instantaneous input vector relative to the hypersurfaces. A boolean function of the outputs of the threhold elements determines which of the output lines is to be true. The result is a Multi-State Decision Element (herein after denoted by MSDE).

2. 3.2 Function Generation Decisions

The function generation decision process may be modeled by sample and holds and a function computer. For convenience in modeling, the function is restricted to linear combinations of the sampled and held signals. The result is called a Proportional Decision Element (herein after denoted as PDE).

2. 3. 3 Complete Models of Discrete Human Operator Behavior

It w-ill be seen .below that the MSDE and the PDE are sufficient to describe a wide variety of discrete human operator behavior. By properly selecting the structure of the tw-o elements it is possible to develop easily mechanized systematic identification algorithms.

By utilizing an MSDE to control the sample and hold operation in the PDE, a very convenient identification procedure results. This procedure has the effect of uncoupling the timing of the decision portion of the model from the function generation portion.

2. 4 The Status Of Models For Discrete Control Behavior In Human Operators

No attempt will be made here to consider the large body of work which is concerned w-ith the continuous input-output behavior of human operators. That this study is possible at all is due, in part, to the fact that the transfer characteristics of human operators in single axis tasks are so w-ell understood. This allows attention to be concentrated here on a rather specific type of human operator behavior.

2. 4. 1 Visual Scanning Models

In a very comprehensive manner, Senders, Elkind, et al [34-7] conducted experiments concerned w-ith the visual scanning behavior

of operators. Unfortunately, these studies are not applicable to the deterministic modeling of human operators. The experimental tasks involved either monitoring of uncorrelated displays for limit conditions or pilot eye motions during instrument flight in which only the pilot's eye motions were recorded. It would be interesting to speculate on the status of deterministic scanning models had the actual instrument readings been recorded simultaneously.

The models treated the human operator as a single channel device with the displays queueing up for attention. Probabilities were used to determine which display deserved attention next. The probabilities were computed from long term properties of the displayed signals, means, higher moments and bandwidth. The models do not utilize the transient data displayed.

The recent literature on human operator modeling contains an increasing number of investigations involving multi-axis tasks.

Almost all of the investigators deliberately suppress visual scanning by displaying all signals on a single integrated display. In a study by Levison and Elkind [19] an uncoordinated two axis tracking task with separate displays was identified assuming eye position to be known. No attempt was made to synthesize a model for the operator's scanning behavior. In any case, the displays presented uncorrelated

signals, and there is no reason to assume that the scanning behavior would be deterministic.

The lack of experiments in w-hich separated displays present correlated signals, motivated the experiment described in Chapter 6. An experiment was performed in which two separated displays presented aircraft attitude and altitude to an operator w-ho controlled the elevator position in a pitch axis aircraft simulation. A deterministic model for the operator's scanning behavior is synthesized.

2.4.2 Pulsatile And Incremental Control Behavior

In 1964 Knoop [10] developed a continuous non-linear human operator model w-hich generated incremental control actions. The non-linearities simulated known non-linear characteristics of human operators. The identification procedures did not utilize the operator's input-output behavior, but depended on optimal control considerations for some parameters while others w-ere manually adjusted to produce an adequate match w-ith the experimental data.

In a similar study, Gould [11] utilized a force computer to generate incremental control actions. Gould's basic human operator model is reproduced in Figure 2. 1. The output of the Force Program Element is an incremental change in controller position. The magnitude of the change is determined by the error and the error rate.

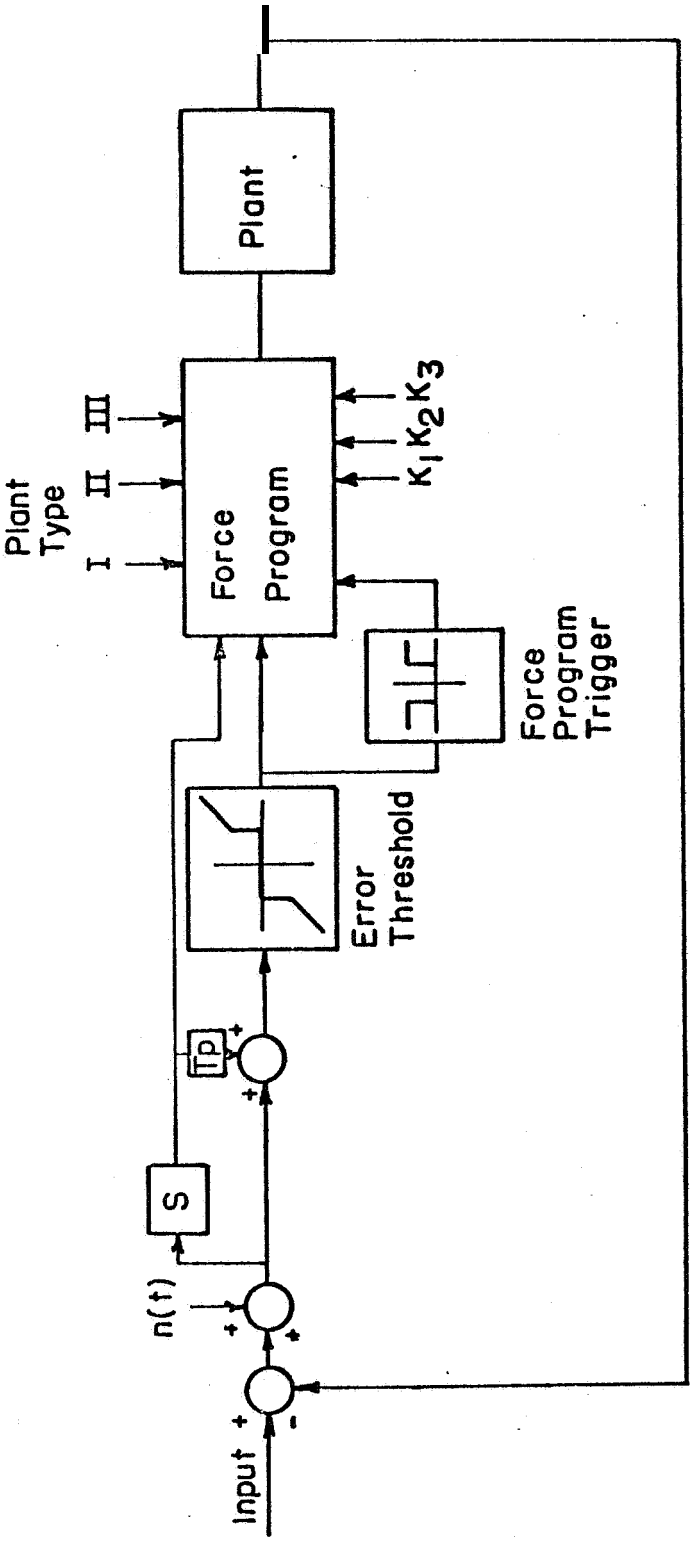

FIGURE 2.1 - Discrete Model of Gould

A threshold element reflects the operator's error dead zone. A bang-bang element triggers a control action when the predicted error exceeds a threshold.

No systematic identification procedures are presented and the model is not easily adapted to other classes of discrete control behavior.

An experiment quite similar to that of Gould is presented in Chapter 5. The operator produces pulsatile rather than incremental control actions. The non-linear elements are combined with the force computer and the complete model synthesized using the discrete elements developed in this dissertation.

A model for pulsatile control actions was proposed by Bekey and Angel [4]. The model structure is developed using asynchronous finite state automata theory. Based on threshold decisions, a single pulse event (rate correction) or a double pulse event (position correction) is generated. The resultant model structure is quite similar to the model presented in Chapter 5 of this study, No attempt w-as made to identify models of human operators.

2. 4. 3 Detection and Switching

When human operators are given differnt plants to control, they select different control policies. For a controlled element of

the form

$$G(s) = K_1 + \frac{K_2}{s} \qquad (2.1)$$

Gould found that the operator's output could be classified into two types of behavior. The type of behavior that predominated depended on the values of K_1 and K_2. A series of experiments in which K_1 and K_2 were changed systematically was used to determine the parameters of a pattern recognition element. The parameters of the recognition element were obtained by plotting the two types of behavior on the K_1, K_2 plane and visually selecting a decision surface that separated the points corresponding to the two types of output behavior. If the model contains a subsystem that estimates K_1 and K_2 then the appropriate force program can be selected.

A more general adaptive switching model is described by Miller and Elkind [9]. Miller and Elkind studied the performance of human operators in compensatory manual tracking with sudden plant changes. The plant transitions involved changing the sign and/ or the magnitude of the plant gain. The tracking task is reproduced from Ref. [9] in Figure 2.2.

Only three possible plant changes could be made from any given starting or base plant. The operator was required to perform the following discrete functions:

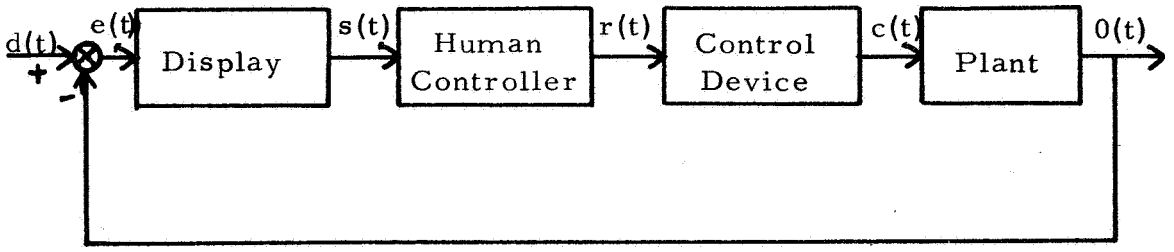

(A)

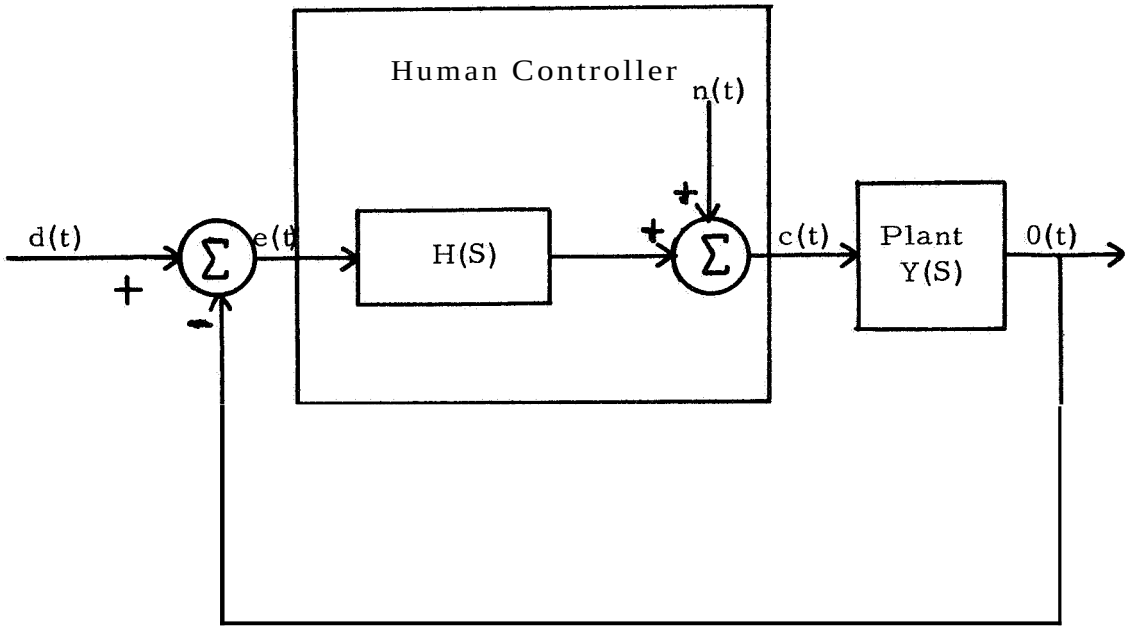

(B)

Figure 2.2 Tracking Task of Elkind and Miller

1) Detect the plant change

2) Determine which of the three possible plants had been selected

3) Modify his performance characteristic to match the new plant

Of the three types of discrete action, the first will best suit the purpose of this discussion.

The experimental data included the following:

a) The inputs $e(t)$ and $\dot{e}(t)$ to the human operator

b) The human operator output

c) A binary signal controlled by the operator that signals his first recognition of a plant change

d) The binary control signal that caused the plant change

The model proposed by Miller and Elkind is shown in Figure 2.3. Part A of the model detects the plant transition and initiates action in Parts B and C. Part B uses trial and error switching of dynamic elements to identify the new plant.

Based on the results of the plant identification, a new human operator describing function is selected to provide satisfactory tracking performance.

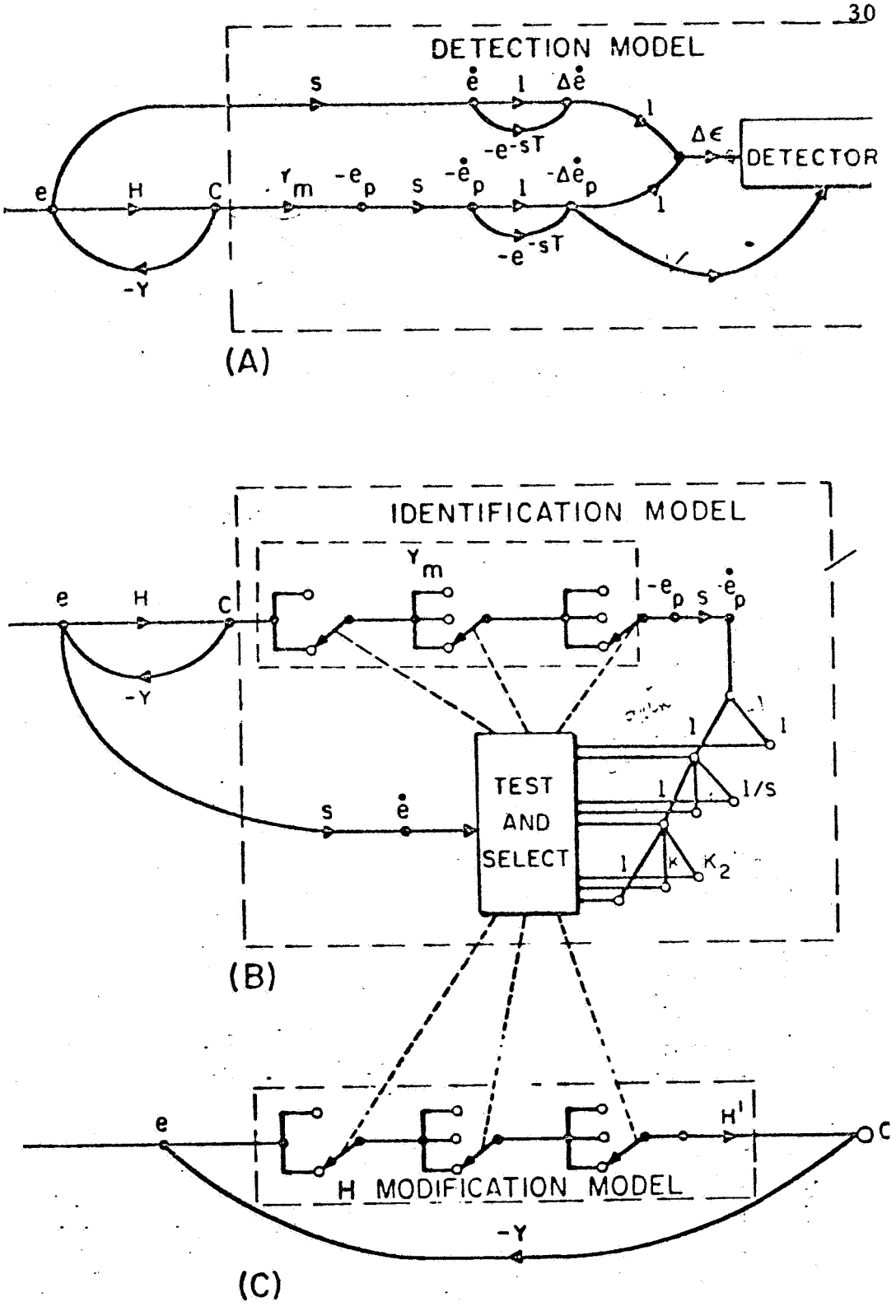

FIGURE 2. 3 - Detection and Switching Model of Miller And Elkind

2.4.2 The Detection Model

The detection model may be more easily studied from Figure 2.4 which is redrawn and labeled version of Figure 2.3

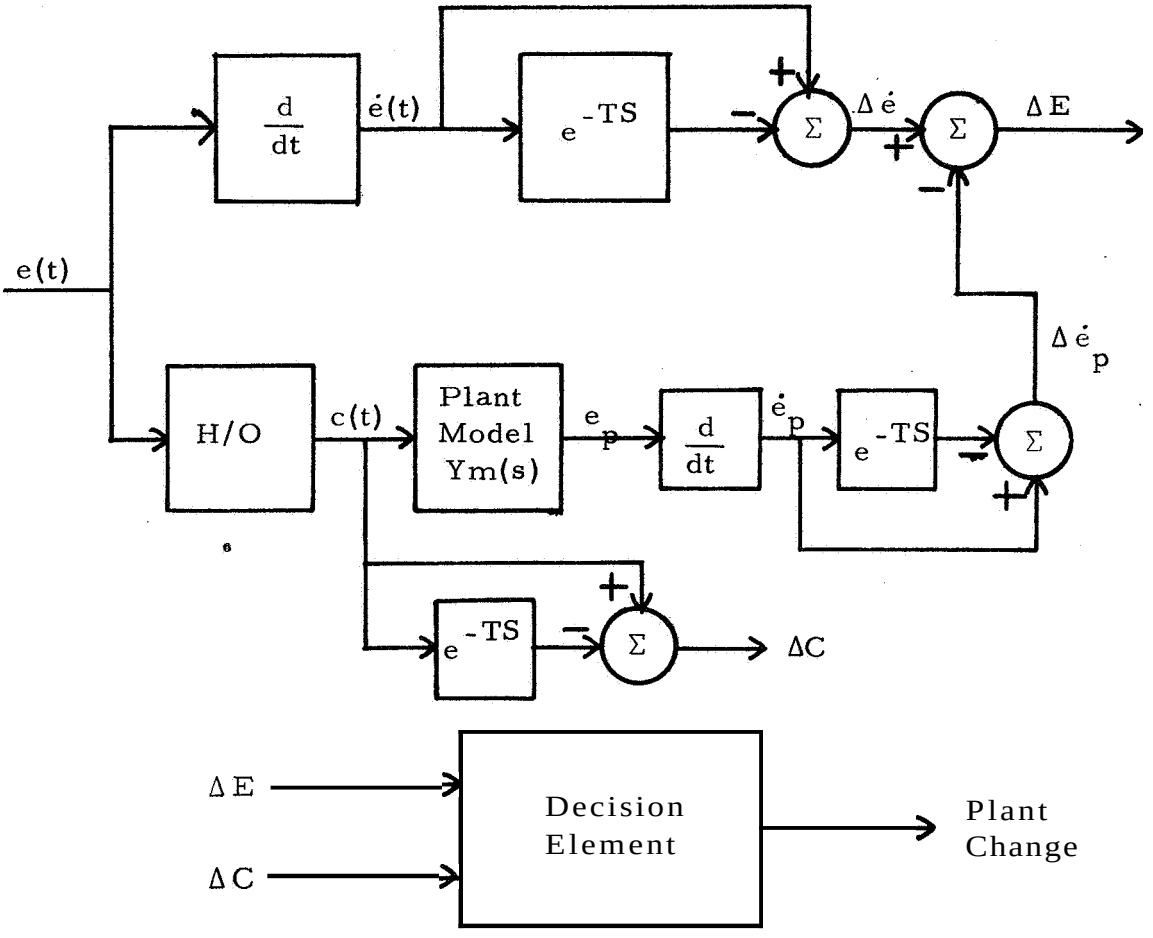

The time of the plant change is easily determined, as is the time at which the linear describing function of the operator changed, This may be seen in Figure 2.5 where the operator gain is plotted as a function of time during a plant transition. The change in the

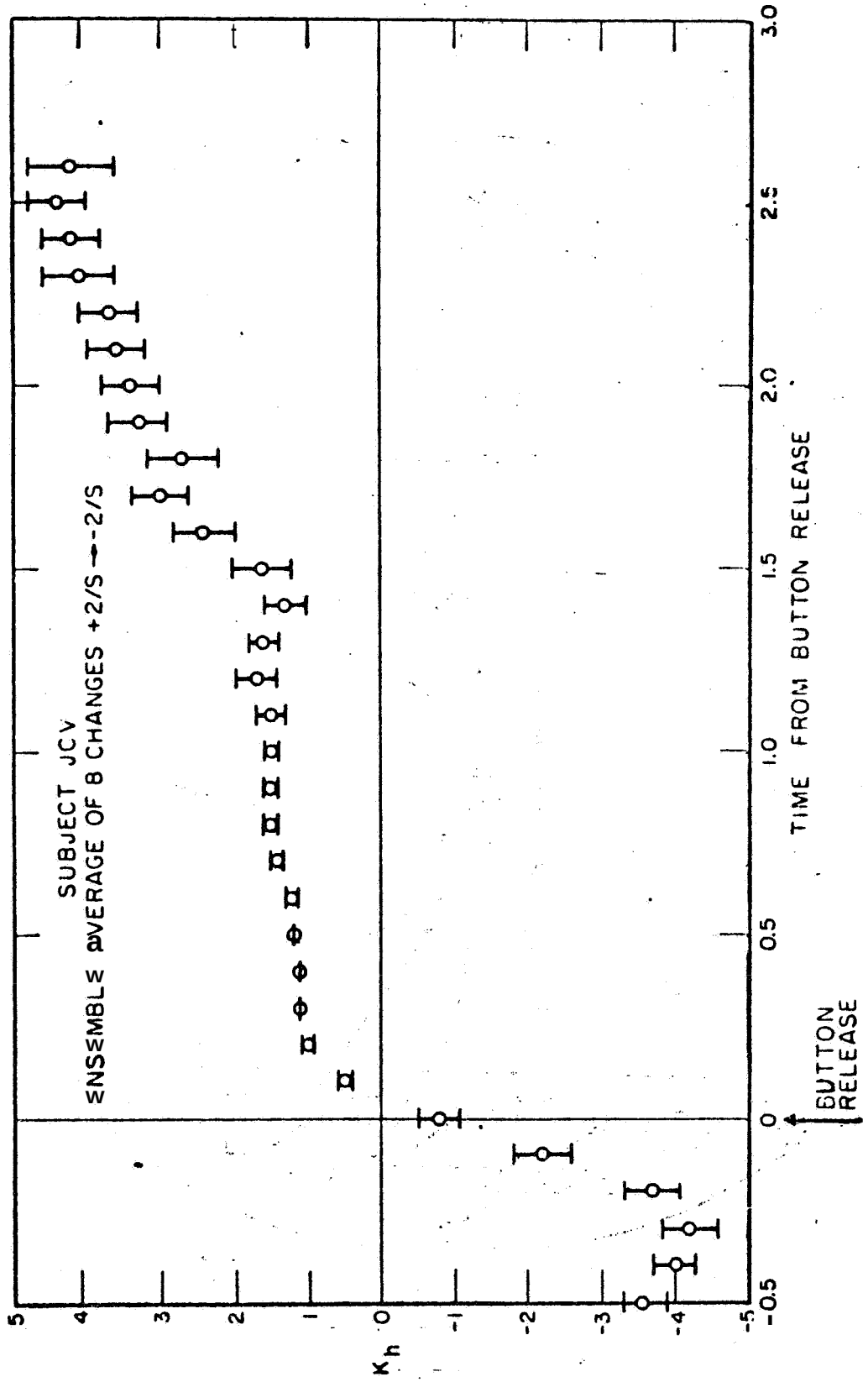

FIGURE 2.5 - Gain of Operator During A Sudden Plant Transition (Miller and Elkind, 1965)

describing function leads the conscious recognition of the change by 100 to 300 milliseconds.

If the values of **AE** and **AC** just after plant transition are plotted, a linear relationship is found, Figure 2.6. This curve can be used as a decision surface, to detect plant changes. If particular values of **AE** and **AC** lie below- the line, the plant has changed. If they are above it, then no plant change has occurred. There is the usual dead space around the origin where the operator elects to make no decisions.

Miller and Elkind obtained the coefficients of the detection model from the graph in Figure 2.6. The points plotted were obtained by recording ΔE and **AC** one "reaction time" before the overt operator action. No attempt was made to adjust the model coefficients, **or** to identify the operator's reaction time.

In a different approach to the same problem, Weir and Phatak [43] devoted their attention to the switching behavior of the operator during sudden plant transitions. Their model contained three phases: (1) retention, in which the operators describing function remains unchanged, (2) optimal control, in which the operator acts as a time optimal bang-bang control system, and **(3)** adjustment to steady state tracking with the new plant. Complete models were obtained for

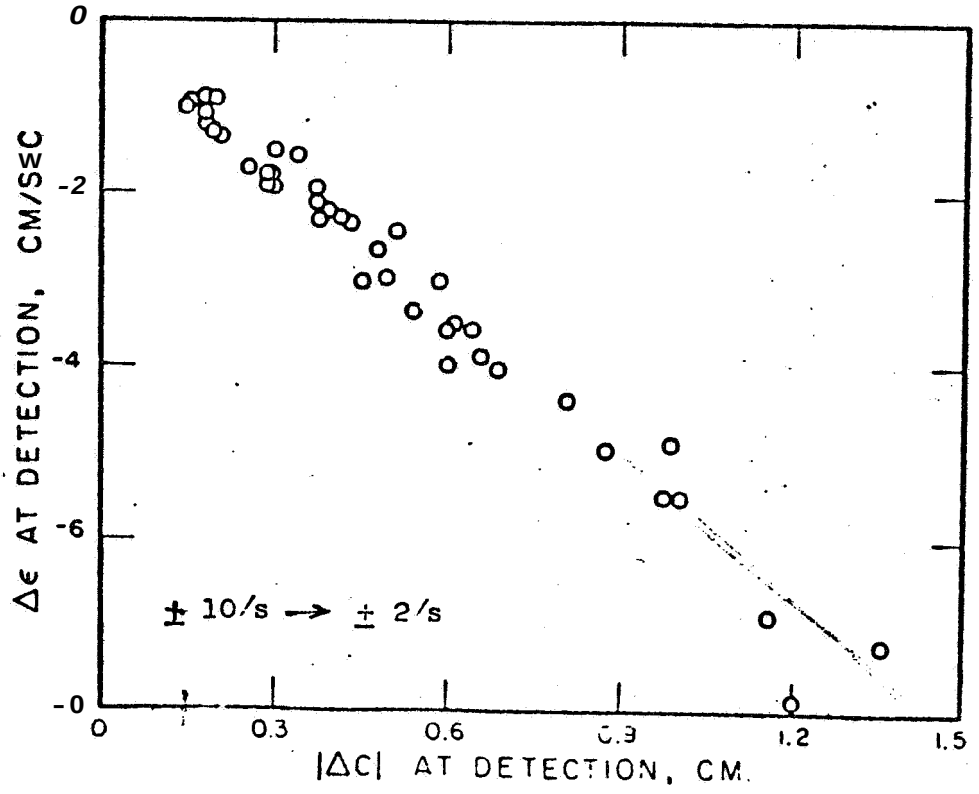

FIGURE 2.6 - Decision Surface For Detection Element (Miller and Elkind, 1965)

operators during each phase, however, no attempt w-as made to synthesize a detection and sequencing system.

2.4. 4 Summary Of The Literature Review-

The characteristics of discrete control behavior, found in a number of experiments have been reviewed. In the next chapter the structure of two general purpose decision elements (the MSDE and PDE) for modeling discrete control responses is presented. It w-ill be show-n that the resulting elements are sufficiently general as to include all of the types of behavior observed in the studies reviewed in this chapter.

CHAPTER 3

BLOCK STRUCTURED DECISION ELEMENTS

3. 1 General Features Of Decision Elements

This chapter presents two types of decision elements in a block diagram form suitable for configuring models of discrete human operator behavior. Subsequent chapters will describe systematic identification schemes and typical applications of the decision elements.

The input-output relationships of the decision elements 'are sufficiently general as to allow- a wide variety of discrete human operator behavior to be modeled. It is hoped that the generality of the blocks w-ill, combined with their identification schemes, allow- discrete behavior to be modeled in the same manner that continuous operator behavior is modeled by describing functions, and pow-er spectral density measurements.

The first decision element described below- is the Multi-State Decision Element (MSDE). The inputs to the element are continuous time varying signals and the outputs are binary signals. The MSDE is intended to model operator decisions betw-een discrete alternatives, for example: sw-itch closures, eye motions betw-een separate

1

displays, decisions to initiate discrete or pulsatile control actions, etc. If the binary outputs are view-ed as the states of a digital register, then each possible decision of the operator can be decoded from the contents of the register. In its simplest form, the MSDE can be viewed as a switching locus generator.

The second element described below- is the Proportional Decicion Element (PDE). The inputs to the PDE are continuous time varying signals and one or more binary control signals. The output of the PDE is a scalar function of the input signals at a time determined by a binary control signal, the scalar output appears at a time determined by the same **or** another binary control signal. The binary control signals may be derived from a timing circuit, or in most cases, from an MSDE. The PDE is intended to model the proportional or function generation behavior of human operators. Such behavior might include: the selection of the amplitude and w-idth of a pulsatile control action, the magnitude of a step change in throttle position in an aircraft, etc. An MSDE decides when to make the change and the direction of the change and a PDE determines the amount of the change.

3.2 The Multi-State Decision Element MSDE

Based on the analysis in the previous chapter, it can be assumed that a multi-state decision process is utilized by human

operators, when a decision must be made betw-een distinct alternatives.

3. 2. 1 Definition of the Basic MSDE

An input-output relaticnship for a general multi-state decision element (henceforth designated MSDE) may be based on the assumption that portions of the input space formed by the linear combinations of the signals applied to the MSDE are associated with desired binary output states:

$$\bar{h} = \bar{B}\ (T(f(x))\ ) \qquad (3.1)$$

where x is an n vector of time varying input signals, f(x) is an m vector of time varying functions of the input vector x, forming decision surfaces in the input space, T is an m vector of time varying binary signals resulting from a threshold operation on the vector f(x), $\bar{B}$ is a **p** vector of boolean functions of the binary signals T(f) and finally, $\bar{h}$ is a **p** vector of binary output signals, only one of which may be true at a time. This relationship is summarized in Figure 3.1.

The components of the input vector x, may be any signals which enter into a causal relationship with the binary output vector $\bar{h}$. These signals may be deterministic signals from the system, random

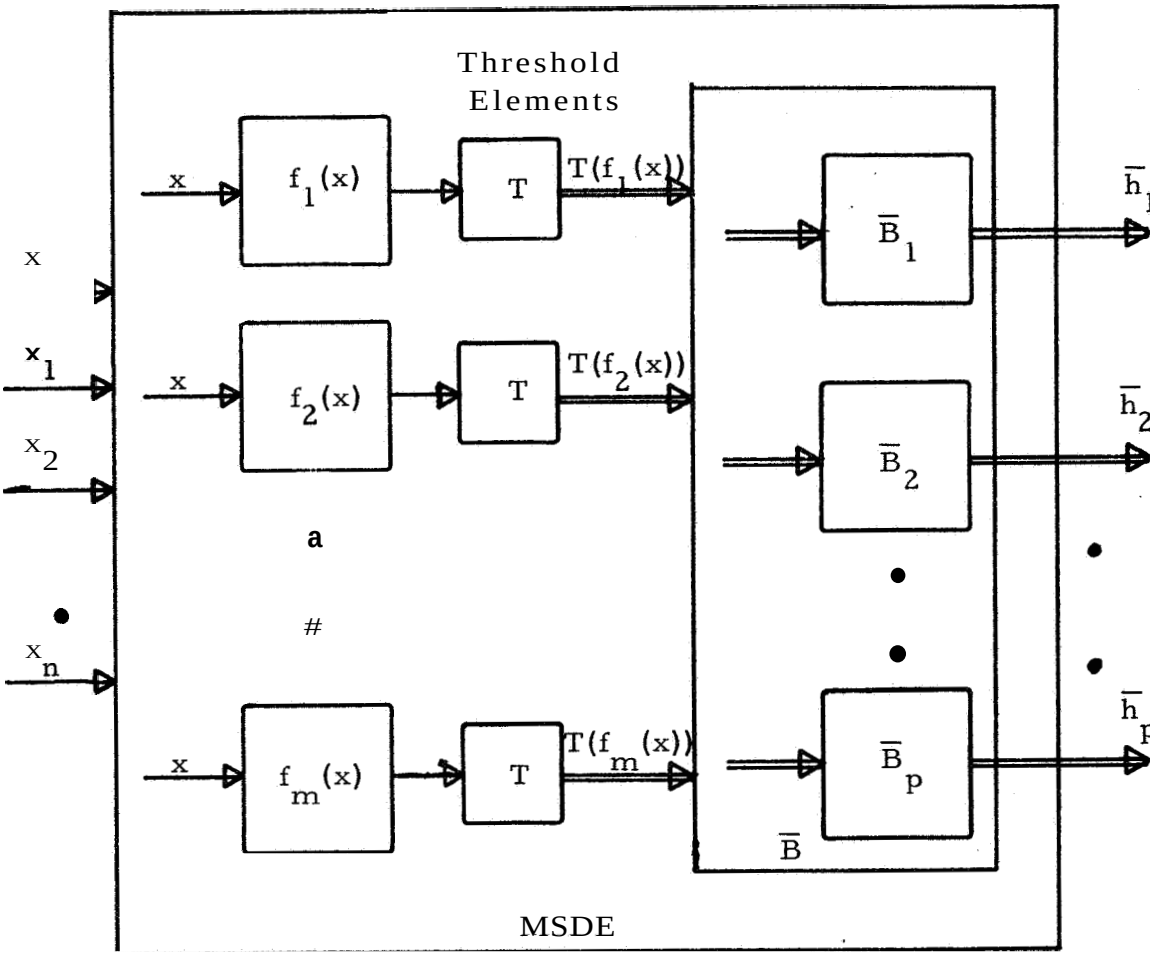

Figure 3. 1 The General Multi-State Decision Element (MSDE)

signals, past samples of the signals, time delayed signals, human operator outputs, etc. The signals may be continuous analog signals, discrete signals, outputs of hold devices, binary signals and encoded continuous signals. The outputs of the MSDE are binary signals and for convenience, it may be assumed that one and only one at a time

may be true. Each component of the output vector, $\bar{h}$, corresponds to a possible state in the system being modeled.

The MSDE is a pure combinatorial network w-ith no direct feedback paths. If storage is a necessary part of the process being modeled, it must be obtained by including delayed or sampled and held signals as additional components of the input vector. Theoretically the identification process described below allows the input vector to contain an unlimited number of components. Practically, the time required to complete the identification depends on the number of components.

3.2. 2 Extension Of The MSDE To Include Time Delay

In order to synthesize and identify models of human operators w-hich reflect discrete decision making behavior, the operator's discrete action must be measurable. That is, it must be possible to measure or infer from observable signals the exact time the operator changed state and the state arrived at. Decisions of this type will be called overt or measurable decisions. In many human operator modeling situations, the model decision must precede the overt action, allowing the model to simulate reaction time and possibly computational or thought processes. The MSDE described by equation 3. 1 and shown in Figure 3, 1 is suitable for the development of models

w-hich produce a change in state at the same time that the human operator executed his discrete act.

The MSDE is easily modified to reflect this behavior by re-defining the input-output equation. The output of the MSDE w-as defined as:

$$\bar{h} = \bar{B} [T(f(x))] \tag{3.2}$$

and a delayed MSDE output may be defined:

$$\bar{b} = e^{-\tau s} \bar{h} \tag{3.3}$$

where τ is the time delay required between the covert or inaccessible human operator decision and the overt decision τ seconds later. The general MSDE shown in Figure **3.1** is redrawn in Figure **3.2** to reflect this additional requirement.

The direct output vector, $\bar{h}$ may be used to trigger input dependent sampling devices, initiate computational processes, etc. The delayed output $\bar{b}$ may be used to initiate the control action.

If the decision element is used to model an overt control action, the time delay element is not needed. This might be the case if the actions being modeled were: operation of a pushbutton, switch

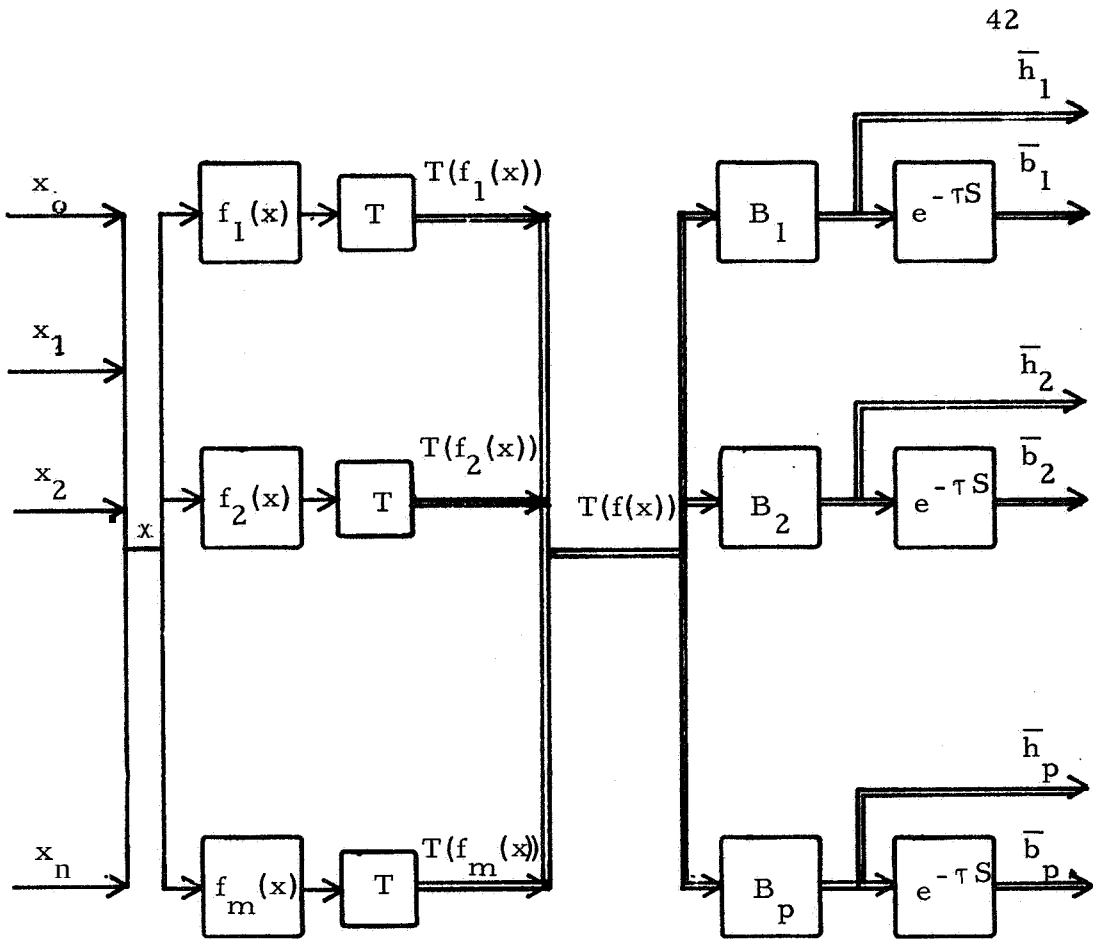

Figure *3.2* Modified MSDE

closures, eye motions, etc. For these actions there is no need to separate the covert decision from the overt act.

3.2. 3 Complete Structure Of The MSDE

The input vector traces out an event trajectory in the space formed by linear combinations of the components of the input vector. The position of the event trajectory relative to the decision surfaces of the MSDE determines which of the p output lines is to be true.

The proper output is obtained by positioning hypersurfaces in the input space such that the event points corresponding to a particular desired output state are separated from all other event points.

If hyperplanes are used to perform the separation, then a rather simple mechanization is possible, and the f_j become

$$f_j(x) = \sum_{i=1}^{n} a_{ji} x_i + a_o \qquad j = 1, 2, \ldots m \qquad (3.4)$$

If an additional component, x_o, is included in the input vector such that

$$x_o = 1$$

then

$$f_j(x) = \sum_{i=o}^{n} a_{ij} x_i \qquad j = 1, 2, \ldots m \qquad (3.5)$$

The threshold operator is defined by

$$T(y) = \begin{cases} & \text{for } y > o \\ 0 & \text{for } y \leq o \end{cases} \qquad (3.6)$$

and

$$T(f_j(x)) = T\left(\sum_{i=o}^{n} a_{ij} x_i\right) \qquad (3.7)$$

If $T(f(x))$ is 1 (true) the event point is above the hyperplane, if $T(f(x))$ is 0 (false) then it is below the hyperplane. By utilizing a sufficient number of hyperplanes and properly selecting the

boolean function, $\overline{B}$ it is possible to generate the decision surfaces required to produce the desired outputs. The complete mechanization of the MSDE is show-n in Figure 3. 3.

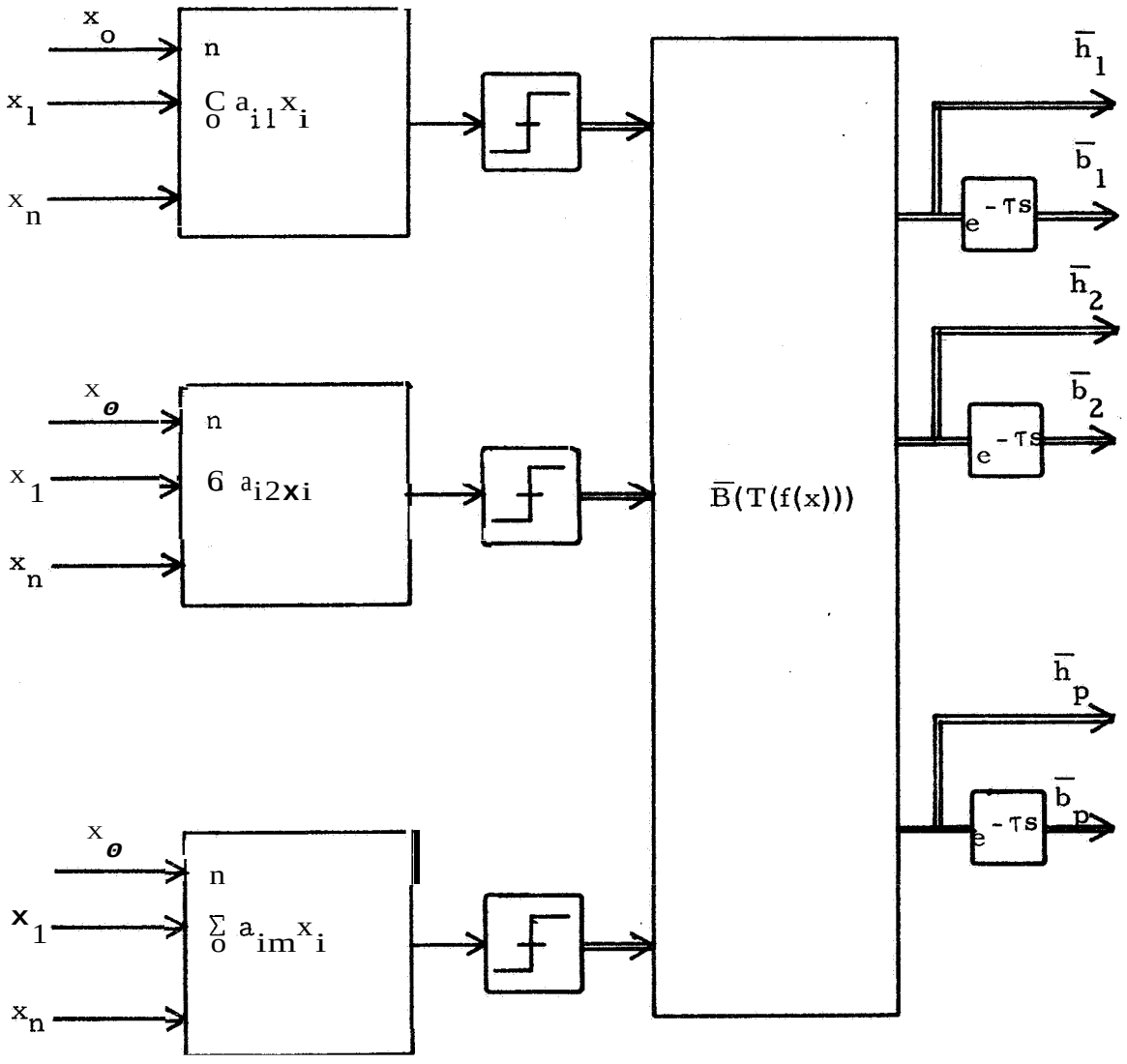

Figure 3. 3 Complete MSDE

3.2.4 Application Of The MSDE To The Generation Of Complex Decision Surfaces

Although the hypersurfaces, generated within the MSDE, are planes in the input space, they may be made to represent complex surfaces by properly selecting the components of the input vectors and the boolean functions, $\overline{B}$. A rather simple phase plane diagram is shown in Figure 3.4. The MSDE is to determine whether the event trajectory is in region a_1, a_2, or a_3, and produce corresponding output states.

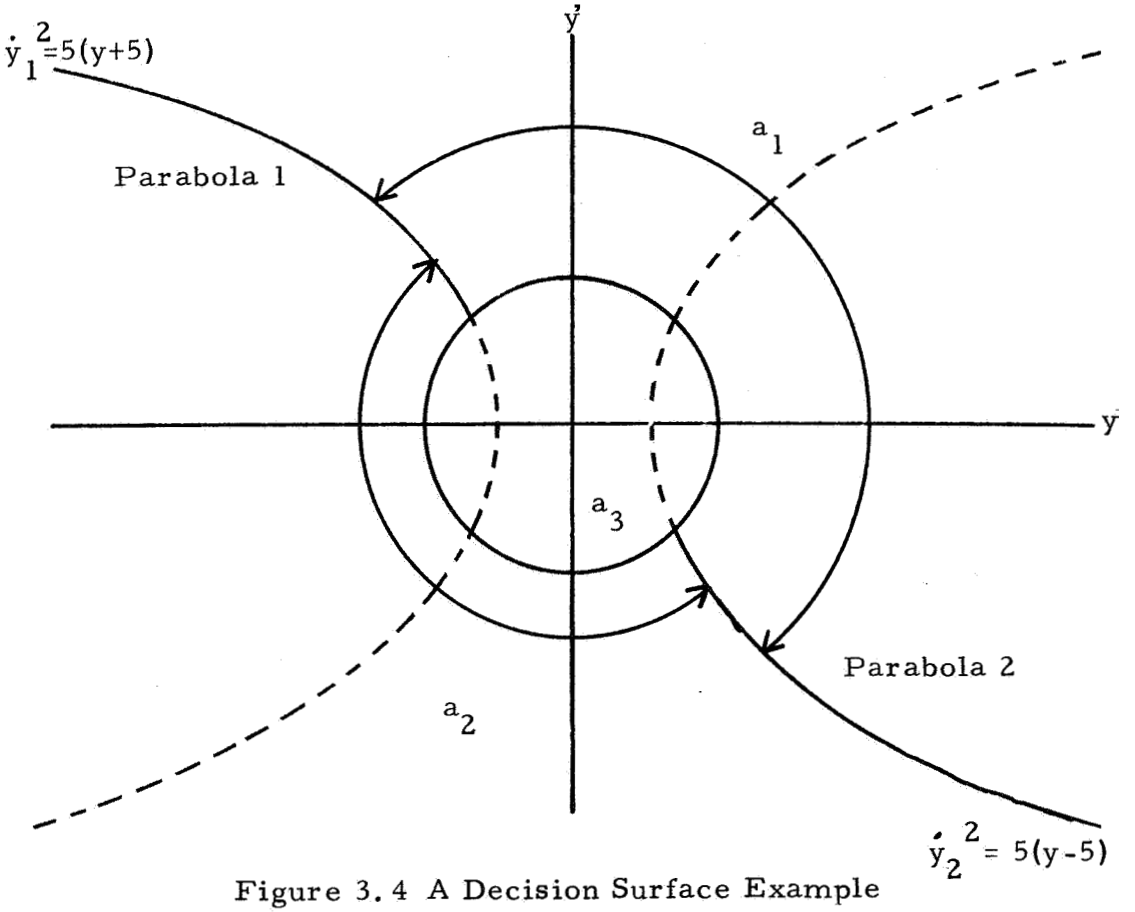

Figure 3.4 A Decision Surface Example

If an input vector is formed from

$$\begin{aligned} x_o &= 1 \\ x_1 &= y \\ x_2 &= \dot{y} \\ x_3 &= \dot{y}^2 \\ x_4 &= y^2 \end{aligned} \tag{3.8}$$

then hyperplanes in the input space may be defined as

$$\begin{aligned} f_1(x) &= x_1 \\ f_2(x) &= x_2 \\ f_3(x) &= x_3 + 5x_1 + 25x_o \\ f_4(x) &= x_3 - 5x_1 + 25x_o \\ f_5 &= x_3 + x_4 - r^2 x_o \end{aligned} \tag{3.9}$$

The resultant threshold functions are tabulated in Table 3. 1.

Table 3, 1 Threshold Functions For the Decision Surface Example

Threshold Functions	Output	Geometric Significance of output
$T(f_1(x))$	1	in the right half plane
	0	in the left half plane
$T(f_2(x))$	1	upper half plane
	0	lower half plane
$T(f_3(x))$	1	outside parbola 1
	0	inside parabola 1
$T(f_4(x))$	1	outside parabola 2
	0	inside parabola 2
$T(f_5(x))$	1	outside circle
	0	inside circle

It is now possible to determine $\overline{B}$ so that three binary output signals, $\overline{a}_1$, $\overline{a}_2$, and a_3 are generated, corresponding to the regions a_1, a_2 and a_3 indicated on Figure 3.4.

$$\overline{a}_1 = [T(f_4(x))]' \cdot [T(f_5(x))] + [T(f_3(x))] \cdot [T(f_5(x))] \cdot [T(f_2(x))] \tag{3.10}$$

$\overline{a}_2$ is written in the same manner, and

$$\bar{a}_3 = [T(f_5(x))]' \tag{3.11}$$

where the primes indicate logical complement.

Thus hyperplanes in the input space may represent complex decision surfaces in the state variable space of the system. The complete MSDE for this example is shown in Figure 3.5.

In more complete examples, below, the MSDE will be applied to modeling of the human operator's decision to initiate pulsatile control actions. In one of the examples it was possible to determine the structure of the decision surfaces from a priori knowledge. The identification consisted of testing and adjusting the free coefficients of the MSDE until an optimum fit was obtained between the models output and the experimental data. In a second example, it was not possible to make any reasonable extimates of the MSDE structure and the identification procedure required a great deal more effort and computer time.

3.2.5 Relationship Between The MSDE And Pattern Recognition Devices

There is a definite relationship betw-een the structure and mechanization of the MSDE and binary pattern recognition devices. The basic concept is the same in both devices, the partitioning of the input space by hyperplanes to establish decision surfaces. In binary

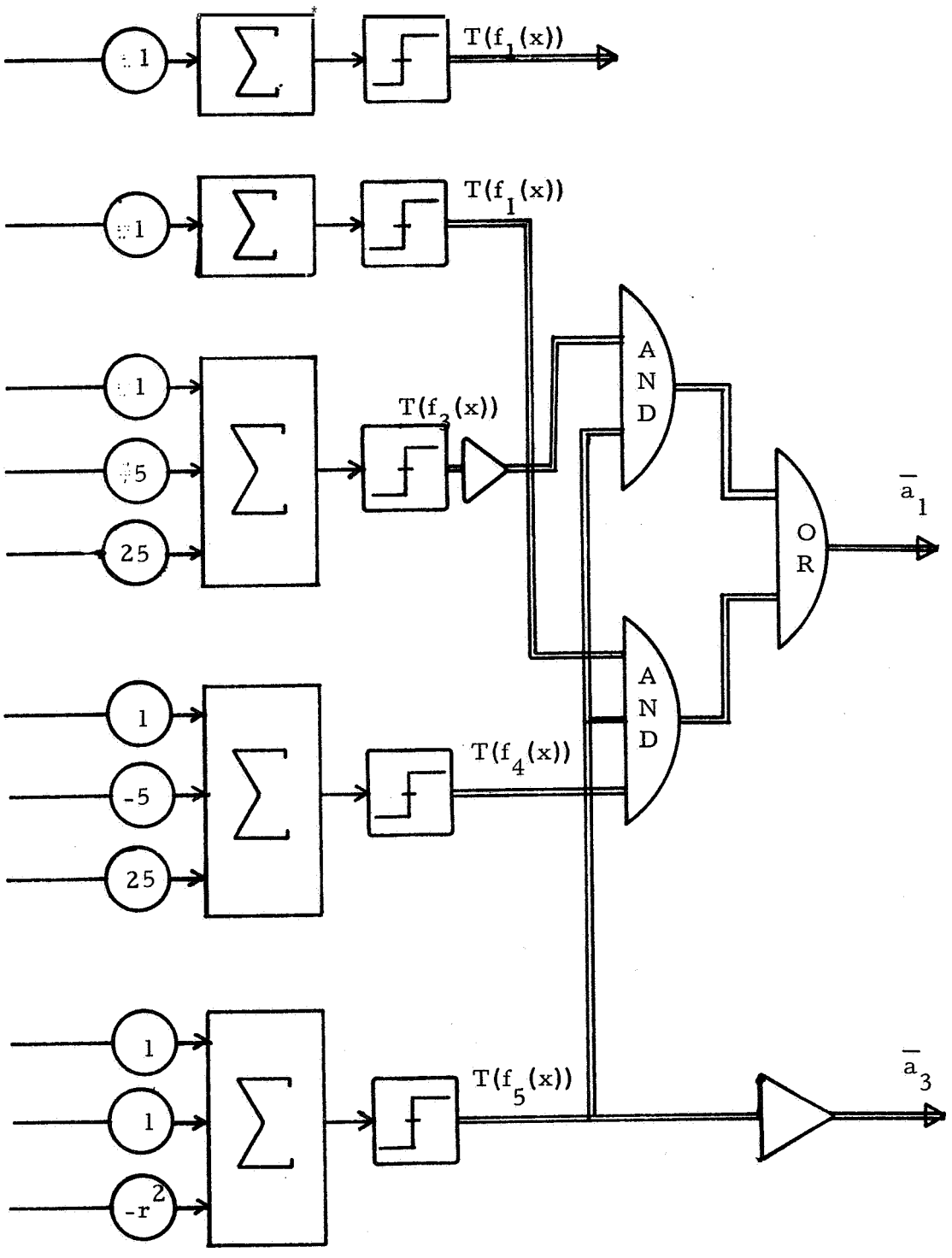

Figure 3. 5 Complete MSDE For Example

pattern recognition devices, the input vector contains only binary signals, and the resultant input space is a binary space. The mechanization of the two devices are identical, their difference lies in the use of only binary inputs in pattern recognizers.

The advantages of the binary recognition device are the ease of mechanization, and the convenient identification algorithms. The disadvantages in their application to human operator modeling result from the need to encode the input signals and the fact that the resultant decision element offers no insight into the process by which the decisions were made.

3.3 The Proportional Decision Element (PDE)

Human operators utilize proportional decisions while performing manual control when they must decide how large, how long or how fast to make a control action. The proportional decision element (henceforth to be denoted as PDE) combines function generators, hold elements and logical structure to produce the discrete decision. This yields a block element which is easily utilized in complete system diagrams to configure human operator models. The output of a PDE may be used to model many types of human operator behavior: amplitude and width of a pulsatile stick motion, time a button or bang-bang controller is closed, etc.

3. 3. 1 Definition Of **A PDE**

The output of the **PDE** is a scalar signal obtained by linearly combining the input signals to the PDE at some time, determined by an applied binary signal $\overline{C}$:

$$x^* = x(t) \mid \overline{C} \tag{3.12}$$

where x (t) is an r vector the components **of** which are time varying signals applied to the input terminals of the **PDE.** The input vector x(t) is sampled and held at the time $\overline{C}$ becomes true. The scalar output, y_1, of the PDE is obtained from

$$y_1 = a' x^* + a_o \tag{3. 13}$$

where a is an r vector containing arbitrary real coefficients and a_o is an arbitrary real constant. If an additional component x_o is added to the input vector x such that

$$x_o = 1 \tag{3. 14}$$

then the constant a_o, may be included in the coefficient vector, a and

$$y_1 = a' x \tag{3. 15}$$

The value of y_1 is held at the output until $\bar{C}$, becomes true again, causing a new value of y_1 to be generated. In some modeling situations an additional delay, τ, is required to simulate the reaction and/or computation time of the operator.

$$y_2 = e^{(a' x)} \tag{3.16}$$

The input-output relationship is summarized in Figure 3.6.

As with the MSDE, the input vector may contain measurements from the system being modeled, the human operator's inputs and outputs, random signals, binary signals, outputs of filters, time delays and hold devices.

The PDE may be interpreted geometrically by considering the r + 1 dimensional space formed by the input vector **x** and the scalar output y. A hyperplane in this space would take the form:

$$y = \sum_{i=0}^{r} a_i x_i \tag{3.17}$$

which is just the equation of the function generation portion of the PDE

$$y = a^I x \tag{3.18}$$

The identification problem consists of finding the best fit hyperplane to the event points. An event point is determined by the input vector at the time the signal $\bar{C}$ becomes true, and the corresponding value of the desired output of the PDE.

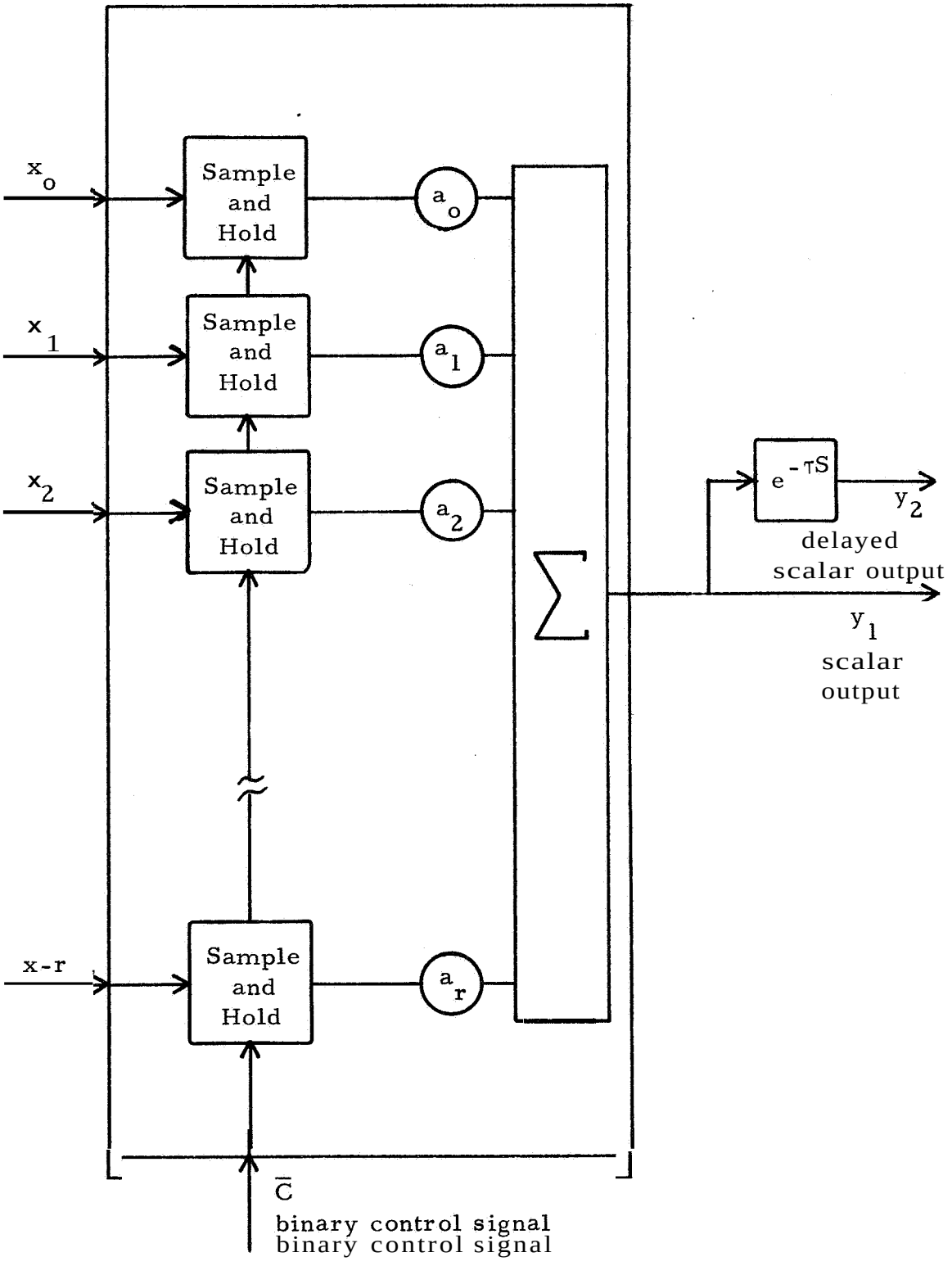

Figure 3. 6 Input-Output Relationship Of The Proportional Decision Element (PDE)

3.3.2 Application Of The PDE To The Generation Of Complex Functions

The use of hyperplanes in the space formed by the input vector and the scalar output is not restrictive. If many functions of a single variable, w, are included in the input vector to the PDE, then a hypersurface is formed in the lower dimensional space of that variable. Consider the following example in which a 6 dimensional hyperplane is equivalent to a two dimensional curve. Let x be the input vector to a PDE the components of which are functions of a single time varying variable, w(t):

$$\begin{aligned} x_0 &= 1 \\ x_1 &= w \\ x_2 &= w^2 \\ x_3 &= w^3 \\ x_4 &= w^4 \\ x_5 &= w^5 \end{aligned} \tag{3.19}$$

The six dimensional hyperplane generated by the PDE is:

$$y = a_0 x_0 + a_1 x_1 + a_2 x_2 + a_3 x_3 + a_4 x_4 + a_5 x_5 \tag{3.20}$$

where y is the scalar output of the PDE, which reduces to a fifth order polynomial in the two dimensional space formed by w and y:

$$y = a_0 + a_1 w + a_2 w^2 + a_3 w^3 + a_4 w^4 + a_5 w^5 \qquad (3.21)$$

Higher dimensional surfaces can be obtained by forming the input vector **x** from the terms of a multi dimensional power series, e. g.

$$\begin{aligned} x_o &= 1 \\ x_1 &= w \\ x_2 &= z \\ x_3 &= w^2 \\ x_4 &= z^2 \\ x_5 &= wz \\ x_6 &= w^3 \\ x_7 &= z^3 \\ x_8 &= wz^2 \\ x_9 &= w^2 z \end{aligned} \qquad (3.22)$$

As many terms may be included as are needed to fit the event points to the accuracy desired.

The advantage in using linear combinations of the components of the input vector lies in the simplicity of the required identification scheme. The identification scheme described in the next chapter can be used to determine the coefficient vector, a, for input vectors of considerable length.

3.3.3 Non-linear PDE's

To represent a three dimensional surface with the PDE requires the terms shown in equation 3.22. The formation of the input vector would require a large number of multiplications. It is not reasonable to presume that the human operator carries out all of this arithmetic.

The operator may be capable of pattern recognition or some other complex process which would require a high order hypersurface in the PDE. This difficulty, resulting from the structure of the PDE, may be overcome by allow-ing models in which the coefficient vector, a, enters non-linearly. For example,

$$y = (a'x)^{\alpha} \qquad (3.23)$$

w-here the vector a and the scalar α are to be determined. The advantage in the non-linear PDE is that complex surfaces can be generated in the state space of the system without introducing a large number of non-linear elements into the model. Such a PDE is shown in Figure 3.7.

Only one non-linear element is required. The disadvantage is that the identification is much more difficult and the resultant coefficients need not be unique or even the best available, as their

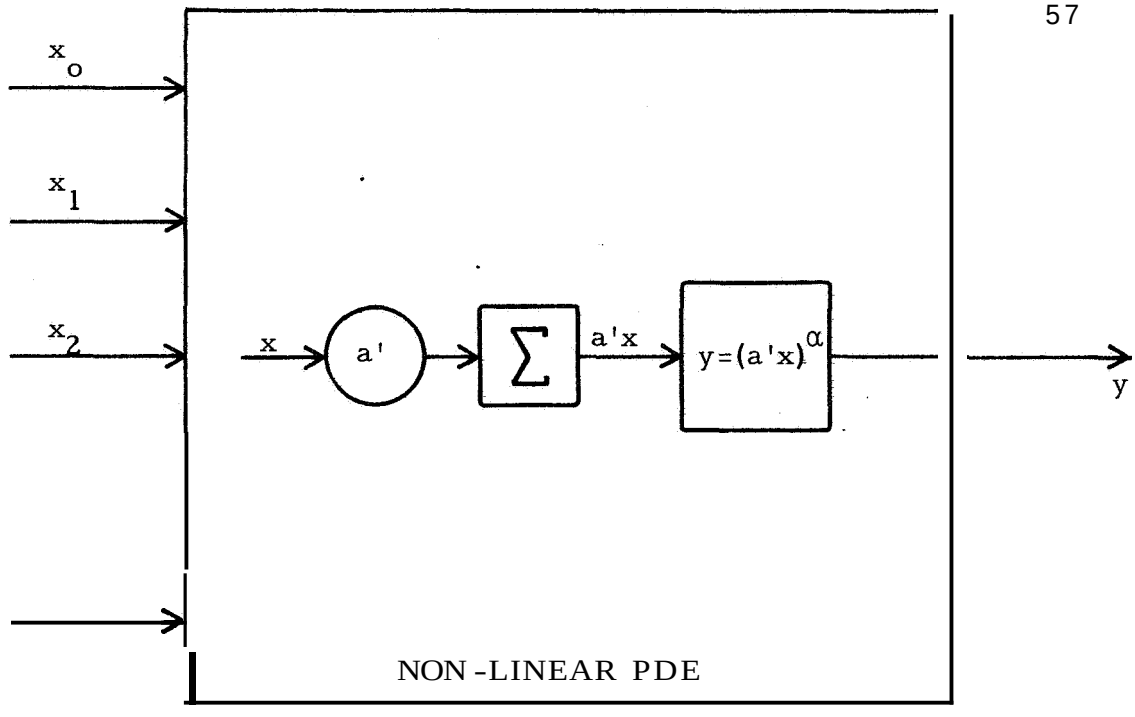

Figure 3.7 A Non-Linear PDE

computation depends on search procedures rather than direct computation.

Once a linear PDE has been identified, snother identification procedure could be used to fit the surface w-ith a non-linear PDE. For most human operator modeling, the linear PDE is sufficient and no attempt will be made here to identify non-linear PDE's.

CHAPTER 4

IDENTIFICATION TECHNIQUES

4. 1 Introduction

This chapter presents identification techniques applicable to general purpose digital or hybrid computers. The procedures are easily prepared as standard programs which might encourage the utilization of the block structured PDE and **MSDE** elements to describe human operator behavior.

4. 2 Identification Of The PDE

The equations defining the PDE were presented in the previous chapter. They were

$$x^* = x(t) \Big| \bar{C} \tag{4.1}$$

where x^* is an r vector the components of which are the values of x(t) at the time $\bar{C}$ becomes true, The PDE may generate two outputs:

$$y_1 = a' x^* \tag{4.2}$$

and

$$y_2 = e^{-\tau s}(a' x^*) \tag{4.3}$$

where y_1 and y_2 are scalars, a is an r vector of unknown coefficients, and τ is an unknown time delay.

It is assumed in the following that the input vector has been selected and that all of the components of the input vector are known functions of time,

The identification of a model is accomplished by adjusting the parameters of the model until a criterion function is minimized. The procedure is shown schematically in Figure 4. 1. It is assumed that the time histories of the r components of the input vector are known. The actual outputs $z(t_i)$ must be known, as well as the times at which the new- values appeared, t_i, i = 1, 2, --N. The binary control signal $\overline{C}$ is assumed to be known. The criterion function corresponding to particular values of a and τ may be computed. The next section describes the parameter selection algorithm.

4.2. 1 The Identification Algorithm

The values of $z(t_i)$ and times at which they appear, t_i, must be known. For convenience define $\underset{\Lambda}{z}$ to be a vector the components of which are the N discrete values:

$$\underset{\Lambda}{z} = (z(t_1),\ z(t_2) \ldots z(t_n)) \qquad (4.4)$$

Similarly, let $\underset{\Lambda}{y}$ be an N vector, the components of w-hich are the N discrete outputs of the model. Assume that the process being modeled is such that τ = 0, i.e. the output and sampling operation

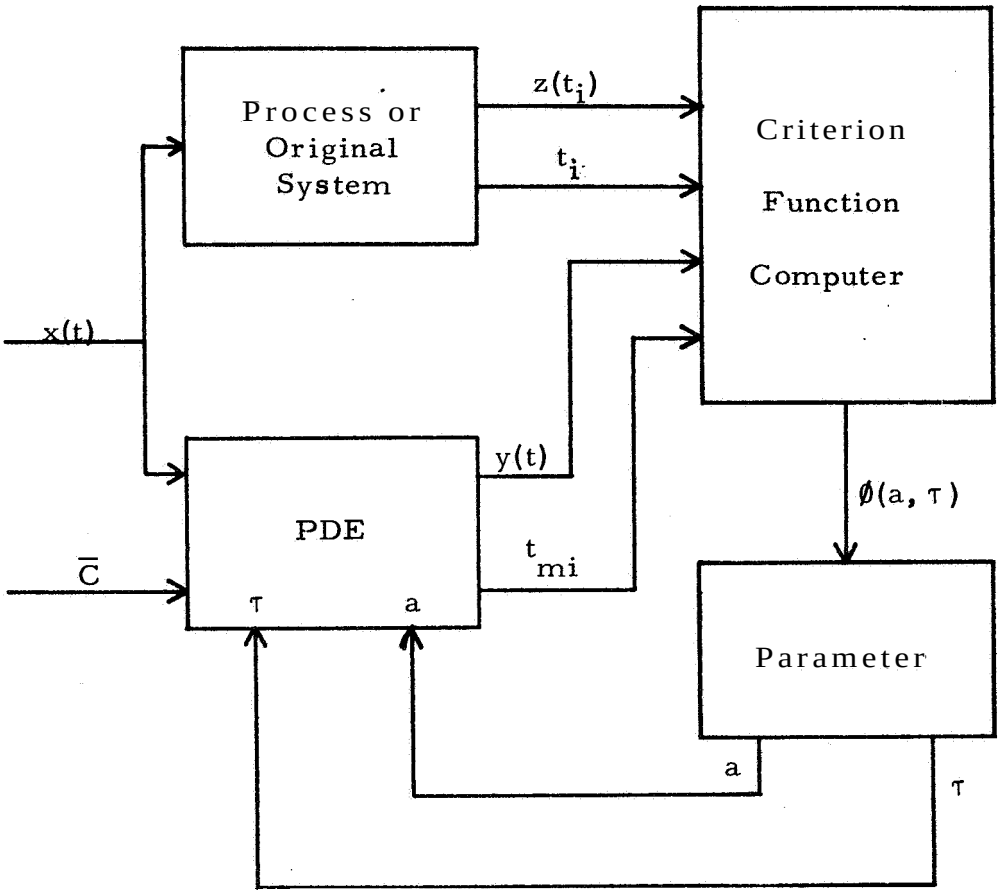

Figure 4.1 The PDE Identification Problem

are simultaneous. This restriction will be removed later. The model output may be written as:

$$\hat{y} = X^* a \tag{4.5}$$

where X^* is an Nxr matrix, the i-th row of which is the transpose of the sampled input vector x^* at the time t_i:

$$X^* = \begin{Vmatrix} x_0(t_1) & x_1(t_1) & x_2(t_1) & \cdots & x_r(t_1) \\ x_0(t_2) & x_1(t_2) & x_2(t_2) & \cdots & x_r(t_2) \\ x_0(t_N) & x_1(t_N) & x_2(t_N) & \cdots & x_r(t_N) \end{Vmatrix} \qquad (4.6)$$

or

$$X^* = \begin{bmatrix} x'(t_1) \\ x'(t_2) \\ \vdots \\ x'(t_N) \end{bmatrix} \qquad (4.7)$$

a model error vector may be defined as

$$E = \hat{z} - \hat{y} \qquad (4.8)$$

and a suitable criterion function is:

$$\phi = E' E \qquad (4.9)$$

from equation 4. 8

$$\phi = (\hat{z} - \hat{y})' (\hat{z} - \hat{y}) \qquad (4.10)$$

and substituting for $\hat{y}$ from equation 4. 5

$$\phi = (\hat{z} - X^* a)' (\hat{z} - X^* a) \qquad (4.11)$$

multiplying out

$$\phi = \hat{z}' \hat{z} - a' X^{*\prime} z - z X^{*} a + a' X^{*\prime} X^{*} a \qquad (4.11)$$

since ϕ is a scalar, each term of this equation is also a scalar. By symmetry

$$a' X^{*\prime} \hat{z} = \hat{z}' X^{*} a \qquad (4.12)$$

Thus ϕ may be written as

$$\phi = z' z - 2a' X^{*\prime} z + a' X^{*\prime} X^{*} a \qquad (4.13)$$

The model error vector is minimized by minimizing the scalar criterion function. Since ϕ is quadratic in the parameter vector, a, it is unimodal and by construction, its stationary point is a minimum. The gradient of ϕ is

$$\nabla_a \phi = -2X^{*\prime} \hat{z} + 2 X^{*\prime} X^{*} a \qquad (4.14)$$

The stationary point of ϕ is obtained from

$$\nabla_a \phi = 0 \qquad (4.15)$$

which yields

$$X^{*\prime} X^{*} a = X^{*\prime} \hat{z} \qquad (4.16)$$

finally, solving for the parameter vector a:

$$a = [X^{*\prime} X^{*}]^{-1} X^{*\prime} \hat{z} \tag{4.17}$$

where $[\,]^{-1}$ indicates matrix inversion.

If

$$\det [X^{*\prime} X^{*}] \neq 0 \tag{4.18}$$

then the parameter vector, a, which results is unique. Since the criterion function was based on the squared model error, the parameter vector, a, minimizes the sum of the squared errors.

The optimization procedure developed above is equivalent to least squares regression. Since the coefficients, a, enter linearly, the identification may also be viewed as the solution of an over-specified set of simultaneous equations

$$\hat{z} = X^{*} a \tag{4.19}$$

which results in N equations in r unknowns.

4.2.2 Interpretation Of Results And Graphical Aids

The PDE may be viewed as a multi-dimensional function generator. If the input vector is formed by algebraic operations on two signals, say $q_1(t)$ and $q_2(t)$, then the N event points $(z(t_i), q_1(t_i), q_2(t_i))$ may be plotted. The model event points generated by the PDE $(y(t_i), q_1(t_i), q_2(t_i))$ may be plotted on the same

co-ordinate system, or the surface generated by the PDE can be obtained by systemmatically applying values of q_1 and q_2 to the PDE.

Two dimensional plots of this type are easily obtained. With suitable mechanical aids, three dimensional plots can be made. By viewing these plots, one can locate areas of poor model performance or gain insight into the original process being modeled. In the former case, the input vector can be modified and a new computational cycle carried out.

Beyond three dimensions the plotting process becomes laborious. In these cases, some other form of graphical aid is necessary.

The numerical value of the criterion function may be used to measure the effectiveness of different input vectors. The same information may be presented in a two dimensional plot of $\hat{y}(a_{optimal})$ against $\hat{z}$. If the model were perfect the criterion function, ϕ would be zero and the points $(\hat{y}(a_{optimal}), \hat{z})$ would line on a straight line of unity slope. Systematic model errors w-ill appear as groups of points off this straight line. In many cases the necessary additions to or modification of the input vector can be determined from the $\hat{y}$, $\hat{z}$ plot.

The procedure developed above can be mechanized on any general purpose digital computer. The memory size of the computer places constraints on the dimensionality of the arays, in particular X^*. With even moderate size computers (i.e., the IBM 1620, 1401) it is possible to handle 70 equations in 5 unknowns. If large digital processors are available, the number of equations and unknow-ns that may be treated are practically unlimited. The advantages of computers w-ith graphical display equipment and on line operating systems are obvious.

4. 2. 3 Extension Of the Algorithm To Include The Identification Of Time Delay

In the previous discussion it was assumed the input vector $x(t)$ was sampled at the same time the output appeared in the original system, i. e. at t_i. This is not always the case and this restriction must be removed. In some situations it is possible to determine when the sampling occurred in the original system. If this is the case, then two times t_{si} and t_i may be determined for each of the N output events. The times t_{si} are the times at w-hich the sampling occurred and equation 4. 1 may be redefined as

$$x^* = x(t_{si}) \qquad i = 1, 2, \ldots N \tag{4.20}$$

The identification is carried out by the procedure described above. The output of the function generator portion of the PDE does not appear at the output of the PDE until time t_i. If there is a constant, or almost constant delay between t_{si} and t_i, then a second control signal is unnecessary, and a time delay of magniture τ may be used where

$$\tau = \frac{1}{N} \sum_{1=1}^{N} (t_i - t_{si}) \qquad (4.21)$$

The availability of the sample time, t_{si}, makes this case very similar to that already considered.

A more common situation is one in which the time, t_i, is available and t_{si} is not. The time at w-hich the input vector w-as sampled must be inferred indirectly from the data available: $x(t)$, $z(t_i)$ and the t_i. If the input vector is at all representative of the decision process utilized by the operator, then the model will yield optimum results when the input vector at time $t_i - \tau$ is used. Thus if

$$x^* = x(t_i - \tau) \qquad (4.22)$$

and τ is studied systematically, the value which produces the minimum value of the criterion function is the optimal τ. The resultant value of τ will depend on the particular components of the input vector.

The PDE has been identified by assuming that the time t_i or, in the last case, $t_i - \tau$ is available in the form of a binary control signal $\bar{C}(t)$ which goes from false to true at the time t_i or $t_i - \tau$. If this signal is not available in the model, then it must be generated by a binary MSDE. The inputs to the MSDE may be the same as those used in the PDE, or may include other signals relevant to the decision, which were not relevant to the magnitude of the PDE event. The desired output of the MSDE is the binary signal $\bar{C}(t)$ of the form just described.

This procedure uncouples the identification, in that the magnitude model and the time delay are determined first and the control element last. Procedures to identify both simultaneously would be excessively complex.

4.2.4 Stochastic Properties Of The PDE

Once the identification procedure has been completed, a model remnant vector can be defined

$$E_R = \hat{z} - \hat{y}(a_{opt}, \tau_{opt}) \qquad (4.23)$$

A non-zero remnant results from short term time variations in the process being modeled, random perturbations of the process, noise corruption of the measured signals, and finally model

inadequacies. If it is felt that the model is adequate, then the remnant is a measure of the stochastic processes in the original system. The distribution function of the N components of the remnant vector is easily computed, as are its mean and higher moments. The identification procedure above, is such that the mean is zero. The moments may be useful as measures of performance, state of operator training, etc. Alternatively, noise with the same characteristics could be added to the model output to produce a stochastic human operator model.

It is not feasible here to determine whether the remnant is functionally dependent on the observable signals in the process being modeled or stochastic in origin.

4. 2. 5 Partitioning Of The Input Space

Another aspect of the identification procedure is that it is possible to perform the identification separately in various regions of the space formed by the input vector and the output y.

If the output of the PDE represents arm motion of a human operator, the modeling may be performed for positive arm motions and negative arm motions separately. It is then possible to investigate asymmetric control actions by comparing the two models.

As another example, assume that the input vector to a PDE is formed from error signals presented to a human operator. By modeling the control action resulting from event points inside a hypersphere of radius R separately from those outside, it is possible to study the effects of error amplitude on the operator's response.

4.3 Identification Of The MSDE

The MSDE was designed to mechanize a concept that is easily interpreted geometrically. A priori know-ledge is used to hypothesize a trial structure of decision surfaces, constructed from hyperplanes. Working backward from the hypothesized decision surfaces, the components of the input vector are selected. The space formed by linear combinations of the components of the input vector x(t) is called the input space. The input vector, x(t), is composed of time varying signals. The path traced out by the input vector in the input space is called the event trajectory. When the event trajectory crosses a decision surface the output vector of the MSDE is changed.

The output of the MSDE w-as given in equation 3.1 and shown schematically in Figure 3.1, as

$$\overline{h}(t) = \overline{B}(T\lfloor A\ x\ (t)\rfloor) \tag{4.24}$$

where x(t) is an n vector of input signals, A is an m x n matrix of

arbitrary real coefficients, T is a vector threshold operator action on the m vector Ax such that the components of T(Ax) say T_i are defined by

$$T_i = \begin{cases} 1 & \text{if } (a_{i0}x_0 + a_{i1}x_1 + \ldots + a_{in}x_n) > 0 \\ 0 & \text{if } (a_{io}x_o + a_{il}x_1 + \ldots + a_{in}x_n) \leq 0 \end{cases} \qquad i = 1,2,\ldots m \qquad (4.25)$$

$\bar{B}$ (T) is a **p** vector of boolean functions of the vector T.

$\bar{h}$ is a p vector of binary outputs.

It is assumed that the state of the process being modeled is known, and is denoted by

$$\bar{k}(t)$$

where $\bar{k}$ (t) is a p vector of binary states. The identification of the model is carried out by adjusting the parameter matrix, **A,** until $\bar{h}$ (t) and $\bar{k}$ (t) are identical. The model achieves this **by** producing outputs w-hich are of the proper state and which appear at the correct times. The concept of matching $\bar{h}$ (t) and $\bar{k}$ (t) must be formalized by defining a suitable criterion function.

4. 3. 1 Selection Of **A** Criterion Function For The Identification Of The MSDE

An error function is defined which assigns numerical values to the various ways in which $\bar{h}$ and $\bar{k}$ can occur:

$$E\ (\bar{h}(t),\ \bar{k}(t)\ )$$

If the two states are identical, then E is zero. Various magnitudes are assigned to the possible errors depending on their physical significance.

From the error function, a criterion function can be defined, as

$$\phi\ (A) = \int_{o}^{t_m} E(\bar{h}(t),\ \bar{k}(t))\ dt \qquad (4.26)$$

where t_m is the length of the record $\bar{k}$ (t). ϕ (A) measured the difference between two time varying binary vectors. This alone is not enough to measure the performance of the model. Consider the example of Figure 4.2.

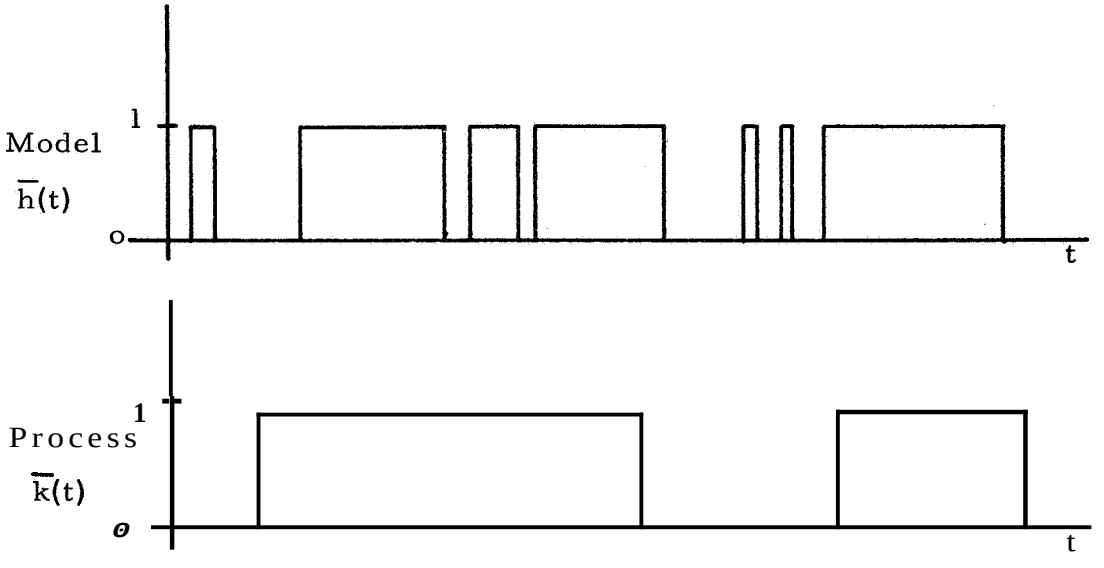

Figure 4.2 Extraneous Model Outputs

As seen from Figure 4.2, the criterion function may be small, without eliminating a large number of extraneous outputs, which because of their short durations, do not significantly affect the value of ϕ. To prevent this, the state change occurring nearest the state change of $\bar{k}$ is arbitrarily called the i^{th} model response. All other responses are false responses and are counted. Let M be the total number of false responses. The augmented criterion function is

$$\phi = K_1 \int_{o}^{t_m} E(\bar{h}, \bar{k})\, dt + K_2 M \qquad (4.27)$$

where K_1 and K_2 are weighting factors.

If the model is required to lead the process by a time τ, then the criterion function must be modified:

$$\phi = K_1 \int_{o}^{t_m} E(e^{-\tau s}\, \bar{h}, \bar{k})\, dt + K_2 M \qquad (4.28)$$

If τ is set to zero, this reduces to the previous case.

4.3.2 The Parameter Adjustment Algorithm

If an initial set of coefficients, A^*, is known, then the criterion function may be evaluated:

$$\phi(A^*) = \phi(a^*_{11}, a^*_{12}, \ldots, a^*_{mn}) \qquad (4.29)$$

If the parameters are incremented and decremented by a fixed

amount A, one at a time, then 2 (n m) values of ϕ are computed. Suppose decrementing one parameter, a_{ij}, by A produces the minimum value of ϕ. A new parameter matrix can be defined by

$$A^*_{new} = (a^*_{11}, a^*_{12}, \ldots, a_{ij} - \Delta, \ldots, a^*_{mn}) \quad (4.30)$$

The process is repeated until none of the trial parameter matrices produce a lower value of ϕ. The value of A can be doubled or halved and the search attemped again. If a better value of ϕ is found, A is returned to its original magnitude and the search resumed. If a better value is not found A is modified again, until A reaches a pre-set limit, at which time the search algorithm is terminated.

The threshold element selected has a useful property

$$T(KAx) = T(Ax) \quad (4.31)$$

if K is a positive non-zero scalar constant. This property makes it possible to normalize the A matrix a row at a time.

If this is done at each step, or periodically, the range of the elements of the parameter matrix is restricted to

$$|a_{ij}| \leq 1 \quad (4.32)$$

The adjustment increment, Δ, may be selected as 10% or 1% of full scale, depending on the particular problem.

4. 3. 3 Selection Of Starting Values

The problem of selecting starting values for the parameter matrix , **A,** is not easily solved. **A** priori knowledge concerning the most likely positions of decision surface leads to the best estimates. **If** a priori knowledge is not available, then random search is used. **A** random number generator is used to produce a large number of parameter matrices. The value of ϕ is computed for each matrix and the best ones used as starting conditions for the search algorithm.

CHAPTER 5

AN ASYNCHRONOUS PULSE-AMPLITUDE PULSE-WIDTH MODEL OF THE HUMAN OPERATOR

5. 1 A Discrete Control Experiment

When the dynamics of a controlled element contain two or more integrations, the performance of the human operator approaches that of a bang-bang system. In particular, a pure inertia (two integrations) usually elicits pulse responses from human operators [14,11]. A mathematical model to represent this output behavior could contain sampled inputs with continuous supervisory control of the sampling. This supervised sampling extends the periodic sampling of previous models [2,3] to aperiodic input-dependent sampling. The pulse nature of the output makes it possible to relate pulse events to decision surfaces in the error phase space [30].

The object of this chapter is to describe the development of a human operator model which produces discrete outputs in response to continuously presented gaussian random inputs. Computer procedures for the complete identification of all model parameters are described.

5.2 Statement Of The Problem

A block diagram of the compensatory tracking situation used in this study is shown in Figure 5. 1 and a portion of a typical tracking record is found in Figure 5.2. An examination of the human operator output (stick position) reveals a sequence of pulses w-hich are roughly triangular in shape. For the purposes of this study the actual human operator output was converted to the idealized human operator output, as seen in Figure 5.2. The selection of symmetric triangular pulses as ideal human operator pulses is arbitrary, and other pulse shapes can be used. Further it was decided to treat each pulse as a separate event, uncorrelated with previous pulses, in order to keep the structure of the pulse model as simple as possible. The use of ore-programmed pulse sequences [2,1] presents an opportunity for future extensions of the work.

The idealized human operator output can be represented by a sequence of three-tuples: time of the pulse initiation, pulse amplitude, and nulse width. If a causal relationship exists between the transient human operator inputs and the pulse outputs, then the input record can be reduced to samples of the input in the vicinity of the pulse initiation. The objective of the present study is the determination of the relationships between these input samples and the pulse output.

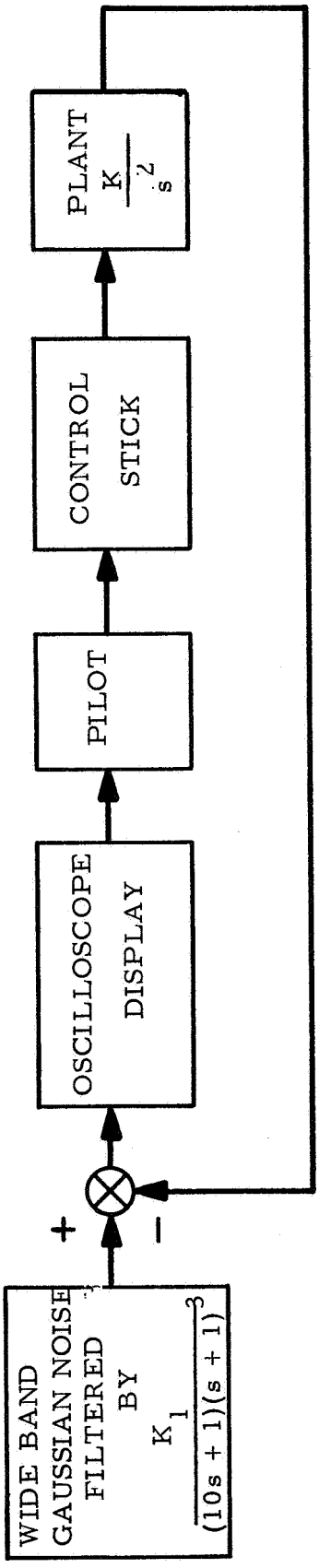

FIGURE 5.1 - Compensatory Tracking System

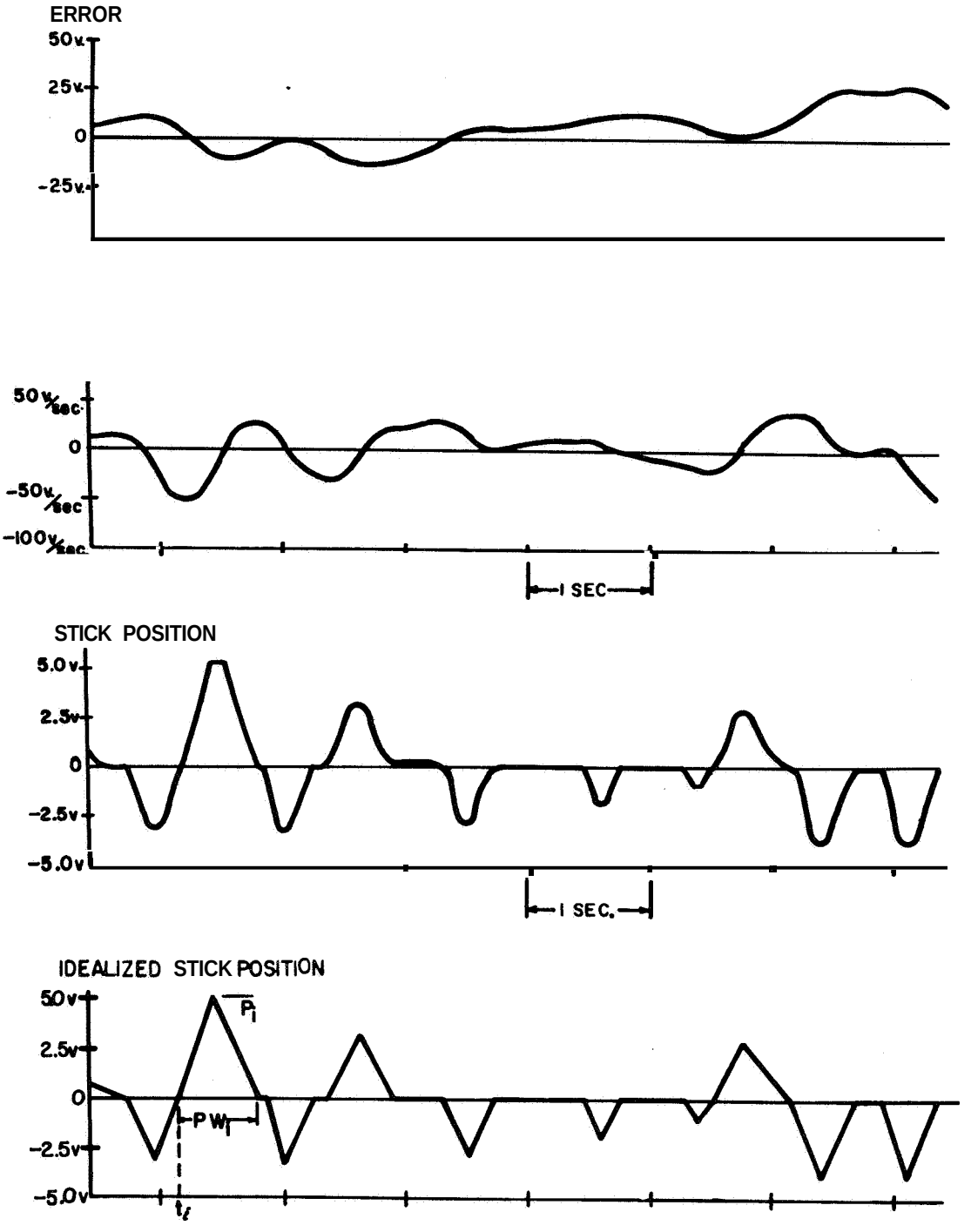

FIGURE 5.2 TYPICAL TRACKING RECORD

Since each event is treated independently, short term human operator variations aye easily computed. These variations are the difference between the model outputs and the actual human operator outputs. The distribution functions of these variations can be obtained and, if desired, can be reinserted as model perturbations. The distribution functions and their associated parameters (mean and moments) can be used as measures of performance and state of training.

5.3 The Experiment

The compensatory tracking task shown in Figure 5.1 was mechanized using an analog computer, an X-Y oscilloscope and side arm control stick. Operator distraction was minimized by placing the manual control station inside a sound proof enclosure with approximately 40 db of audio attenuation. The operator wore an aircraft type headset with lip microphone for communication purposes. The operator sat in achairwithout armrests facing the display oscilloscope. The control stick was adjustable in position and contained an integral arm rest. The operator adjusted the control stick and arm rest into a comfortable position. The oscilloscope was placed at eye level.

The double integrator plant closely resembles an aircraft pitch axis. The input is elevator position and the output is altitude.

In order to preserve this resemblance, the error display was a rotating needle corresponding to a glide path indicator in an aircraft navigational /ILS display. Horizontal needle position represented zero error. The frequency response problems associated with actual instruments were avoided by simulating the glide slope needle with an oscilloscope containing a specially prepared edge lighted reticle.

The control stick and oscilloscope were connected to the analog computer which converted the stick output to a voltage, computed the plant response, and generated the necessary X and Y axis signals for the error display. By solving some of the equations explicitly it was possible to obtain the error and its exact derivative. The inputs to the system were obtained by filtering the output of a low-frequency gaussian noise source. The filter transfer function was:

$$F(s) = \frac{K}{(10s + 1)(s + 1)^3} \qquad (5.1)$$

An FM magnetic tape recorder was used to record tracking data, which was later digitized and stored on a disk file for digital processing.

A single subject received approximately 20 hours training over a period of one month. The training sessions consisted of 10 minutes of tracking with 10 minute rest periods. One of the last

sessions was recorded on magnetic tape, From the 10 minute session approximately 3 minutes of data was subsequently digitized. The sampling interval utilized was 25 milliseconds or 40 samples per second.

The digitized data stored on the disk file was printed out and punched on IBM cards for permanent storage. The following data was punched on IBM cards:

1. The time of the pulse initiation.
2. The time of the pulse termination.
3. The peak amplitude of the pulse.
4. The values of e and $\dot{e}$ at the following times:
    a. One sample after the initiation of the pulse
    b. At the start of the pulse
    c. The 5 samples prior to the start of the pulse

5.4 Hypothesized Human Operator Model

The input to the human operator is the error, $e(t)$. If it is assumed that the operator is capable of differentiating this display variable then $\dot{e}(t)$ is also an input to the operator. The operator's output is a pulsatile control action characterized by a time of pulse initiation, pulse amplitude and pulse width.

It is hypothesized that the pulse amplitude and pulse width were computed from samples of the error and error rate, and the decision to initiate a pulse is based on decision surfaces in the error phase space.

The resultant model structure is shown in Figure 5.3.

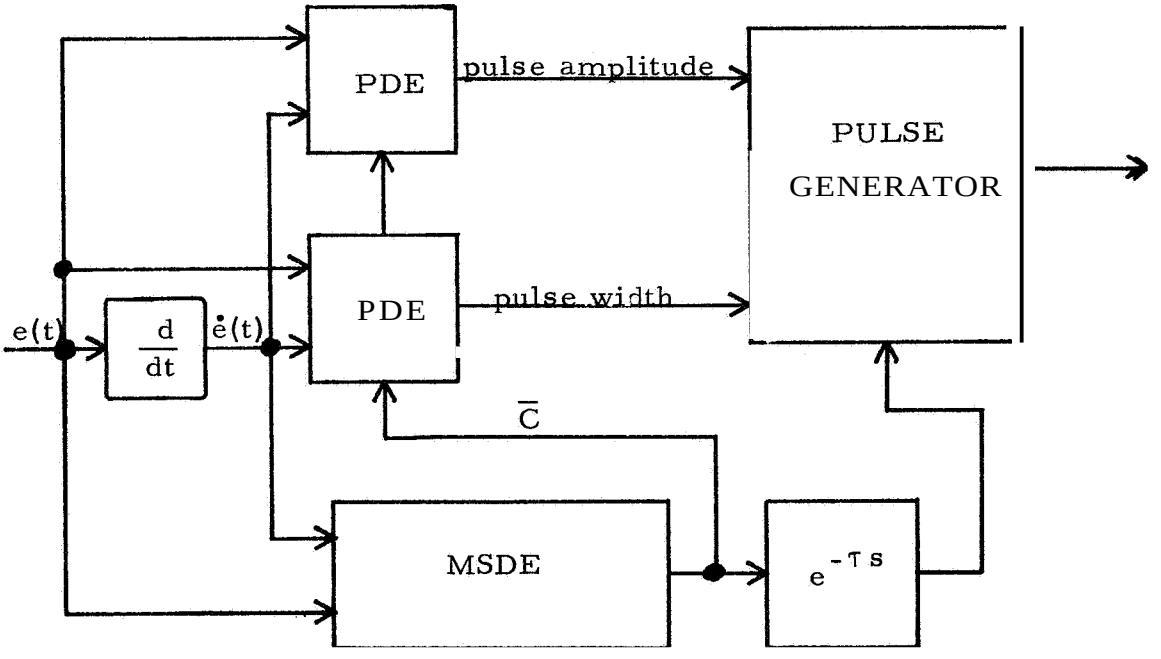

Figure 5.3 Hypothesized Human Operator Model

5. **4.** 1 Pulse Amplitude Model

The amount of pulse amplitude modulation utilized by the human operator is evidenced in the distribution function of the pulse

amplitude, seen in Figure 5.4. Further work is needed to evaluate the significance of the asymmetry in the distribution function.

The time of the pulse initiation is easily measured. This is an overt operator decision. Some time before this, the operator samples the error and error rate and computes the amplitude of the pulse. The process is easily modeled by a PDE, as shown in Figure 5.3.

The PDE's input vector was

$$\begin{aligned} x_o(t) &= 1 \\ x_1(t) &= e(t) \\ x_2(t) &= \dot{e}(t) \end{aligned} \tag{5.2}$$

The input vector is formed from the digitized signals available on punched cards. These cards contain samples of the error and error rate ranging from 0.125 before to 0.025 seconds after the actual pulse initiation. These samples may be viewed as leading the pulse initiation by τ seconds where τ varies between 0.125 and -0.025 seconds in steps of 0.025 seconds.

The resultant form of the PDE takes the form shown in Figure 5.5 where

$$*$$ (5.3)

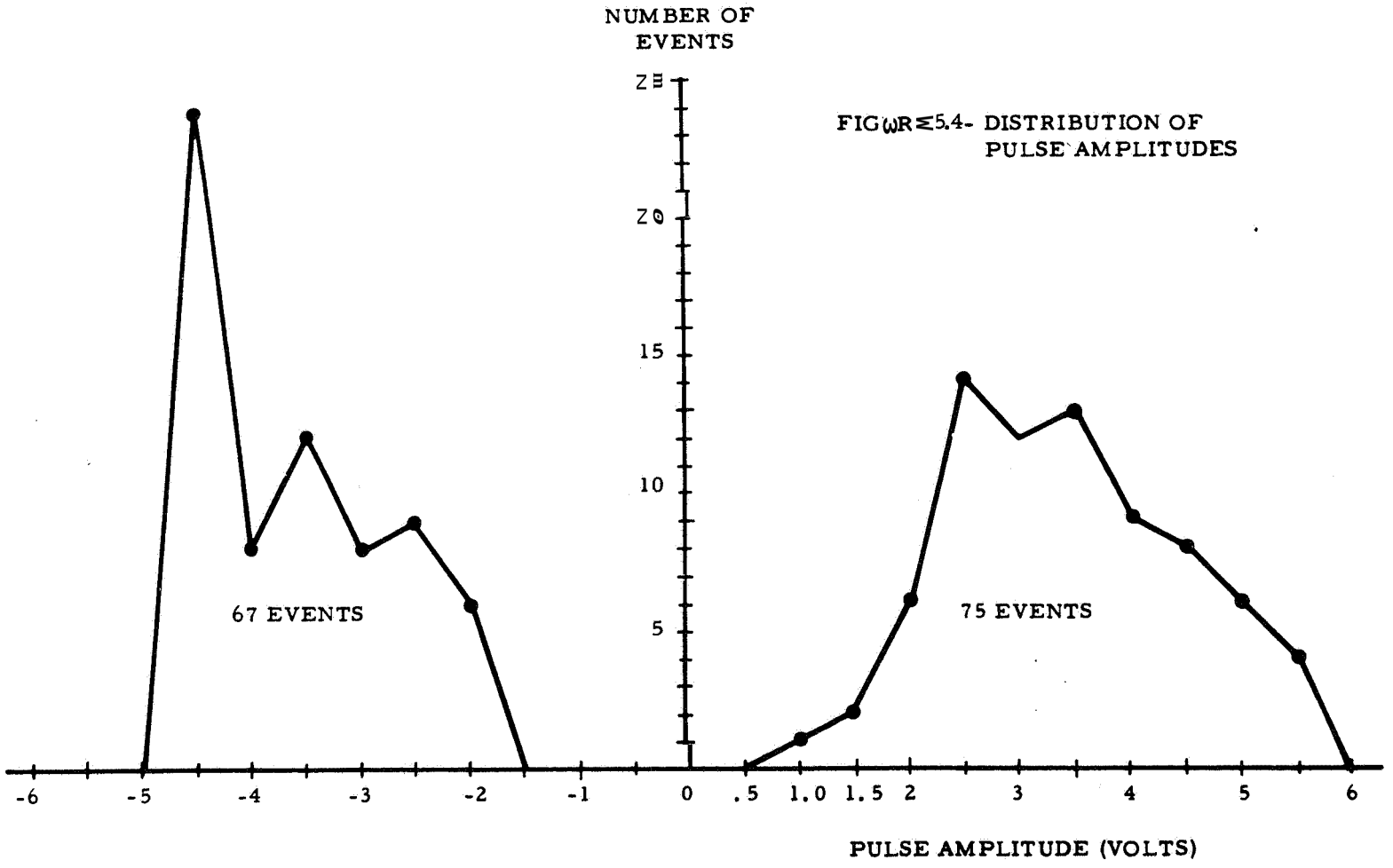

FIGURE 5.4- DISTRIBUTION OF PULSE AMPLITUDES

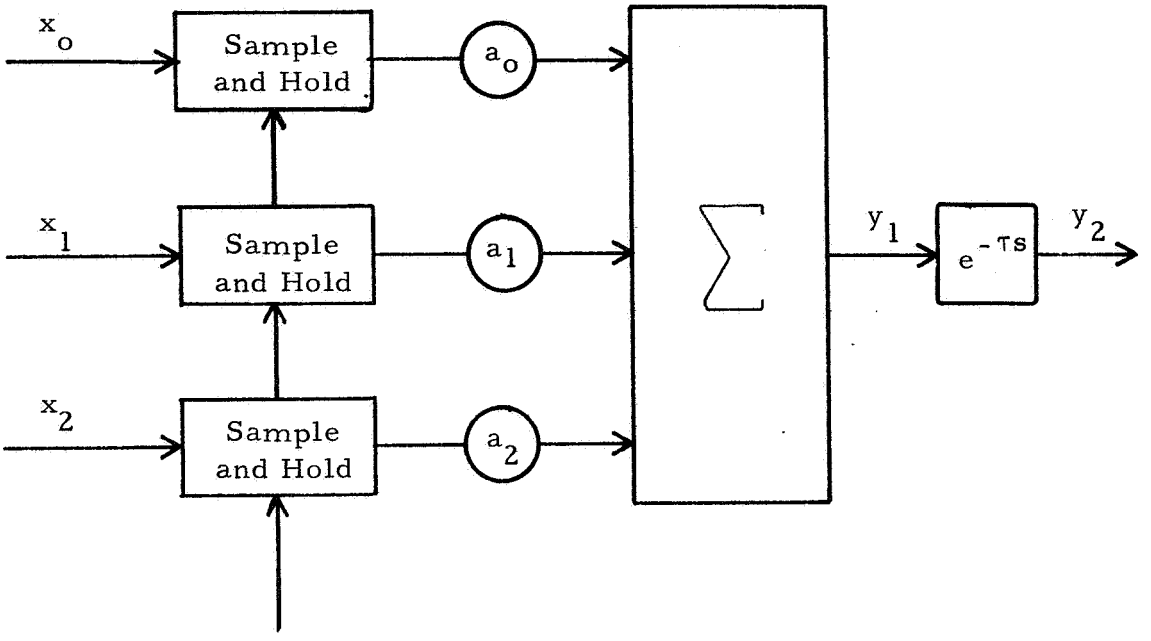

Figure 5. 5 Pulse Amplitude PDE

There were a total of 142 pulse events in the digitized record. Of these 75 were positive control pulses and 67 were negative control pulses. The space formed by $e(t)$, $\dot{e}(t)$ and p_i, the pulse amplitudes, was partitioned about the $p = 0$ plane and the identification procedure performed separately on positive and negative operator control actions. With this partition, it is possible to investigate possible asymmetry in operator control actions.

A digital computer program was written to carry out the identification procedure for **PDE's** derived in section 4.2. 1 and extended to include time delay in section 4. 2. 3.

The inputs to the program were the values of the input vector τ seconds before pulse initiation, where the range of τ was from 125 milliseconds before the pulse to 25 milliseconds after the pulse, in steps of 25 milliseconds. Also supplied were the actual pulse amplitudes, p_i, i = 1, 2, ...N. The computational results are tabulated in Table 5. 1.

TABLE 5.1

τ_1^*	a_1		a_2		a_3		$\phi \times 10^{-6}$	
Polarity	+	-	+	-	+	-	+	-
0.125	-0.060	-0.065	-0.139	-0.145	2.16	-2.02	0.507	0.220
0.100	-0.061	-0.066	-0.134	-0.143	2.16	-1.99	0.496	0.217
0.075	-0.062	-0.065	-0.130	-0.137	2.16	-2.00	0.495	0.222
0.050	-0.062	-0.064	-0.125	-0.131	2.16	-2.04	0.492	0.228
0.025	-0.059	-0.061	-0.118	-0.123	2.19	-2.10	0.498	0.242
0	-0.057	-0.060	-0.112	-0.116	2.22	-2.14	0.504	0.253
-0.025	-0.057	-0.060	-0.106	-0.108	2.25	-2.20	0.509	0.263

As can be seen from Table 5. 1, there is a well defined minimum value of the criterion function ϕ as τ is varied. A plot of the criterion function, ϕ versus τ is found in Figure 5.6. A plot of the pulse amplitudes generated by the optimal models versus the actual pulse amplitudes is found in Figure 5. 7. The points are quite close to the ideal unity slope line. The optimum values for positive and

FIGURE 5.6- CRITERION FUNCTION FOR PULSE AMPLITUDE MODEL Vs TIME DELAY (τ_1^*)

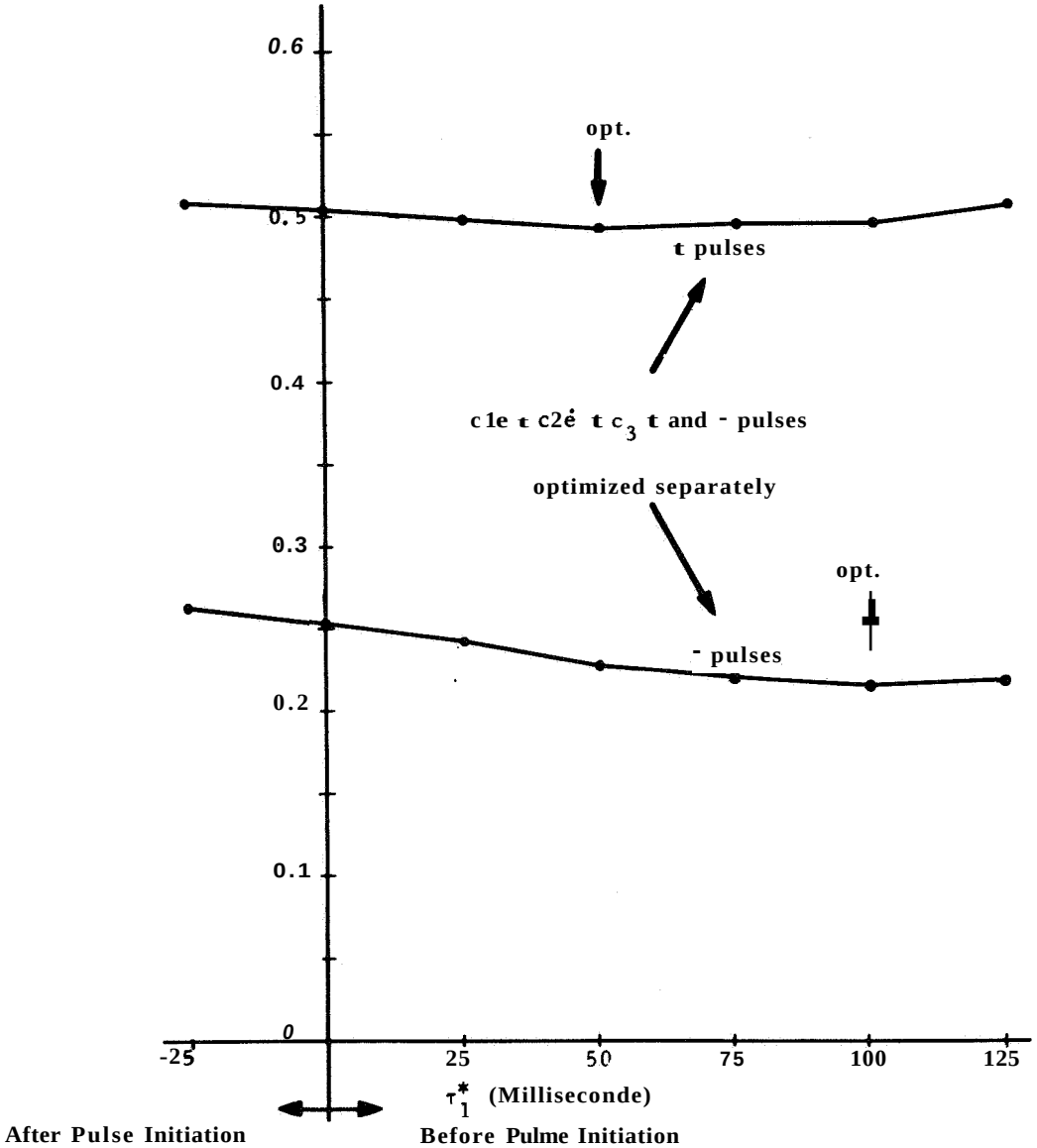

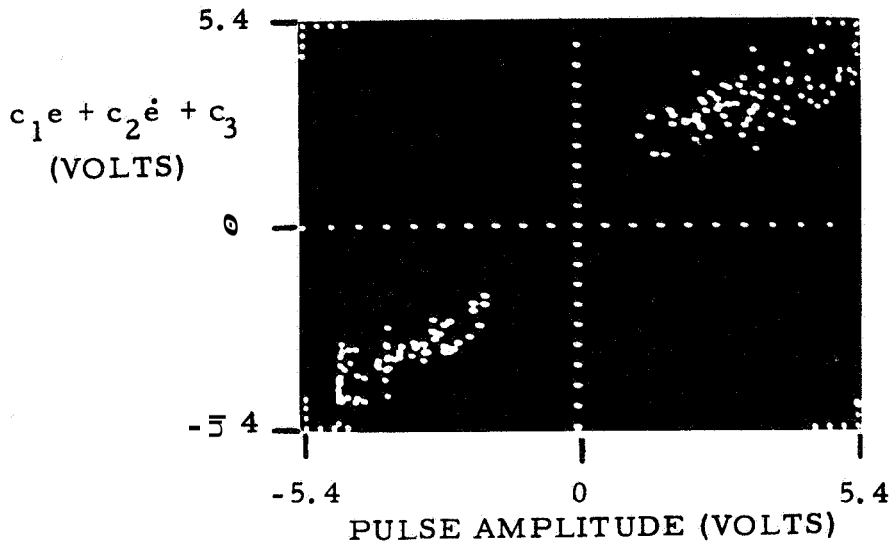

FIGURE 5.7- $c_1e + c_2\dot{e} + c_3$ Vs PULSE AMPLITUDE, POSITIVE AND NEGATIVE PULSES OPTIMIZED SEPARATELY

negative pulses, respectively are a_0 = 2. 16, -1. 99 volts; a_1 = -0. 062, -0.066; a_2 = -0.125, -0. 143; and τ = 0.050, 0. 100 seconds. The symmetry observed in these values contrasts with the large differences in the values of the optimum criterion function ϕ_t = 0.492 and ϕ_- = 0.217. In other words, the positive pulses produced poorer correlation with the actual pulse amplitudes than did the negative pulses. This is also seen in the scatter plot, Figure 5. 7, where the negative pulse events are closer to the ideal line than the positive pulse events. This may be a result of one or more of the following factors: arm motion asymmetry associated with the side arm control stick, incomplete training, or the tendency of the operator to prefer certain portions of the error phase plane.

In a recent experiment by Agarwal, [1] the effective inertia, spring constant, and damping coefficient of the human operator performing forearm control were measured. The results of their experiment are tabulated in Table 5.2.

TABLE 5.2

	Direction of Arm Rotation	
Parameter	Supination	Pronation
J	1.05×10^{-3}	$.4 \times 10^{-3}$
B	1.3×10^{-2}	$.5 \times 10^{-2}$
K	2.5	2.3

The asymmetry in these results tends to support the assumption that the large differences in the criterion functions are a property of side arm controllers resulting from the structure of the operator's neuromuscular system.

An analysis of the differences betw-een the human operator pulse amplitudes and the corresponding model pulse amplitudes serves two purposes. The fidelity of the model is tested and the distribution functions of the human operator variations may be determined. These distribution functions are found in Figure 5. 8 and their mean and standard deviation are found in Table 5.3.

TABLE 5.3

	Pulse Polarity	
	+	-
Mean (volts)	0	0
Standard Deviation (volts)	.80	.58

The sample signal $\bar{c}$ must be generated by an MSDE. The times at which the MSDE must change state may be computed from

$$t_{iM} = t_i - \tau_i \tag{5.4}$$

where t_i is the actual time of the pulse initiation, τ_i is the time delay appropriate to the i^{th} pulse event and t_{iM} is the time at which the MSDE muet change state.

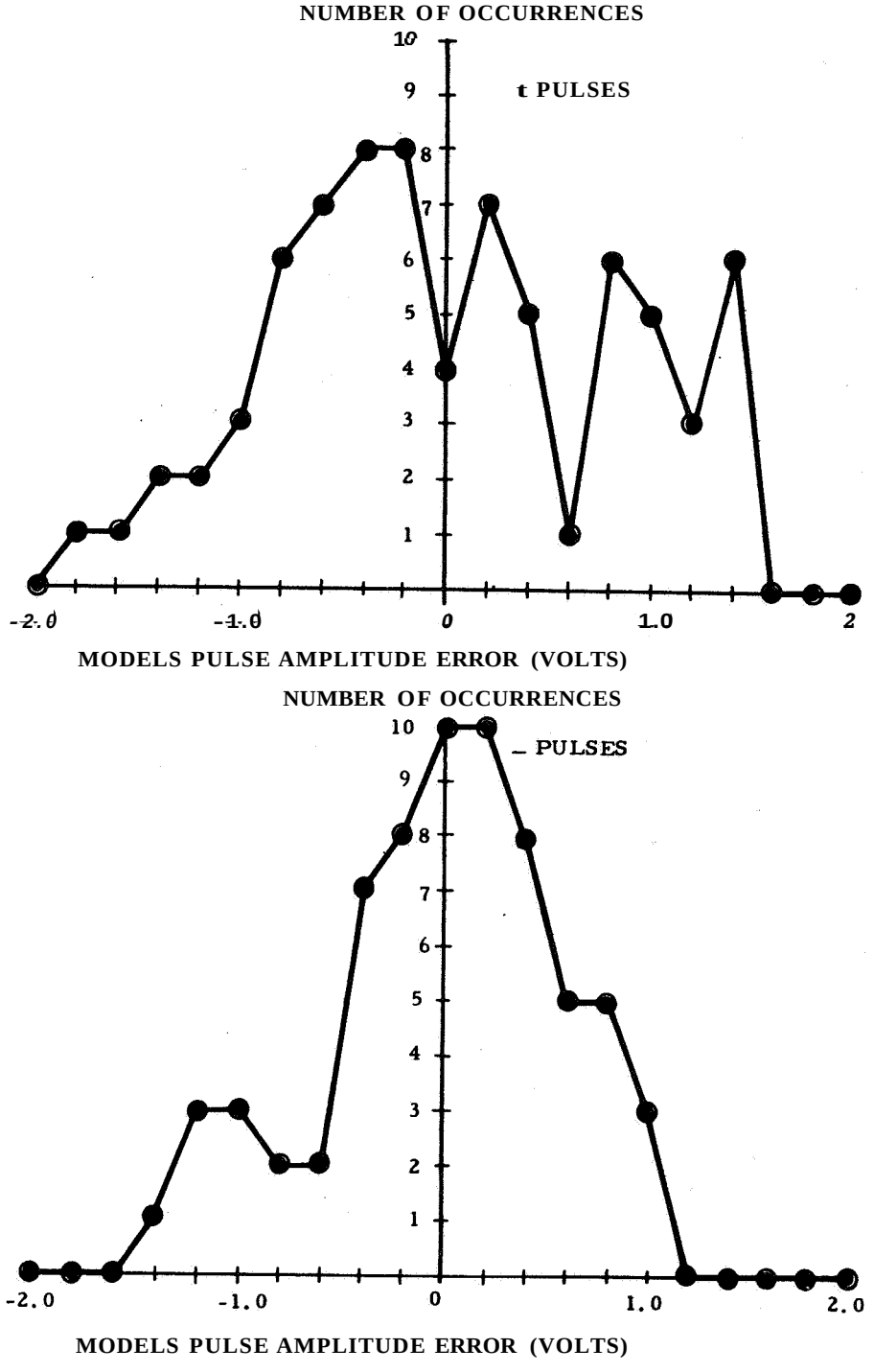

FIGURE 5.8- DISTRIBUTION FUNCTIONS OF MODEL PULSE AMPLITUDE ERRORS

5.4.2 Pulse Width Model

The pulse w-idth of a pulsatile event is easily generated by a PDE. It is assumed that the pulse width PDE is controlled by the same control signal as the pulse amplitude PDE. Preliminary analysis of the tracking records led to the hypothesis that the pulse width w-as proportional to pulse amplitude. This hypothesis leads to a particularly simple input vector

$$x_0 = 1$$
$$x_1 = PA_i \qquad i = 1, 2, \ldots N. \tag{5.5}$$

The resultant PDE is

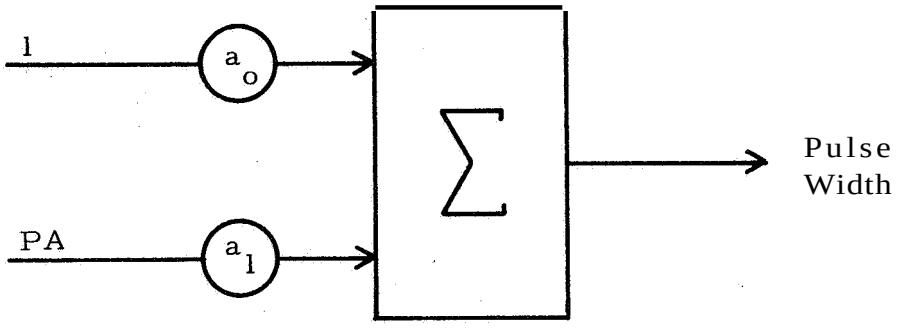

Figure 5.9 Pulse Width PDE

The pulse w-idth model falls into the category of modeling situations discussed in section 4.2.2. The input vector is of sufficiently low dimensionality, that the input-output relationship can be plotted. Such a plot is found in Figure 5.10 where the pulse width is

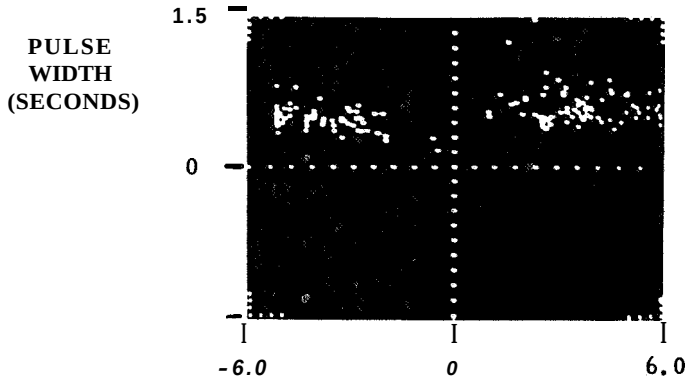

FIGURE 5.10 PULSE WIDTH Vs PULSE AMPLITUDE

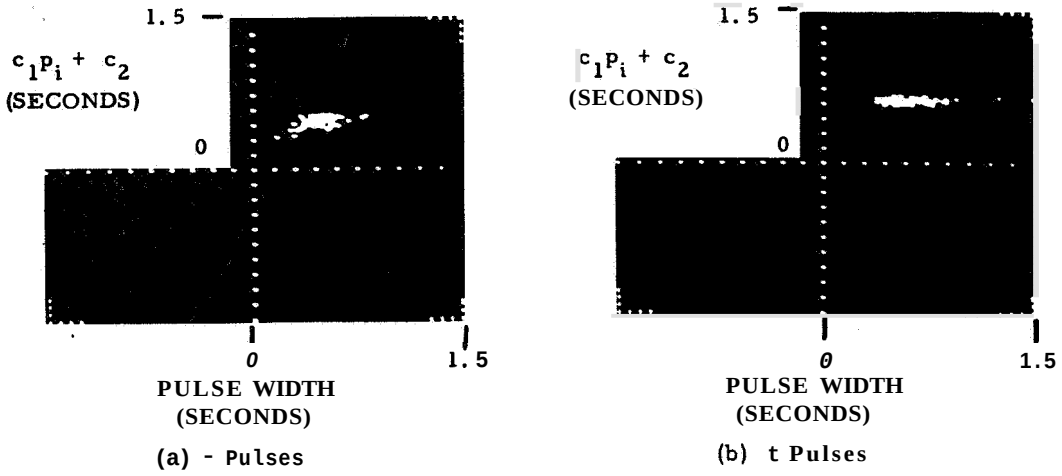

FIGURE 5.11 MODEL PULSE WIDTH Vs ACTUAL PULSE WIDTH

plotted against the pulse amplitude. The PDE fits the event points shown with a straight line. The best fit straight line appears to a horizontal line at the mean pulse width. The computational results are: a_0 = 0. 711, 0. 316, a_1 = -0. 021, -0. 049 for positive and negative pulses respectively. The coefficient associated with the pulse amplitude is small, indicating that the pulse w-idth is almost independent of pulse amplitude. A plot of the model pulse w-idth versus the actual pulse w-idth is found in Figure 5. 11. These plots are further evidence that the pulse width is not strongly dependent on pulse amplitude. The distribution functions of the difference between the actual pulse width and the model pulse w-idth is found in Figure 5. 12. The mean and standard deviation of these distribution functions are found in Table 5.4.

TABLE 5.4

	Polarity	
	+	-
Mean (sec.)	0	0
Standard Deviation (sec.)	0. 05	0. 04

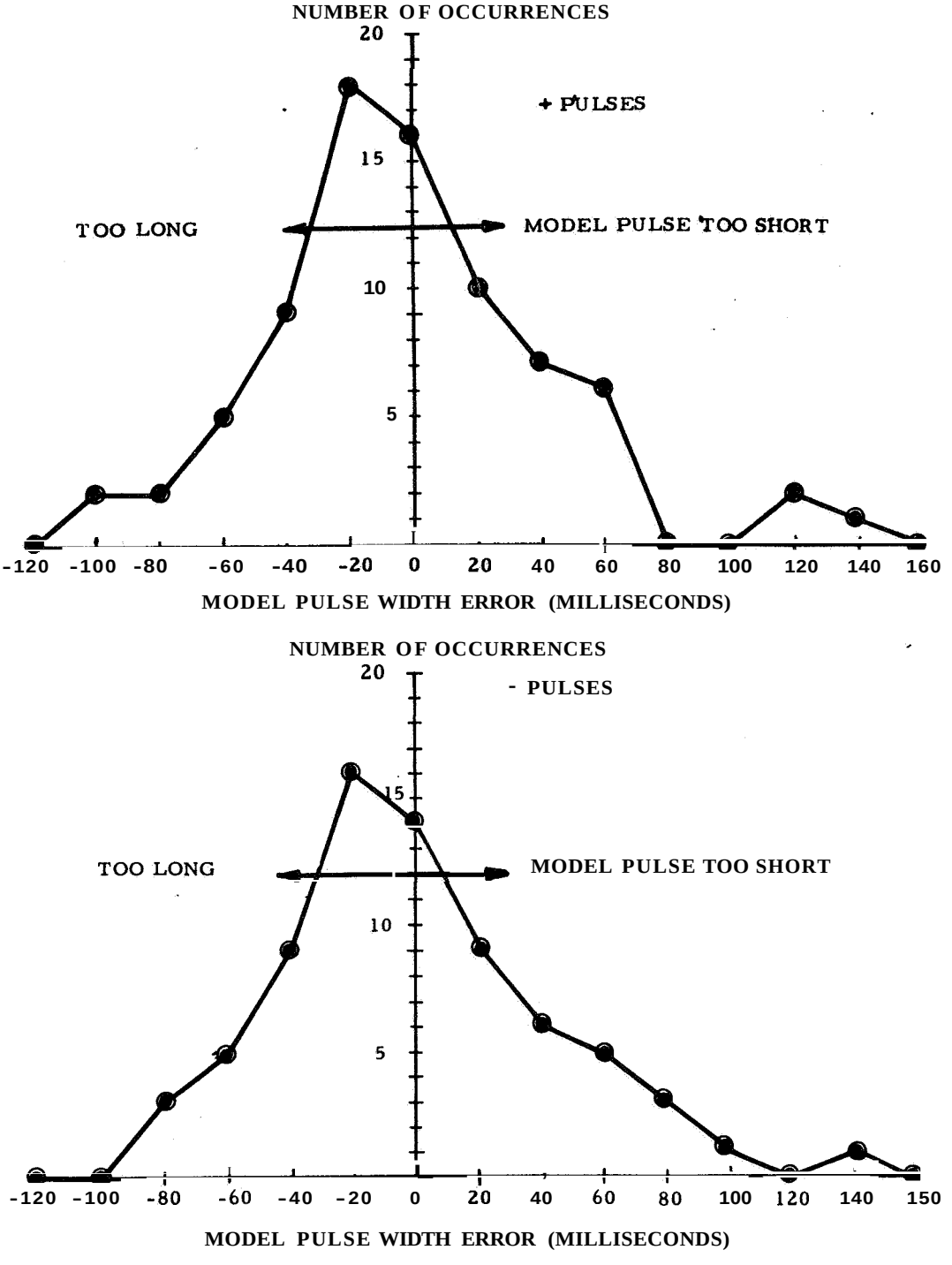

FIGURE 512- DISTRIBUTION FUNCTIONS OF MODEL PULSE WIDTH ERRORS

5.4.3 The Complete Pulse Amplitude - Pulse Width Model

If a binary control signal, $\bar{c}$, is assumed, then the complete pulse amplitude - pulse width model can be constructed as shown in Figure 5.13.

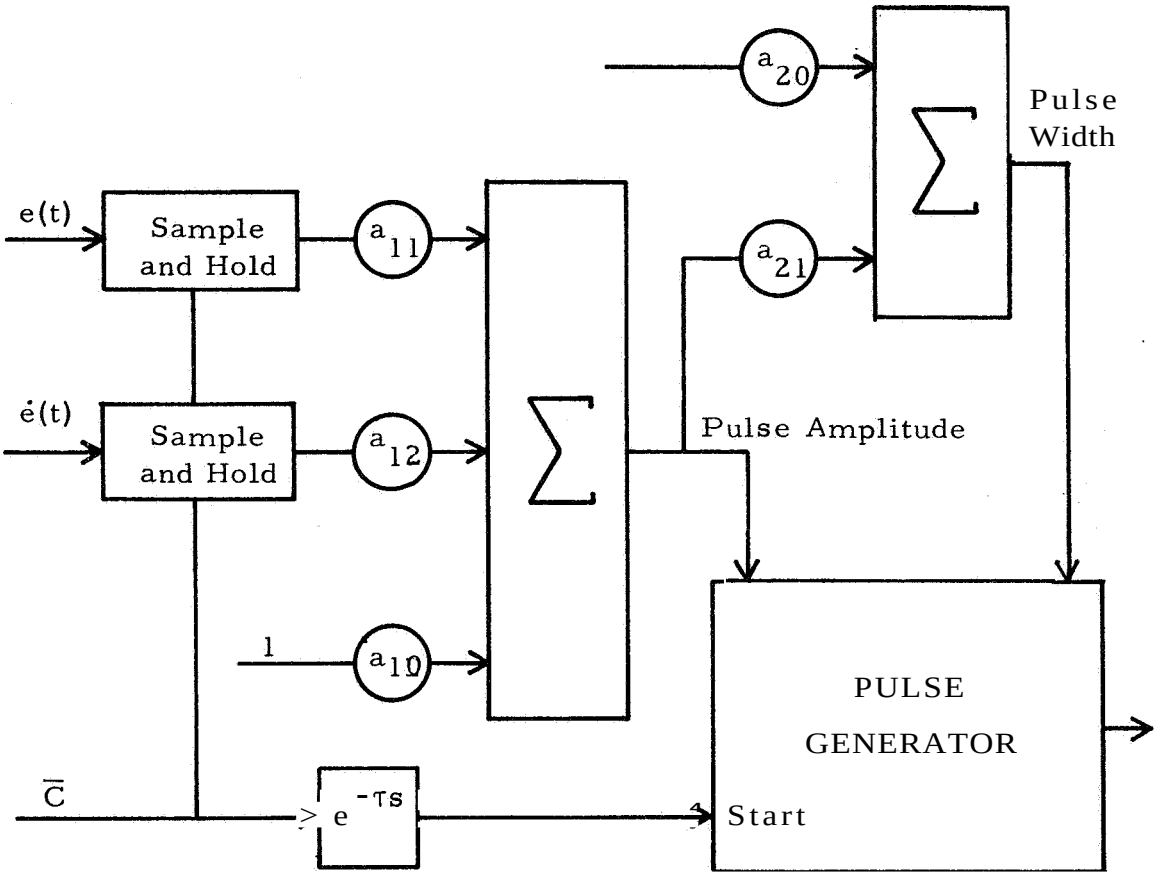

Figure 5.13 Pulse Amplitude - Pulse Width Model

The coefficients, a, and the time delay, τ, depend on the polarity of the pulse. Two arrangements are possible: determine average coefficients and an average time delay, or construct two separate models.

In the next section, the binary control signal, $\bar{c}$, will be generated by an MSDE. The components of the MSDE's input vector will be $e(t)$ and $\dot{e}(t)$. Thus the pulse amplitude - pulse width model shown in Figure 5. 13 contains an input dependent sampler.

5. 4. 4 Pulse Initiation Model

The overt act of generating an output is a measurable event. The time at which the output event is initiated is easily obtained from the tracking record, show-n in Figure 5.2. The pulse initiation process is easily modeled by a binary MSDE, i. e., an MSDE with an output w-hich is either on or off. If this signal is used as the binary control signal, $\bar{c}$, which operates the pulse amplitude and pulse width sample and hold devices, then the desired on times for the N events may be computed from:

$$t_{iM} = t_i - \tau_i \qquad i = 1, 2, \ldots N \qquad (5.6)$$

where the t_{iM} are the time at which the desired output of the MSDE, $k(t)$, becomes true, t_i are the actual times of initiation and τ_i is the time delay obtained in section 5. 4. 1 where $\tau_i = .050$ milliseconds for positive pulse events and $\tau_i = .100$ milliseconds for negative pulse events.

Although the above yields a decision element which generates the desired control signal, it does not necessarily reflect the human

operator's behavior. The decision to initiate the pulse might w-ell be made prior to the decision to sample and hold the input vector. This possibility may be investigated by selecting a criterion function for the MSDE adjustment algorithm that allows the time delay to be computed. This may be achieved by assuming that the operator ignores the input vector during a pulsatile event, and does not resume monitoring the input vector until the pulse output event is complete. This results in the following procedure for evaluating the MSDE criterion function: apply the time varying input vector until one of tw-o possibilities occurs--the MSDE generates an output, or the actual time of a pulse initiation is exceeded. If the MSDE produces an output, compute the time by w-hich the signal leads the next actual pulse initiation. Resume applying the input vector starting at the end of the pulse event. If the MSDE produces no output prior to the actual time of initiation, the event has been missed. A tally is kept of the total number of misses. Ideally, an MSDE will be found such that an output is produced exactly τ seconds prior to the actual time of initiation for every pulse event. If the MSDE is representative of the operator's behavior then this time delay will be larger than or equal to the time delay associated with the sampling process.

This may be formulated by defining a criterion function as follows:

$$\Phi = \frac{K_1}{N-M} \sum_{i=1}^{N-M} [\tau - (t_{im} - t_i)]^2 + K_2 M$$

and

$$\tau = \frac{1}{N-M} \sum_{i=1}^{N-M} (t_{im} - t_i) \qquad (5.7)$$

where t_i is the actual time of pulse initiation, t_{im} is the time at which the MSDE output became true, and M is the number of missed events.

The time delay, τ, is the mean lead time of the MSDE. The first term of the criterion function is just the standard deviation of the lead times $(t_{im} - t_i)$.

The results of the pulse amplitude model clearly demonstrate the ability of the human operator to estimate the derivative of a displayed signal. The MSDE input vector was selected with the assumption that the decision to initiate a pulse is based on a relatively simple decision surface in the error, error rate phase plane, A number of error phase plane trajectories w-ere sketched, Figure 5. 14. The trajectories start (circles) at the termination of a pulse event and end (crosses) at the initiation of the next pulse. An inspection of

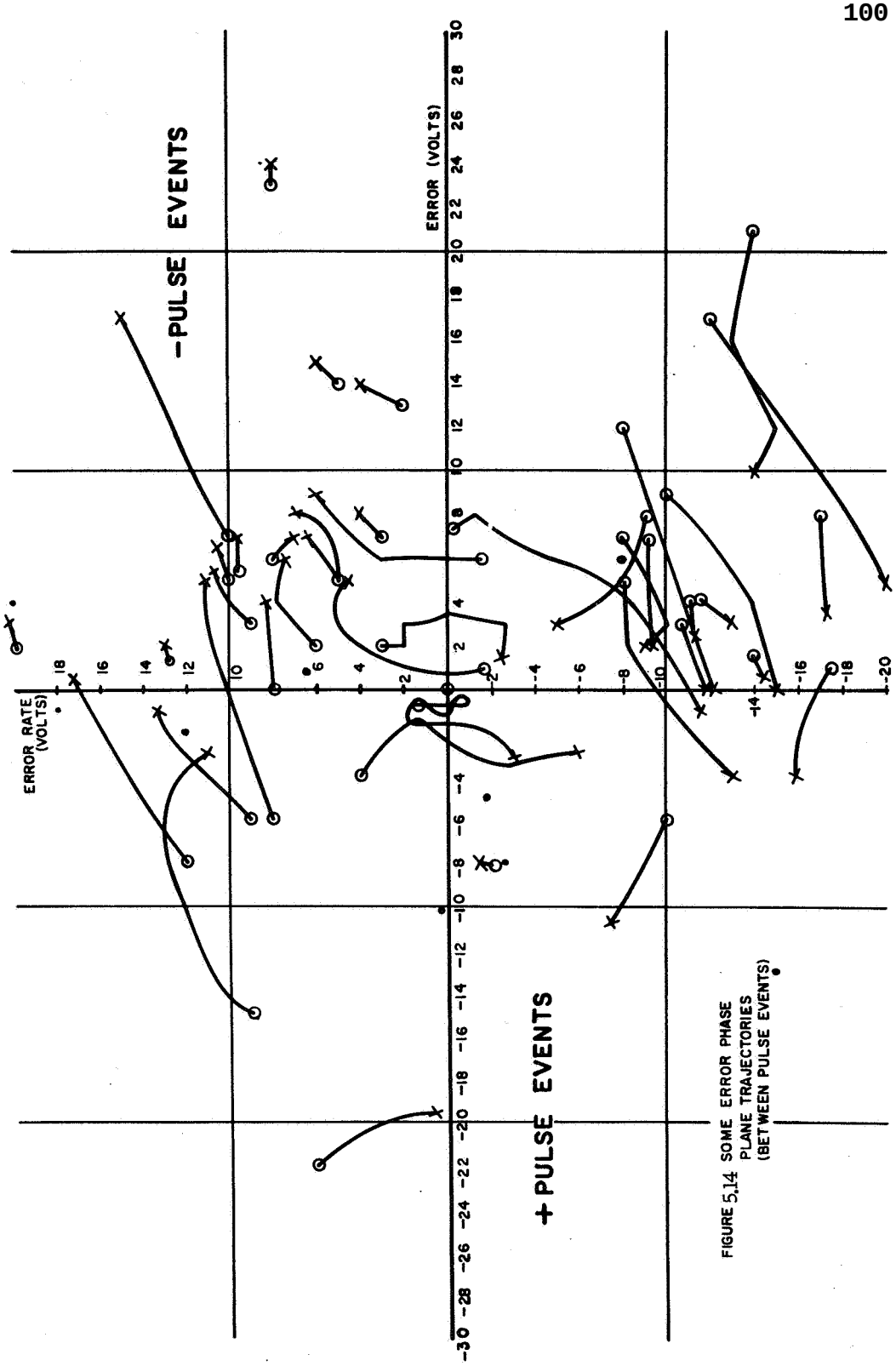

FIGURE 5.14 SOME ERROR PHASE PLANE TRAJECTORIES (BETWEEN PULSE EVENTS)

these trajectories led to the observation that the human operator utilizes the favorable error rate in the second and fourth quadrants and allows the system to coast until the magnitude of the error is sufficiently small. If, at the time the error rate is still large, a new pulse event is initiated. A further observation is that an error, error rate dead zone exists inside of which no pulse events are generated. This is consistent with other human operator tracking experiments [2,4].

Based on the above analysis, decision surfaces in the error phase space were selected. These surfaces are shown in Figure 5.15.

An MSDE is easily constructed to realize these decisions surfaces. There are two surfaces described by

$$\begin{aligned} \dot{e}^2 + e^2 &= R^2 \\ \dot{e} + m e &= 0 \end{aligned} \tag{5.8}$$

and

$$e = 0 \tag{5.9}$$

where R is the radius of a circular dead zone and m is the slope of a line through the origin, as shown in Figure 5.15.

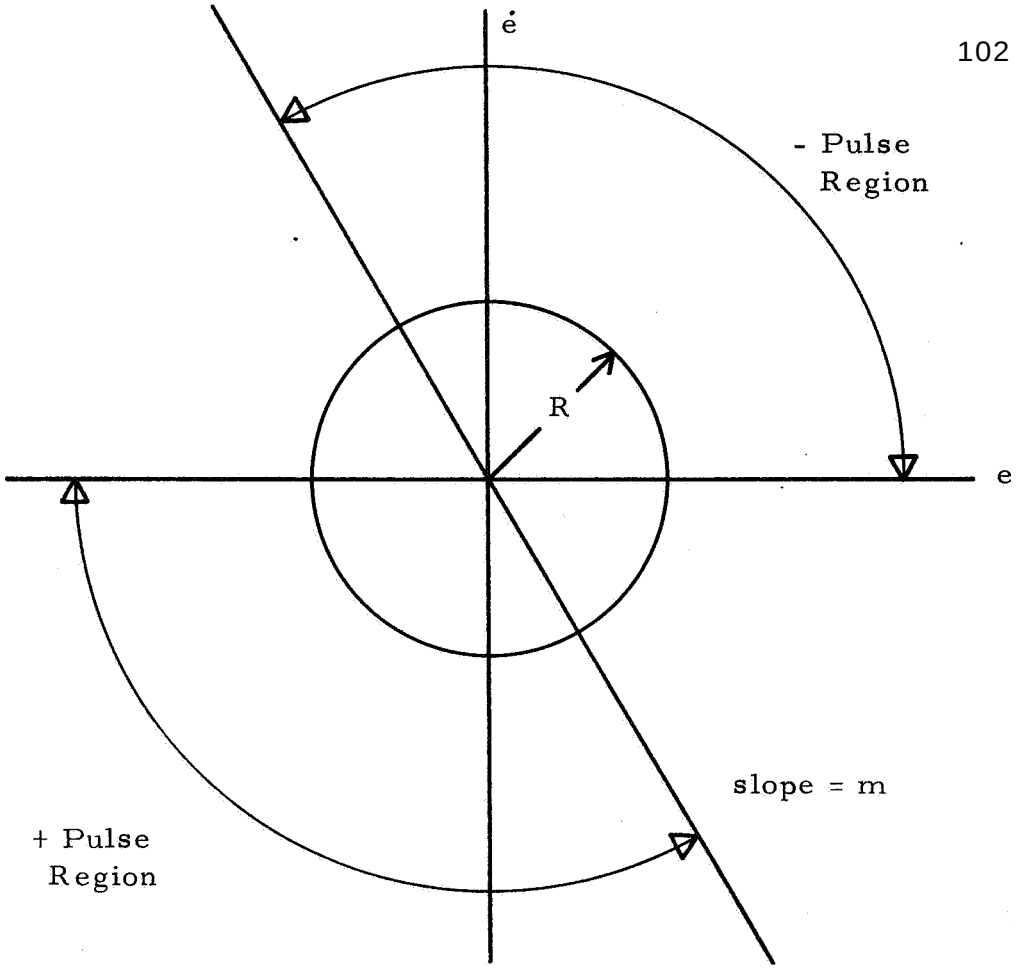

Figure 5. 15 Decision Surfaces For Pulse Initiation MSDE

The input vector is

$$
\begin{aligned}
x_0 &= 1 \\
x_1 &= e(t) \\
x_2 &= \dot{e}(t) \\
x_3 &= e^2(t) \\
x_4 &= \dot{e}^2(t)
\end{aligned}
\qquad (5.10)
$$

The resultant MSDE is shown in Figure 5. 16.

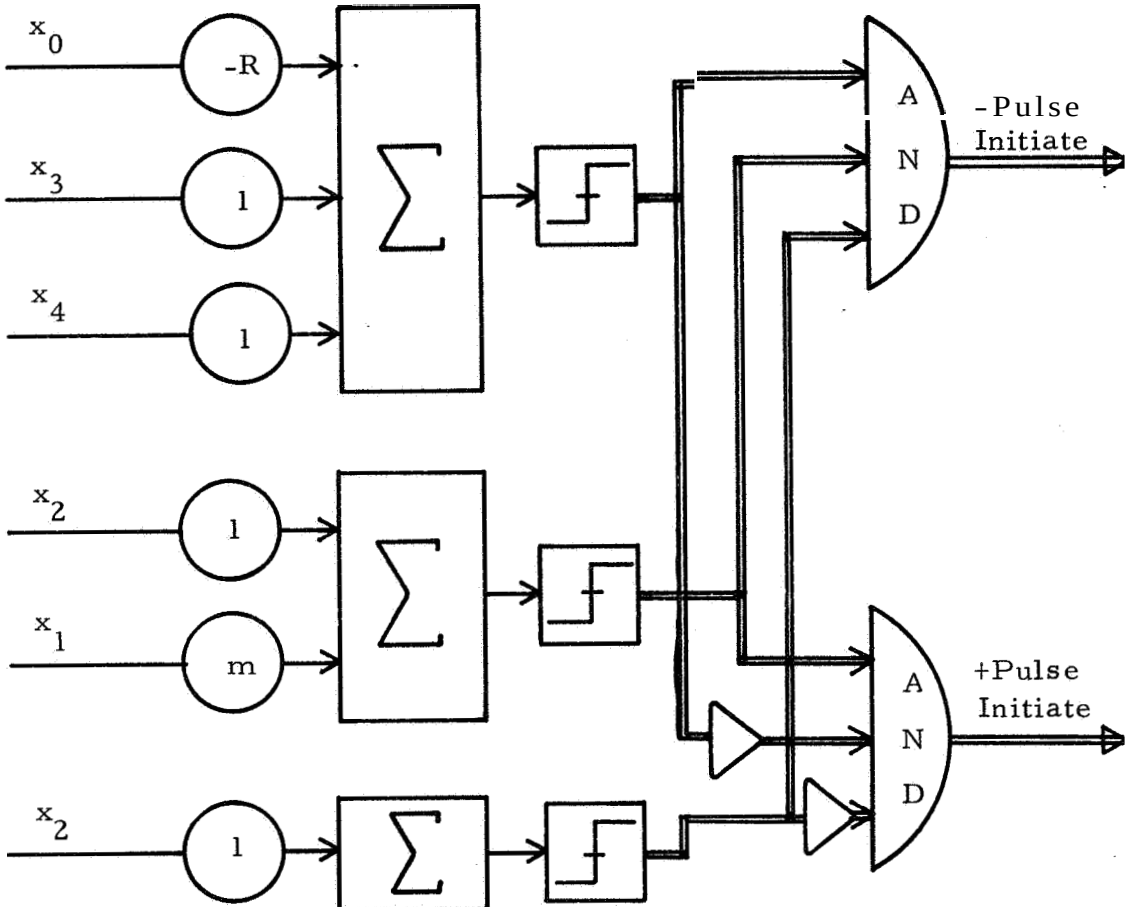

Figure 5. 16 The Pulse Initiation MSDEZ

The **MSDE** contains only two arbitrary constants which must be identified. Rather than utilize the adjustment algorithm developed in section **4.** 3, it was decided to perform a systematic study of the admissible values of **R** and m. This is feasible when the number of parameters is sufficiently small, and their ranges well defined.

The computational results are seen in Figure 5, 17. The optimum parameter values are R = 4.0 volts and m = **-1.43.** The value of τ which results from these parameter values is τ = 0.200 milliseconds. The pulse initiation model may be studied by plotting the distribution function of the times the model produced an output relative to the actual time of initiation. Such a plot is found in Figure 5. 18. **A** peak is observed at 100 milliseconds before actual pulse initiation. These MSDE outputs do not lead the actual event by the required 200 milliseconds. This is consistent with the experimental data, **as** there are a number of Dulse events which are separated by less than 200 milliseconds. **A** plot of the distribution function of the times between pulse events is found in Figure 5. 19. Again, a peak is observed at 100 milliseconds. Thus, if the model makes a decision to initiate a pulse at the first available instant, i. e. exactly at the completion of the pulse event in progress, the decision will still be less than 200 milliseconds prior to the actual initiation of the next pulse. Two mechanisms may account for this result. The first is that the operator resumes monitoring of the input vector some time before the completion of the pulse. The second, and most likely is that the operator had decided to generate two or possibly more pulses before he initiated the first one.

FIGURE 5.17 - PULSE INTERVAL CRITERION FUNCTION
OVER THE R, m PARAMETER SPACE

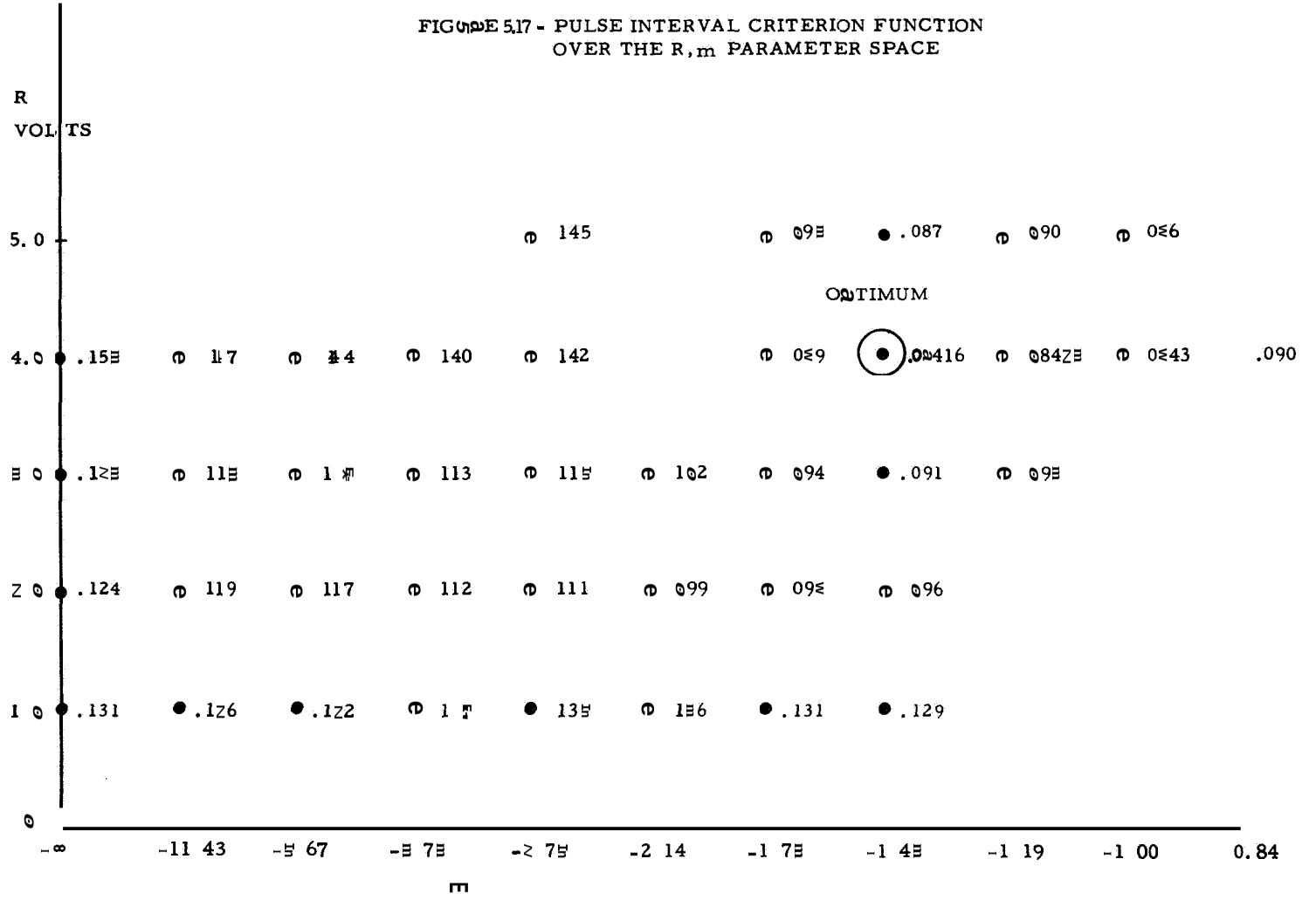

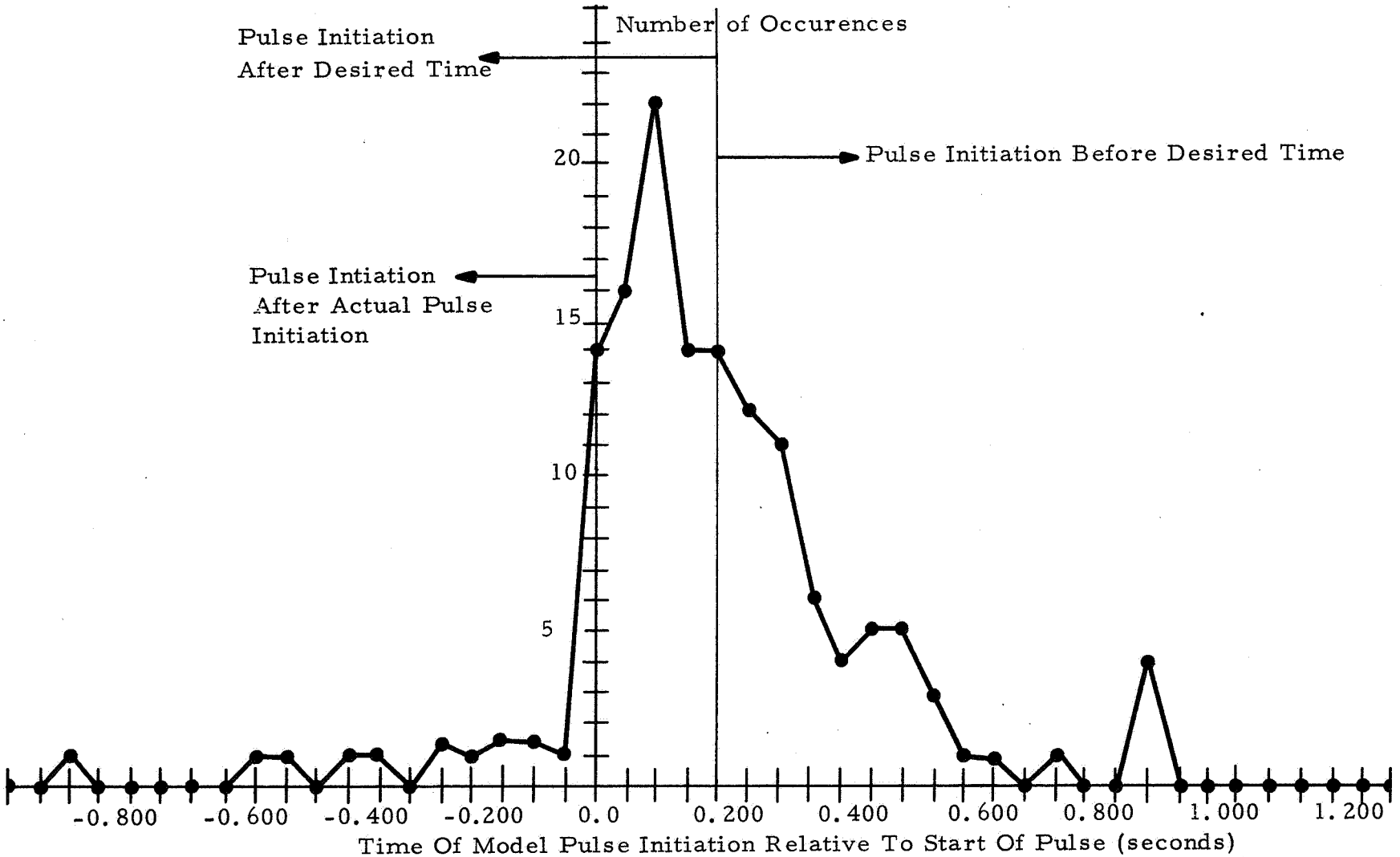

FIGURE 5.18 - Distribution Function Of Pulse Initiation Model Errors

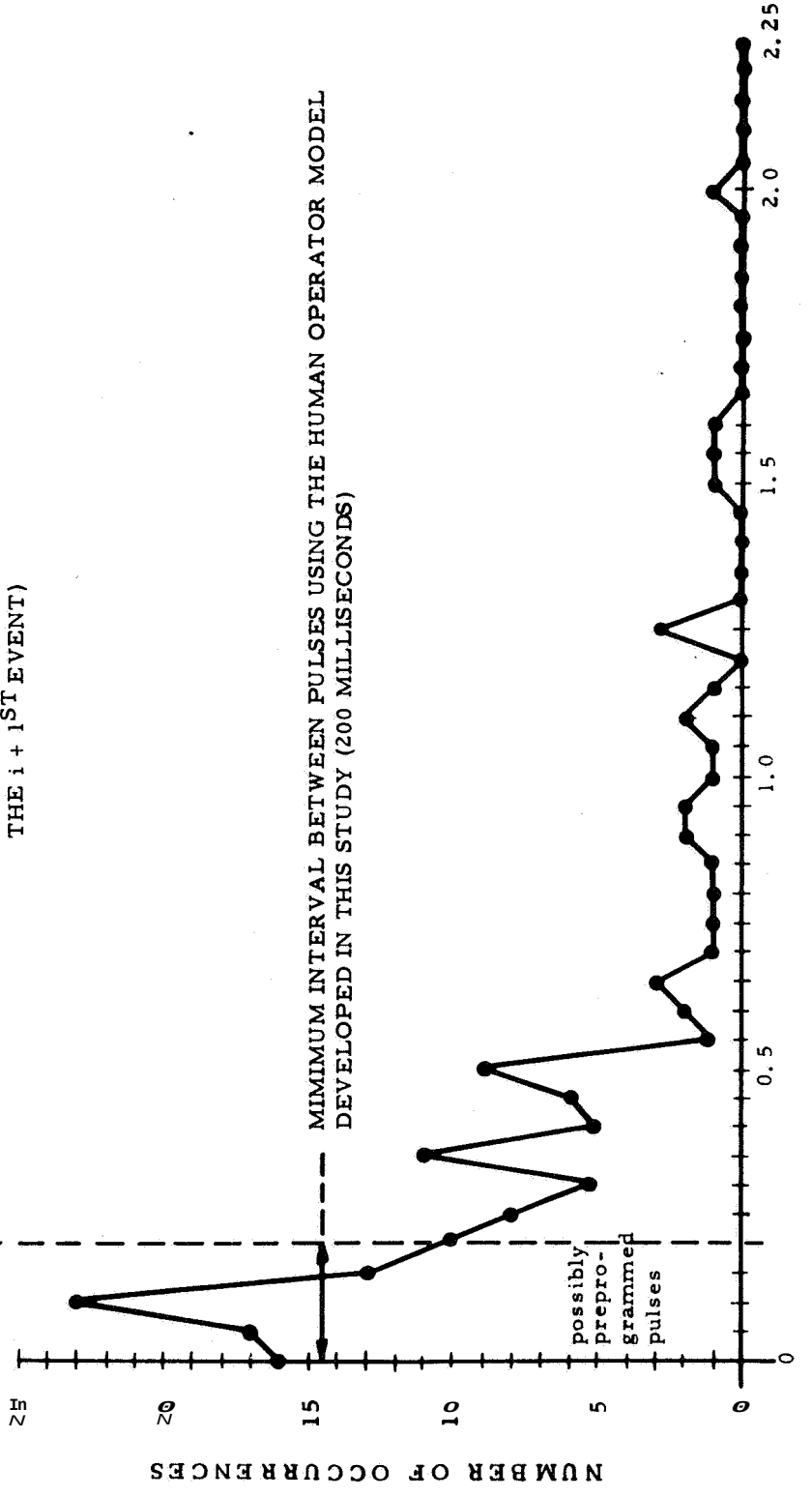

FIGURE 5.19 - DISTRIBUTION FUNCTION OF THE MAGNITUDE OF THE TIME INTERVAL BETWEEN PULSE EVENTS (FROM THE TERMINATION OF THE i^{TH} EVENT TO THE START OF THE $i + 1^{ST}$ EVENT)

The operator generates single pulses to achieve rate corrections and pulse sequences to achieve position corrections. Human operator models to represent preprogrammed pulse sequences have been proposed by Bekey and Angel [4] and Tomovic and McGhee [42]. The inclusion of a Dreprogrammed pulse sequence generator represents a logical and necessary continuation of this study.

The use of more complex decision surfaces is clearly indicated. These results do, however, demonstrate the applicability of the MSDE and the PDE to the modeling of discrete behavior in human operators.

Since the decision to initiate the pulse event leads the decision to sample the inputs, it may be hypothesized that the initiation of an output pulse by the human operator is a complex process which consists of several phases as follow-s:

(a) Somew-here near the completion of an output pulse, monitoring of e and $\dot{e}$ by a decision element is resumed.

(b) When the error trajectory enters pre-selected regions of the phase plane, a decision to produce a pulse is made

(c) Some time later the input vector is sampled and the amplitude and width computed.

(d) Some time after (c) the pulse is initiated.

5. 5 The Complete Human Operator Model

The complete human operator model is shown in Figure 5.20. An interesting feature of the model is the input dependent sampling which takes place in the pulse amplitude PDE.

5. 6 Summary of Results and Conclusions

The PDE and MSDE may be used to contruct identifiable human operator models for discrete control behavior. The resultant model contains a completely identified input dependent sampling element.

The parameters of the human operator model shown in Figure 5.20 were obtained from experimental data taken from one subject in an advanced state of training. No records were made of the error or measures of the error as a function of training, The computational results brought to light a number of interesting results:

(1) The delay time τ between the model's decision to pulse and the actual event was 200 milliseconds. The value is within the range of reaction times reported in the literature

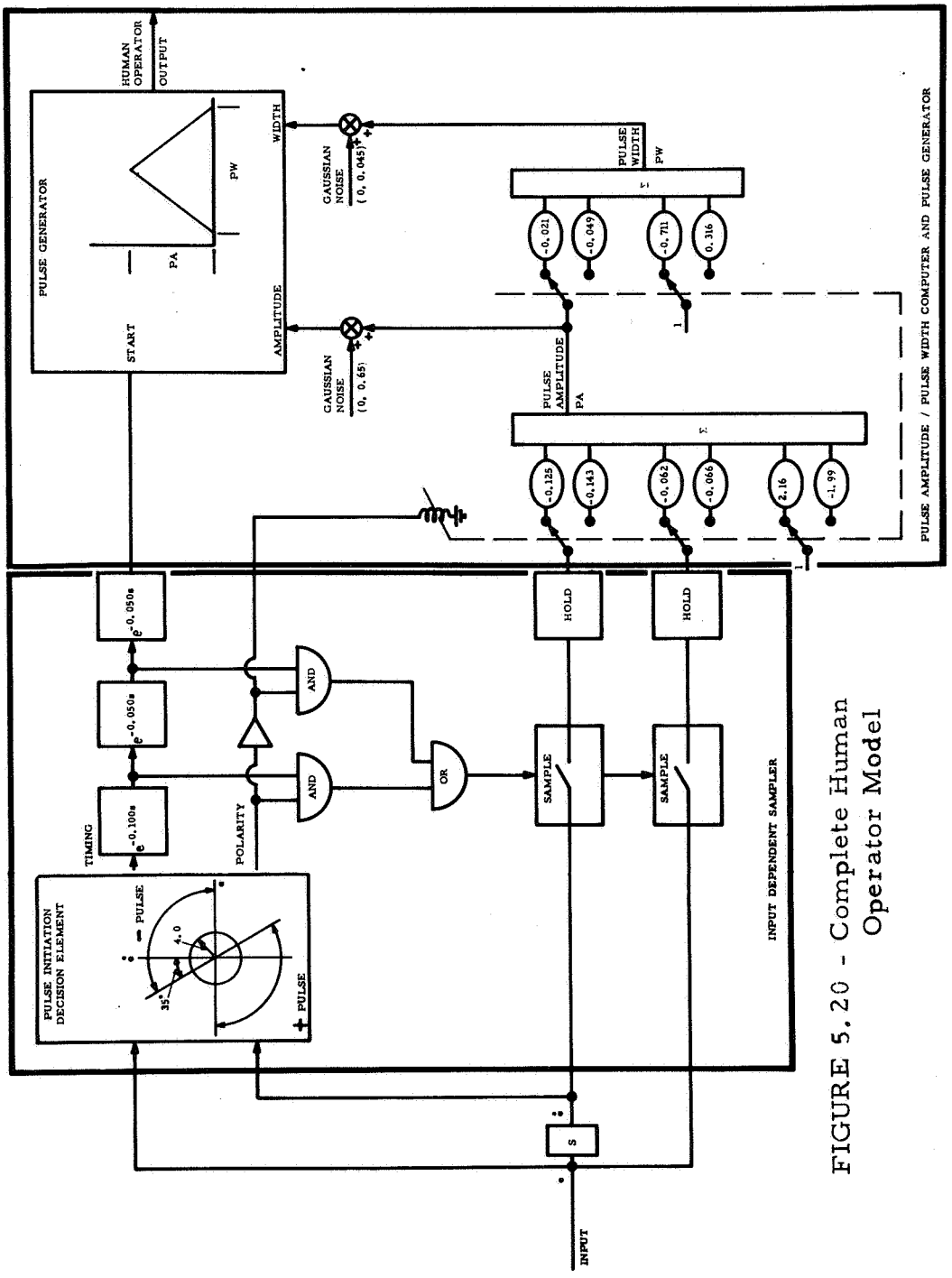

FIGURE 5.20 - Complete Human Operator Model

(2) The numerical values for the time delays in Figure 5. 20 lead to the following sequence: (1) A decision is made to generate a pulse, followed by (2) a pause of 100 - 150 milliseconds, (3) e(t) and ė (t) are sampled, (4) during the next 50-100 milliseconds the amplitude and width of the pulse are computed'and (5) the pulse is generated.

(3) The pulse amplitude and pulse w-idth models for negative pulses produce better correlations with the experimental data than the models for positive pulses. This is clearly apparent in the scatter plot, Figure 5. 7 and in the values of the criterion function, Figure 5.6. This may be the result of incomplete training, the design of the side arm controller used, the position of the subject's arm relative to the controller or a characteristic of the particular human operator in this experiment. The results of Agarwal [1] are cited in support of the hypothesis that this is a characteristic of side arm controllers.

(4) The pulse amplitude models for positive and negative pulses are quite similar, despite considerable asymmetry in pulse amplitude distributions, Figure 5. 4.

(5) The results presented in Figure 5. 19 strongly indicate that human operators utilize some pre-programmed pulse sequences.

(6) If the differences between model results and experimental tracking data are viewed as the result of short term human operator variations, then the statistics of the human operator variations are easily determined, tables 5.3 and 5.4.

From the present study it is not feasible to determine w-hether the model errors observed are random or functionally depending on the human operator inputs and input-output history. Further studies should include preprogrammed pulse elements, more complex error phase plane decision surfaces, and the effects of training on the model parameters and their associated distribution functions.

CHAPTER 6

A MODEL FOR THE TRACKING BEHAVIOR OF HUMAN OPERATORS USING MULTIPLE COORDINATED DISPLAYS

6.1 Scanning Behavior Of Human Operators

There are many physical systems in w-hich the operator's control actions are based on information obtained from tw-o or more sources. The aircraft instrument panel show-n in Figure 1.3 is an excellent example of such a system. The information presented by the instruments is deterministic and coordinated in that the state of the aircraft can only be determined by reading a number of instruments.

Models which describe the scanning behavior of human operators have been described in the literature. These studies may be divided into three groups. Group I contains situations in w-hich the display devices presented uncorrelated signals. The operator's control action consisted of monitoring the displays for limit conditions and actuating a button or sw-itch. Group I also contains multi-axis control tasks in w-hich the displays are uncorrelated w-ith each other. Group II contains situations in w-hich the displays presented

deterministic, coordinated signals, but the signal time histories were not utilized. Group III contains situations in w-hich the displays presented deterministic, coordinated signals whose time histories were recorded simultaneously with the operator's eye position.

Models for the scanning behavior of operators in Group I and II situations have been presented [5,35]. In all of the investigations described in the literature, the behavior modeled is the distribution function of the fixation times for each instrument, and the distribution function of the various inter-instrument transitions. The resultant scanning model depends on the long term properties of the displayed signals; signal mean and higher moments, or bandw-idth. The instantaneous signals viewed by the operator are not utilized.

Models for Group III situations have not been published to the present time; the purpose of this chapter is to synthesize a deterministic model for an operator's scanning behavior in a Group III experiment. The control task described in the preceding chapter was the pitch axis of an aircraft. The operator viewed a single display w-hich presented altitude error and operated a control stick which positioned the aircraft's elevator. The altitude error display may be viewed as an ILS/Glide Slope Needle or simply a high-low indicator in a terrain avoidance system. If a second display is added,

w-hich presents the aircraft's pitch attitude, the control system becomes a Group III task if both displayed signals and the operator's eye position are recorded.

This chapter presents the results of such an experiment. A complete human operator model is synthesized and identified. Discrete decision elements, operating on the displayed signals, are utilized to model the scanning behavior of the operator.

6.2 The Tracking Task

The tracking task consists of maintaining an aircraft at a constant altitude while flying over rather bumpy terrain. The inputs to the operator are aircraft attitude (pitch angle) and altitude error. The operator's output is elevator position. A block diagram of the control system is found in Figure 6. 1

The operator must scan or commutate between the two displays in order to operate the system. The two displays w-ill be referred to as the LEFT display (attitude) and the RIGHT display (altitude error).

Terrain avoidance and ILS/NAV systems utilized similar pitch axis displays. A terrain avoidance task may be performed at constant throttle, while ILS climbs and descents depend heavily on throttle control. Thus, a terrain avoidance task w-as utilized.

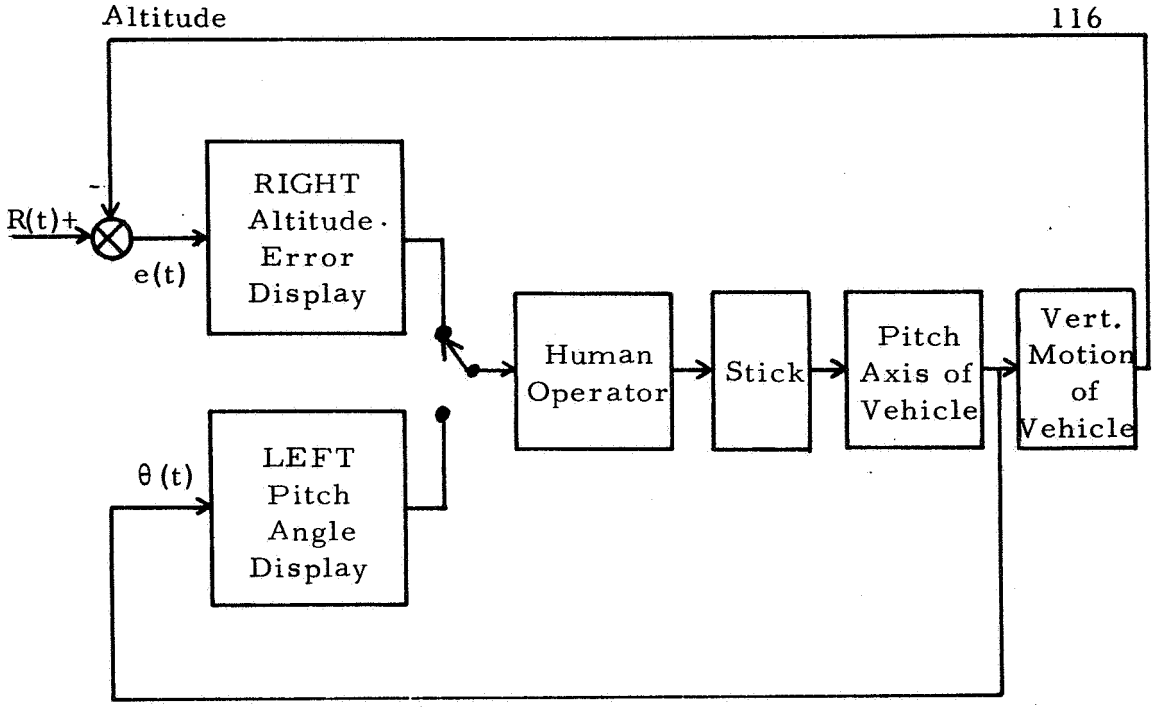

Figure 6. 1 The Tracking Task

The operator w-as instructed to keep the instantaneous error as small as possible w-ithout allowing the pitch angle to exceed t 40 degrees.

6. 3 The Experiment

The transfer functions for the pitch axis and the vehicle altitude w-ere selected so that the operator produced pulsatile control actions. The transfer functions w-ere:

$$\frac{\text{Pitch angle (degrees)}}{\text{Stick Otuput (volts)}} = \frac{2}{s(s + 2)} \qquad (6.1)$$

$$\frac{\text{Altitude (feet)}}{\text{Pitch angle (degrees)}} = \frac{50}{s(s^2 + 10s + 100)} \qquad (6.2)$$

The display gains were:

Pitch attitude: 10 degree/cm of vertical displacement

Altitude error: 100 feet/cm of vertical displacement

The stick gain was:

3 volts/ degree of rotation

The tracking station is shown in Figure 6. 2

The operator sat in a long range transport pilot's chair, which could be adjusted vertically to suit the operator. The sidearm controller was also adjustable and contained an integral arm rest, Frequency response problems associated with actual aircraft instruments w-ere avoided by utilizing oscilloscopes with specially prepared edge lighted reticles. The oscilloscope displays are seen in Figure 6. *3*.

The transfer functions w-ere mechanized on an analog computer, Seven signals available at the analog computer were recorded on FM magnetic tape:

1. the operator's eye position
2. stick position
3. pitch angle, $\theta(t)$
4. pitch rate, $\theta^{o}(t)$
5. altitude error, $e(t)$
6. altitude error rate, $e^{o}(t)$

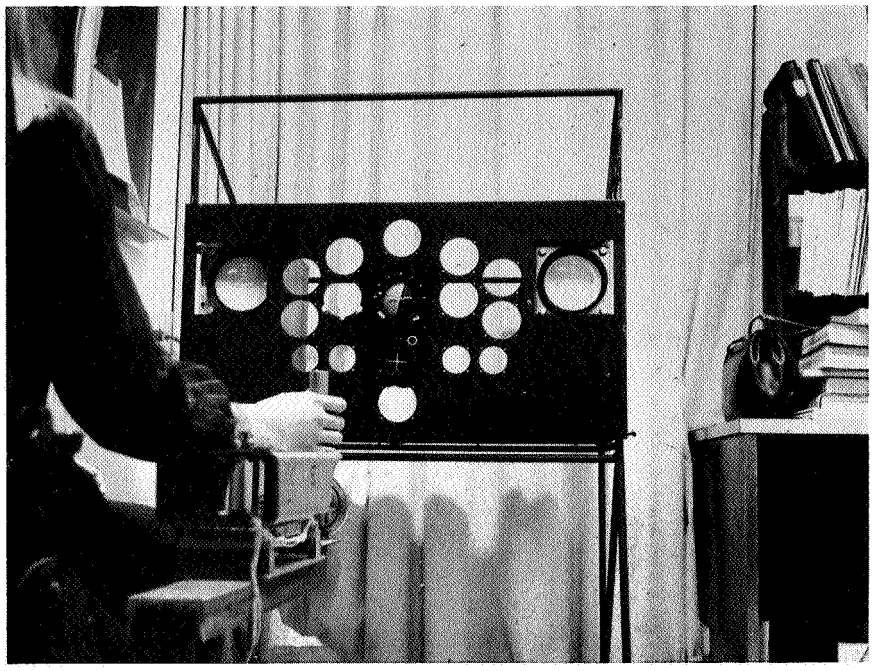

a. Display Configuration

b. Pilot's Seat and Sidearm Controller

FIGURE 6. 2 - Tracking Station

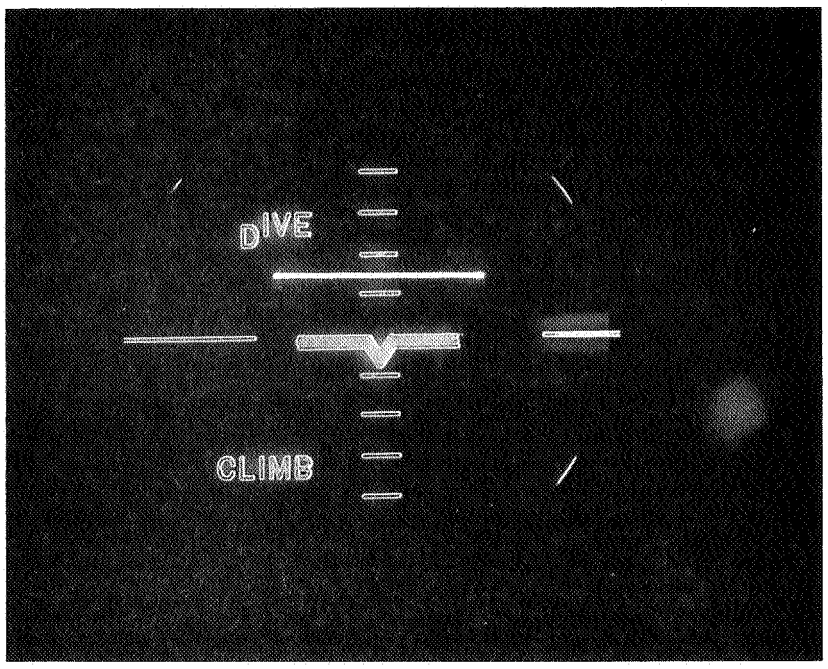

a. RIGHT Display Reticle

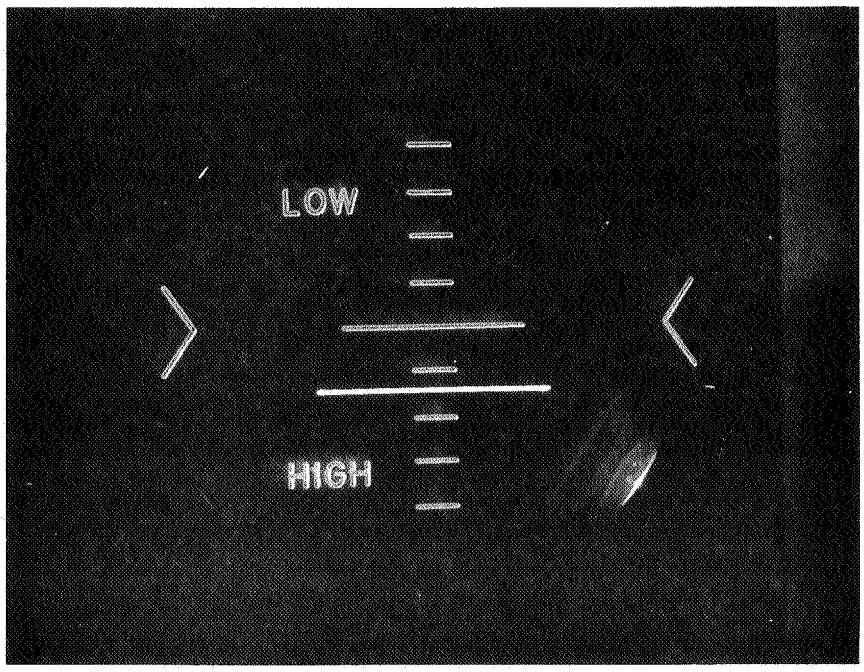

b. LEFT Display Reticle

FIGURE 6. 3 - Illuminated Displays

The input to the system w-as obtained by filtering low frequency gaussain noise. The filter transfer function w-as:

$$F(s) = \frac{100K}{(s+1)^3 (s+a)} \qquad (6.3)$$

The nominal values of K and a were 30 and 10 respectively. The values of K and a w-ere adjusted to control the difficulty of the task.

A single subject received approximately **30** hours of training over a period of three weeks. The training sessions consisted of six minutes of tracking and five minutes of rest. One of the last sessions w-as recorded on magnetic tape and subsequently digitized. The sampling interval was 25 milliseconds or 40 samples per second.

6.4 Measurement of Eye Position From Electro-ocular Potentials

According to Young [52], Schott [55] demonstrated a relationship betw-een eye motion and periorbital potential variations as early as 1922. Mowrer, Ruch, and Miller [56] found that by placing electrodes on the skin around the eye, potential differences could be measured between electrodes w-hich resulted from eye motions in the plane formed by the two electrodes and the eye's center of rotation. These potentials are often referred to as electro-ocular potentials,

The potential changes due to eye motion are approximately 20 microvolts per degree of rotation. The gain and stability of D. C. amplifiers have only recently reached the point where these potentials are easily measured. If a pair of electrodes are placed laterally on either side of the eye, then the potential difference between them may be used to determine lateral eye position. This potential may be increased by placing lateral electrodes near both eyes and connecting them in series. A reduction in the number of electrodes required may be obtained by eliminating the two middle electrodes. The resultant electrode placement may be seen in Figure 6. 4

The left and right electrodes were connected to the differential inputs of a high gain, high common mode rejection amplifier, The center electrode was connected to the guard or common input. The amplifier contained a variable bandwidth low pass filter. The filter cutoff was set to 10 cps to eliminate 60 cps noise pickup.

The system was calibrated by asking the subject to look at a spot midway between the two displays. The amplifier offset was used to zero the amplifier output. With an amplifier gain of 2500, 30 degrees of eye motion produced an output of approximatley 2 volts. Some subjects electro-ocular potentials contained a small D. C. level in addition to the eye motion potentials. If the amplifier is to

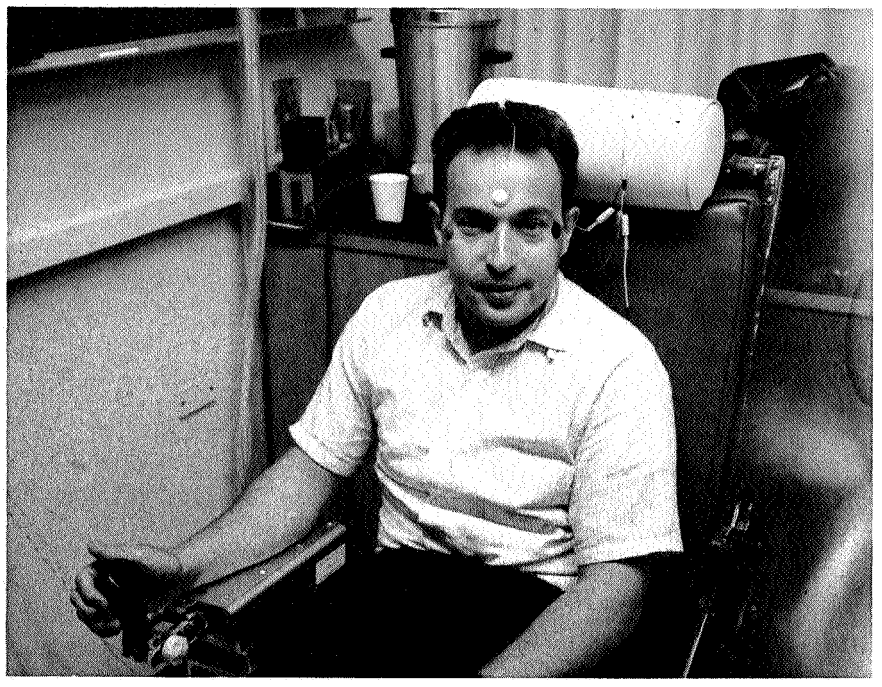

FIGURE 6.4

Subject Showing Location of Biopotential

Skin electrodes For Eye Motion Measurements

be kept out of overload, the gain must be reduced, This reduces the signal to noise ratio and makes it difficult to detect the eye motions.

When this becomes troublesome the circuit shown in Figure 6.5 was used in series with one of the electrodes.

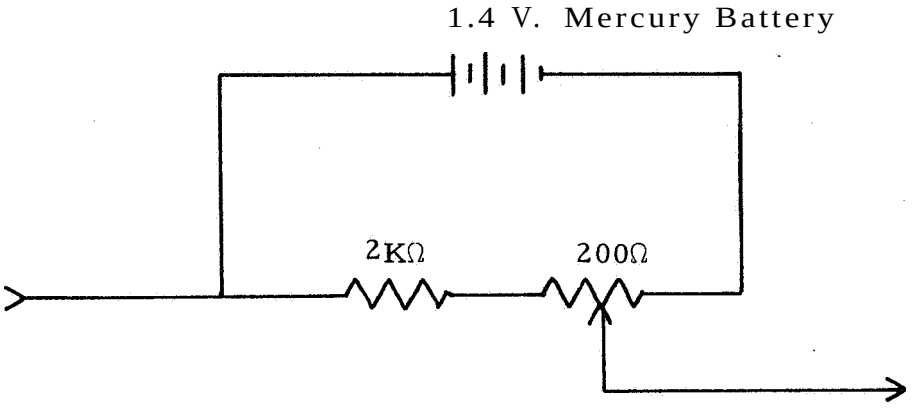

Figure 6.5 D. C. Potential Correction Circuit

The polarity of the correction is reversed by reversing the battery in its holder, The potentiometer is adjusted periodically to insure that the amplifier output is within its specified voltage range.

The electro-ocular potential was used to determine which of the two displays the subject was viewing. A portion of a typical eye motion record is shown in Figure 6.6. As can be seen from this figure, no difficulty is encountered in determining which display is being viewed. For this reason, no attempts were made to accurately calibrate the system or to eliminate slow- D. C. drifts.

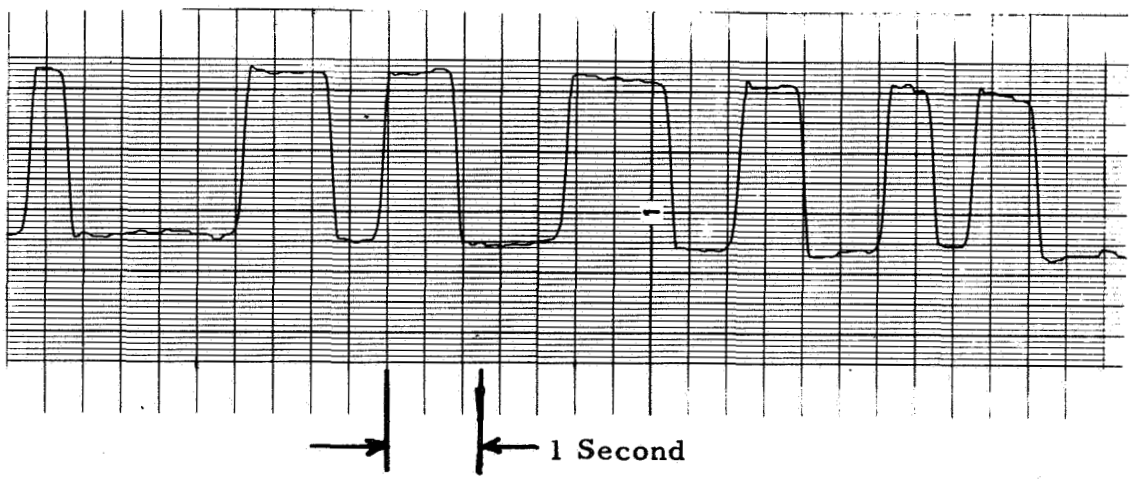

Figure 6.6 Typical Eye Motion Record

6.5 The Experimental Data

As described previously, a single subject received approximately 30 hours of training. One of the last six minute tracking sessions was selected for detailed study. The FM tape recording was digitized by sampling all seven recorded channels every 25 milliseconds.

Digital computer programs were written to correct for zero offset and gain errors introduced by the FM recording process. These corrections were computed from the zero and ± 100 volt calibration signals recorded at the end of the run.

The digitized record contained the time histories of the follow-ing signals:

1. eye motion
2. stick motion
3. pitch angle $\theta(t)$
4. pitch rate $\dot{\theta}(t)$
5. altitude error $e(t)$
6. altitude error rate $\dot{e}(t)$
7. altitude command input

A typical portion of the tracking record is seen in Figure 6. 7. The start of the run w-as located on both the digitized record and strip chart recording. All time measurements were made relative to the start of the session.

The transient eye motion data was converted to integer digits as shown in Figure 6.8.

The operator is assumed to be view-ing the LEFT display when the code digit is 6, 1 or 2, and the RIGHT display when the code digit is 3, 4 or 5. A total of 216 eye motion cycles left to right and back again were located in the digitized record.

The time history of the stick motion w-as examined. As can be seen from Figure 6. 7, it is strongly pulsatile. The stick

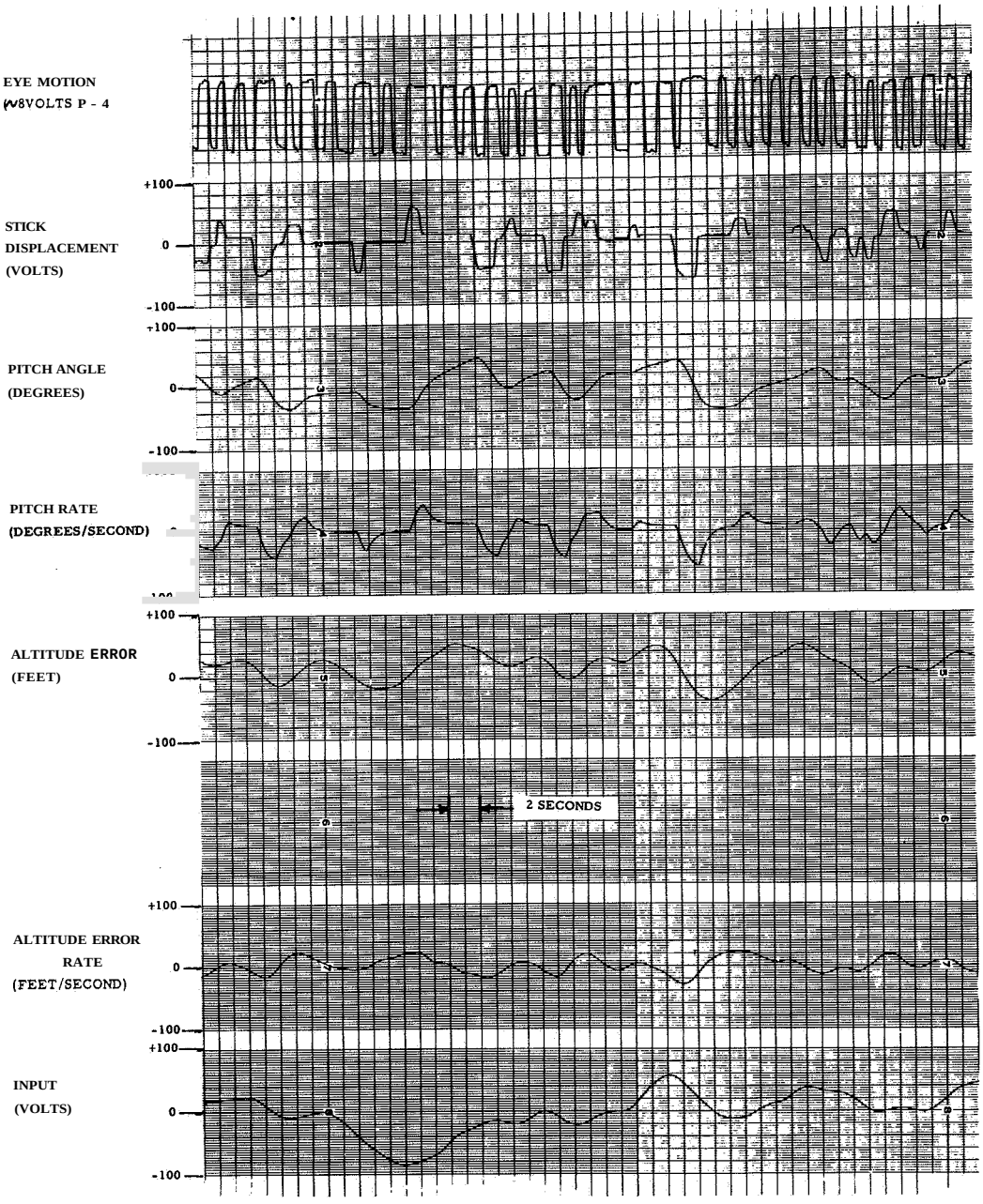

FIGURE 67 A TYPICAL TRACKING RECORD

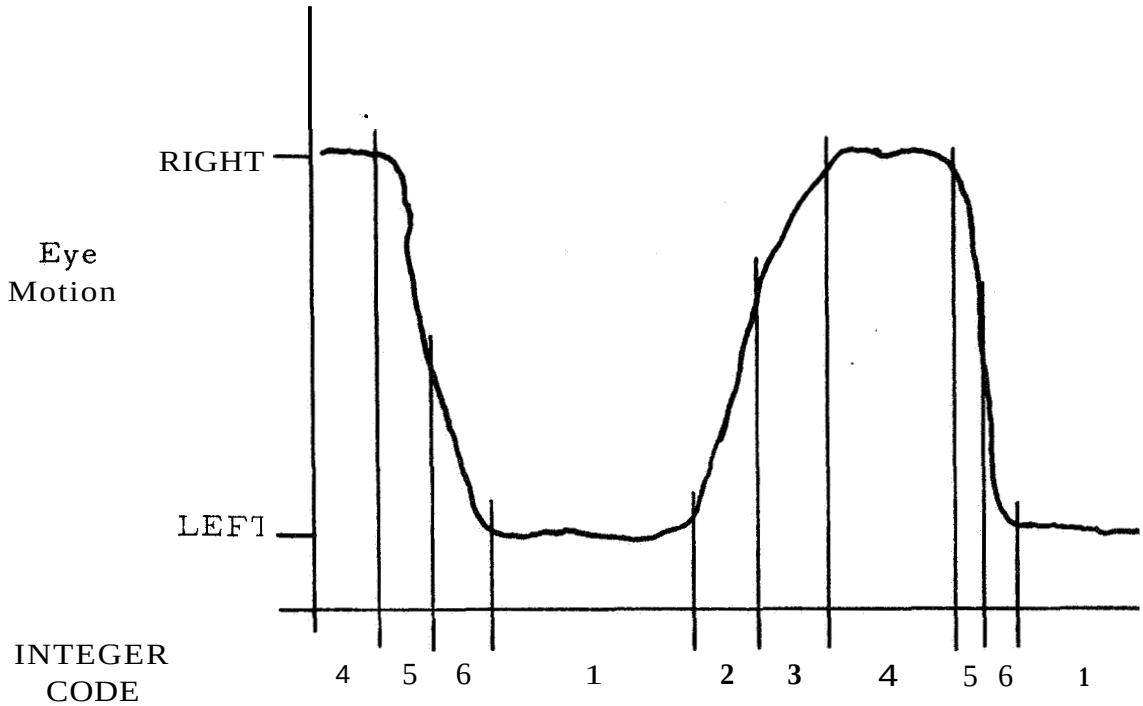

Figure 6. 8 Discretization of Eye Motion Data

motions were idealized as triangular shaped pulses, as shown in Figure 5.2 of the nreceding chapter. The time of the pulse initiation, time of nulse termination, and the amplitude of the pulse were recorded. If a pulse w-as Dart of a sequence of pulses, the zero crossing point w-as used to estimate the initiation and termination times.

6.6 The Proposed Model

The only difference between the experiment described above and the experiment of the previous chapter is the scanning behavior of the operator. Since the operator's outputs are oulsatile, much of the model will be identical to that of the previous chapter. There are, however, twice as many signals available to the operator. The task of modeling the resultant behavior is considerable as the dimensionality of the signal space renders intuitive and graphical aids useless. Instead systematic modeling procedures must be relied upon.

The ability of operators to estimate rates of change of displayed variables is well established. Thus, when the operator looks directly at a display, the signal and signal rate are assumed to be available continuously. If direct or foveal vision is assumed to be the only source of input to the operator, then signals in the periphery are not available. When the operator moves his eyes from one display to the other, it may be assumed that the last observed values of the signal and signal rate are stored. A scanning model which reflects this description is found in Figure 6.9.

The element which models the operator's decision to switch displays is hypothesized to be an MSDE.

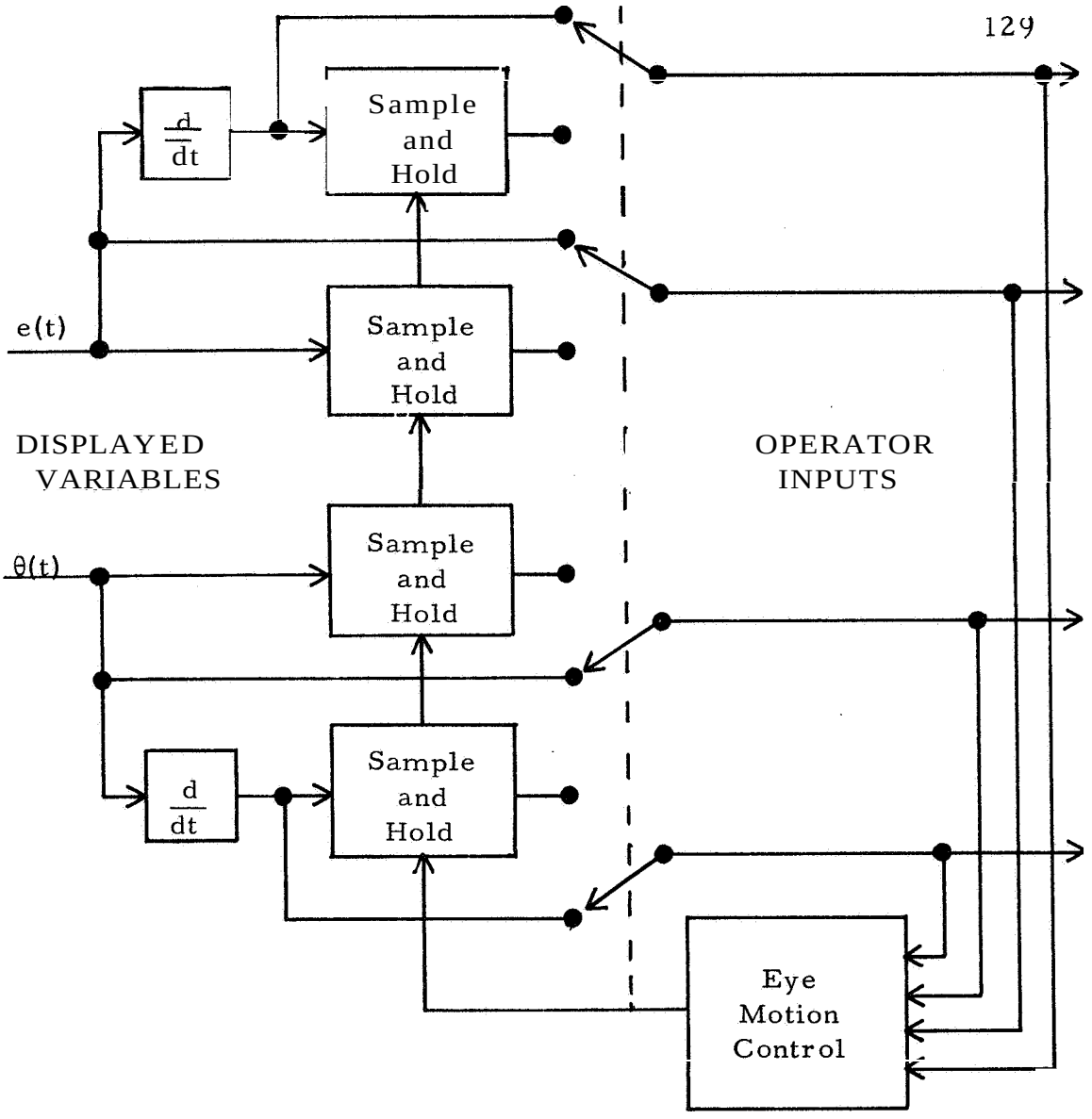

Figure 6.9 Scanning And Signal Processing System

The remaining portion of the operator model shown in Figure 6.10, follow-s from the results of the previous chapter.

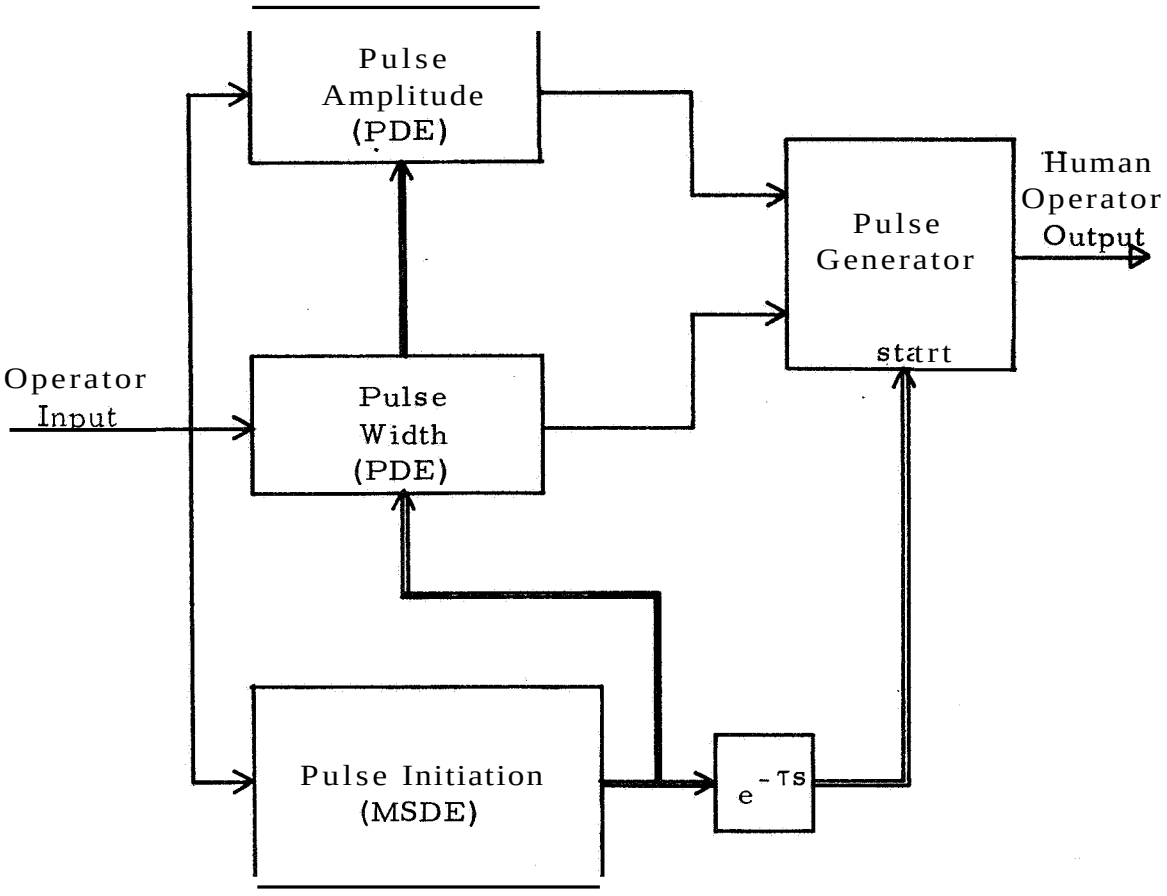

Figure 6. 10 Proposed Human Operator Model

6. 6. 1 Comments On The "Operator Input"

The "operator input" as defined above consists of tw-o continuous signals and tw-o discrete, sampled and held signals. There are, consequently, at least four inputs to the decision elements used to synthesize the model. The input vectors to each element will contain at least 5 components. The decision space will be at least

six dimensional. This makes it almost impossible to select reasonable decision surfaces from a priori knowledge of the system. The possibility that the operator utilizes three dimensional decision surfaces and forms more complex surfaces by combining them is investigated below.

6.7 Identification Of The Pulse Modulation Model

The control actions of the operator were idealized above as triangular pulse events. Each event consisted of a time of initiation, a pulse amplitude and a pulse width. The validity of this idealization will be investigated below. The results of the previous chapter clearly demonstrate the applicability of PDE's to the modeling of the operator's decision as to the amplitude and width of the pulse to be generated. The physical separation of the display devices prevents the operator from utilizing both displayed signals continuously. The output of the operator's scanning and signal processing system, shown above in Figure 6.9, can be computed from the eye position record. The resultant signals are called the Operator Input. The PDE input vectors will be derived from these signals.

The PDE produces a scalar voltage, the magnitude of which determines the pulse amplitude or width. A binary signal controls the sampling and computation process. The identification procedure

determines this timing signal relative to actual time of initiation of the pulse. Another decision element, described below-, models the operator's decision to initiate a pulse event. The output of this element always leads the actual time of initiation by a known time. The timing of both decision elements is identified relative to the actual pulse initiation.

By algebraic manipulations, all of the control signals can be defined relative to the output of the pulse initiation decision element.

The input vector utilized for both the pulse amplitude and the pulse width PDE's was:

$$
\begin{aligned}
x_0 &= 1.0 & x_8 &= \dot{e}^2(t_1 - \tau) \\
x_1 &= \theta(t_i - \tau) & x_9 &= \theta(t_i - \tau)\dot{\theta}(t_1 - \tau)/100 \\
x_2 &= \dot{\theta}(t_i - \tau) & x_{10} &= \theta(t_1 - \tau)e(t_1 - \tau)/100 \\
x_3 &= e(t_i - \tau) & x_{11} &= \theta(t_1 - \tau)\dot{e}(t_1 - \tau)/100 \\
x_4 &= \dot{e}(t_1 - \tau) & x_{12} &= \dot{\theta}(t_i - \tau)e(t_1 - \tau)/100 \\
x_5 &= \theta^2(t_1 - \tau) & x_{13} &= \theta(t_i - \tau)\dot{e}(t_1 - \tau)/100 \\
x_6 &= \dot{\theta}^2(t_1 - \tau) & x_{14} &= e(t_1 - \tau)\dot{e}(t_1 - \tau)/100 \\
x_7 &= e^-(t - \tau)
\end{aligned}
\qquad (6.4)
$$

where τ is a lead time relative to the time of actual **pulse** initiation, t_1. Further, the signals shown are not the actual displayed

variables, but the Operator Inputs produced by the scanning and signal processing system shown in Figure 6.9.

The components of the input vector form a four dimensional quadratic surface in the space formed by θ, $\dot{\theta}$, e, $\dot{e}$ and the pulse amplitude or width.

6. 7. 1 Computational Results

The identification procedure of chapter 4 was used to identify the coefficients of the PDE's and the associated time delay. As in the previous chapter, the event space was partitioned by modeling the positive pulses separately from the negative pulses. The computational results are seen in Figures 6. 11-6. 14 where the criterion function is plotted against the mean lead time, τ.

Three of the four curves, Figures 6. 11, 6.12, and 6. 14 show strong minimums more than 500 milliseconds after the actual pulse initiation. The mean pulse width is approximately 1.4 seconds. Thus it is possible that the operator selects the amplitude and width while the pulse is being generated, A model which would reflect this type of behavior would require a preview model to determine in what direction and at what rate to move the control stick in advance of the decision as to the final amplitude and width. A model of this type

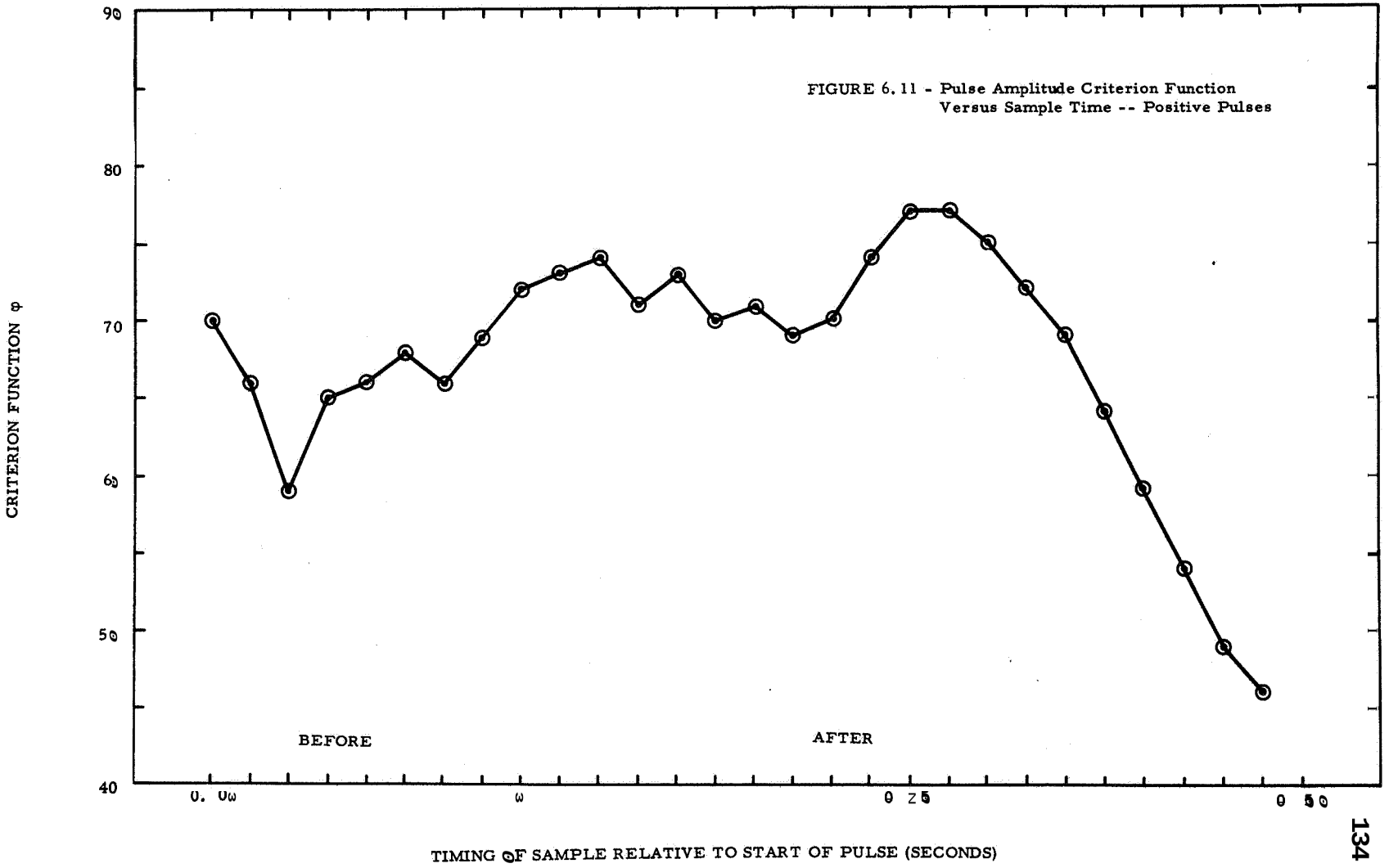

FIGURE 6.11 - Pulse Amplitude Criterion Function Versus Sample Time -- Positive Pulses

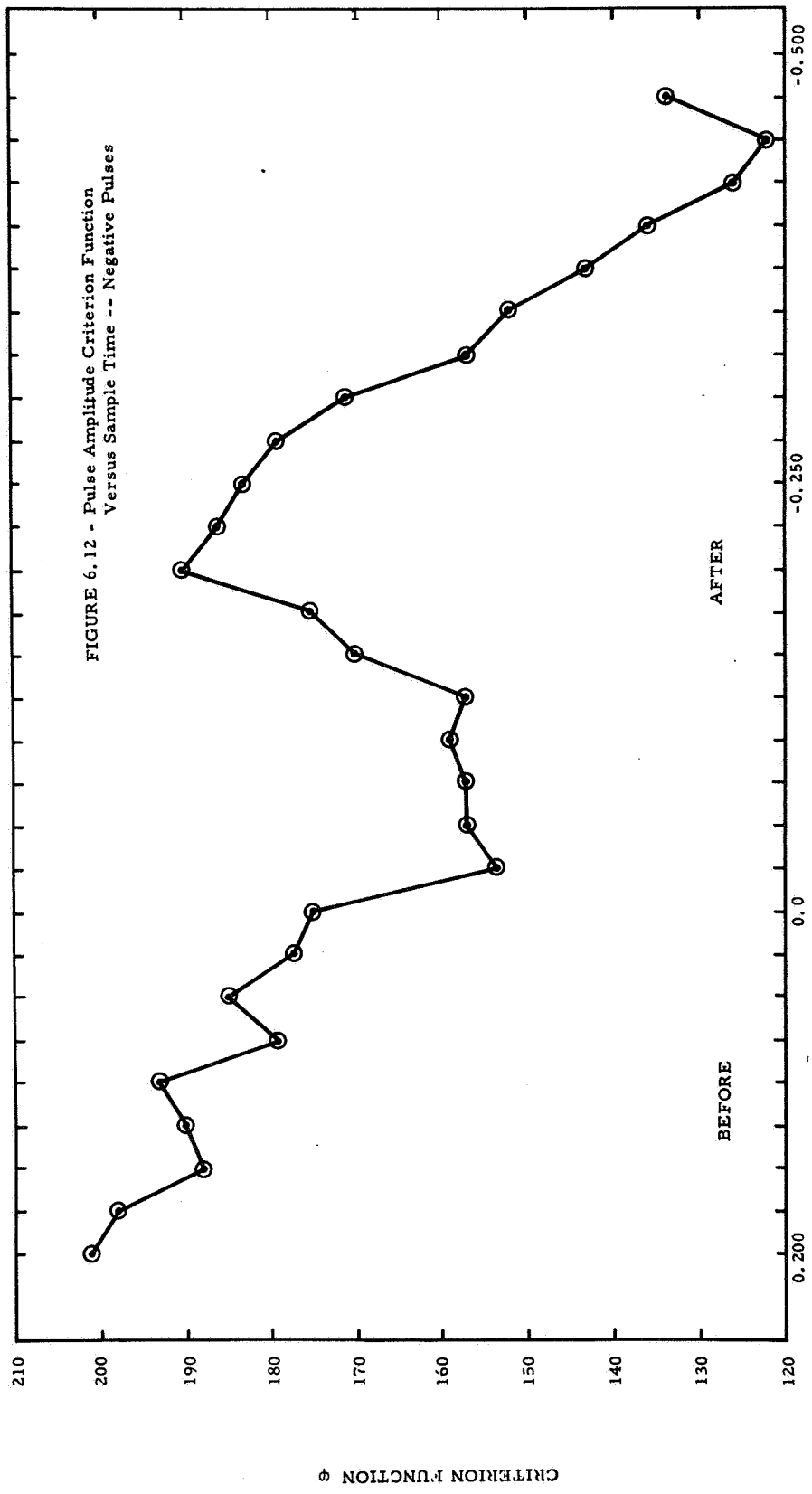
FIGURE 6.12 - Pulse Amplitude Criterion Function
Versus Sample Time -- Negative Pulses
CRITERION FUNCTION Φ
210
200
190
180
170
160
150
140
130
120
0.200
0.0
-0.250
-0.500
BEFORE
AFTER
TIMING OF SAMPLE RELATIVE TO START OF PULSE (SECONDS)

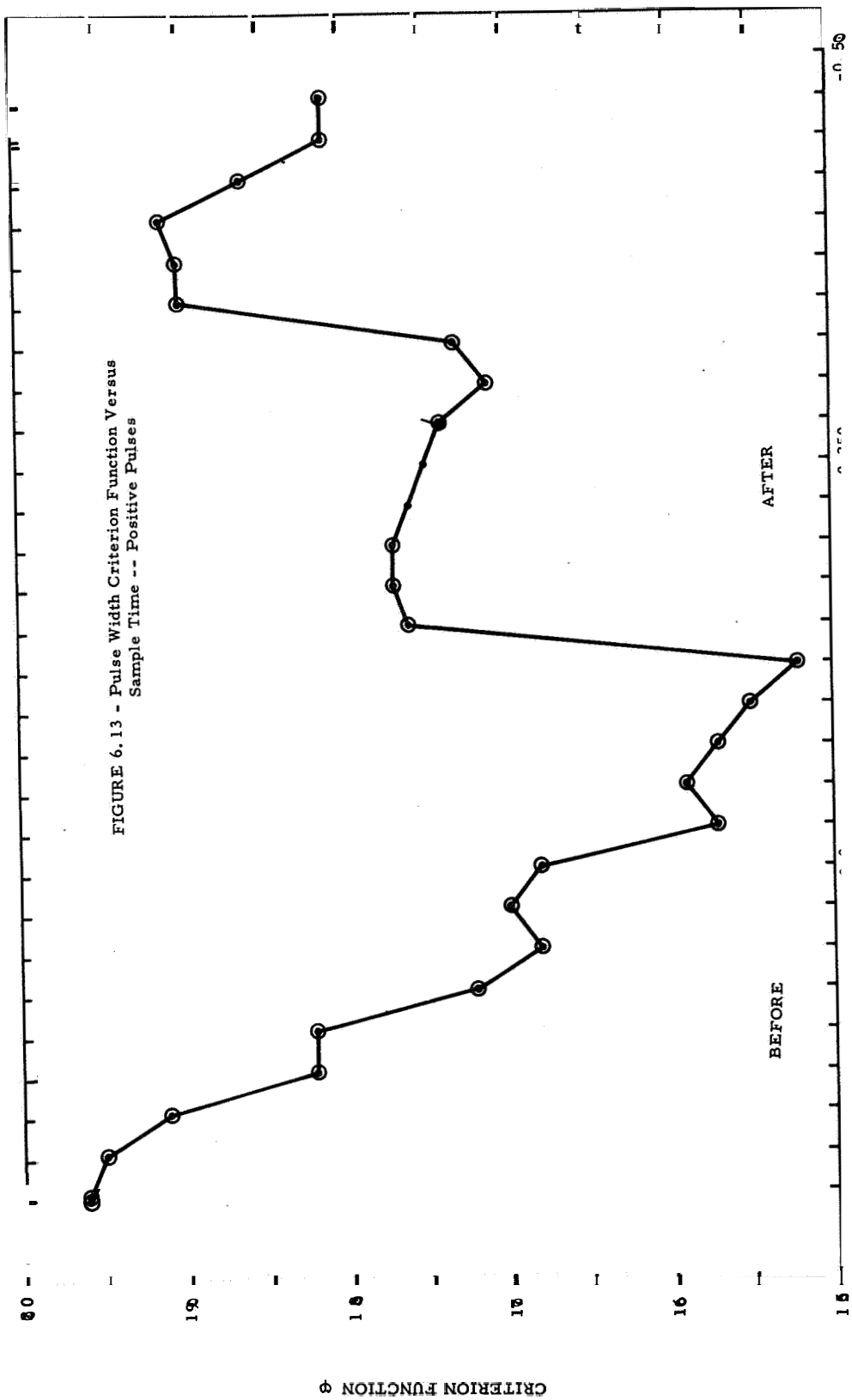

FIGURE 6.13 - Pulse Width Criterion Function Versus Sample Time -- Positive Pulses

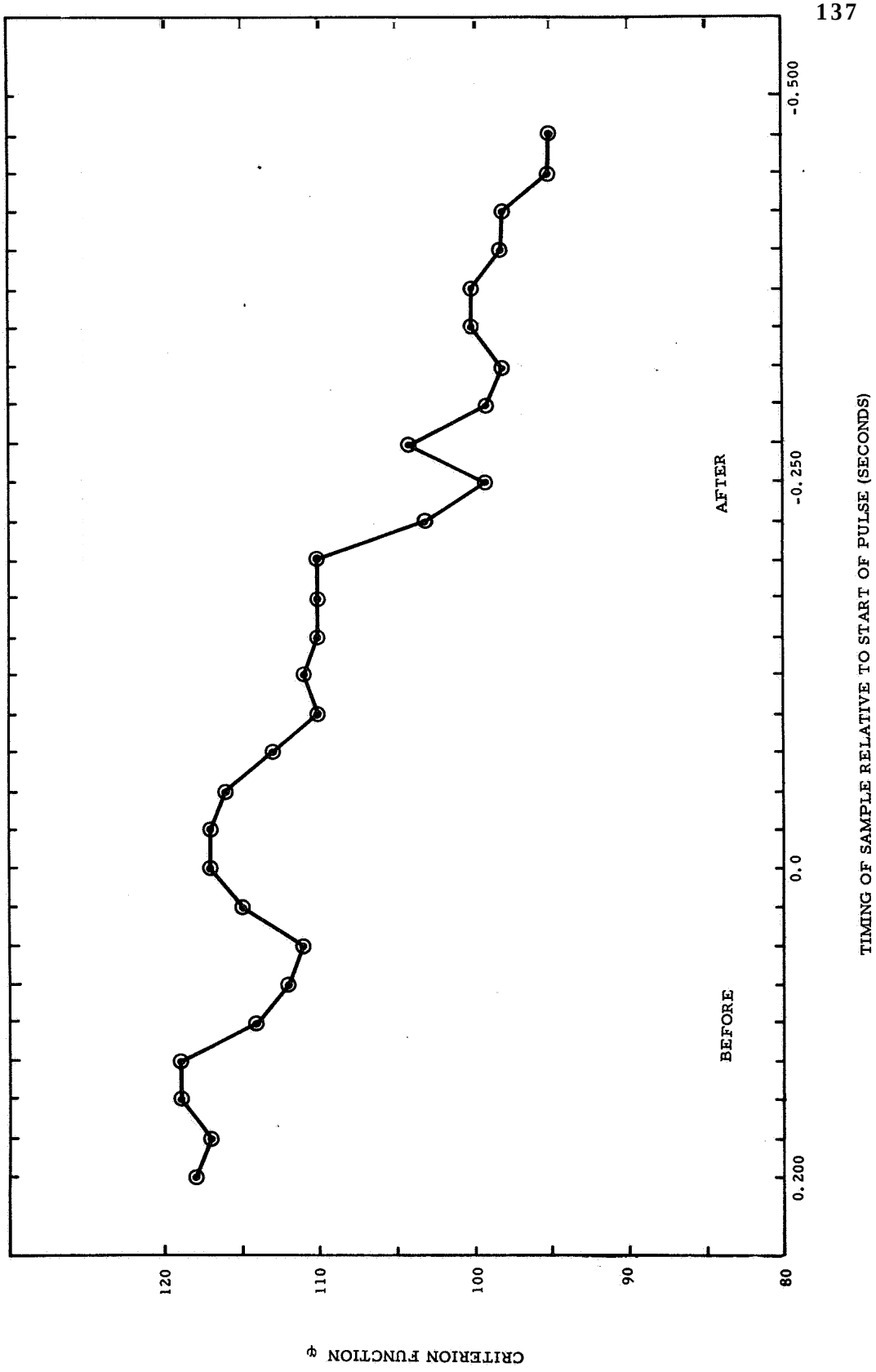
CRITERION FUNCTION φ
120
110
100
90
80
0.200
0.0
-0.250
-0.500
BEFORE
AFTER
TIMING OF SAMPLE RELATIVE TO START OF PULSE (SECONDS)

could be constructed by utilizing four PDE's two for preview- and two for precise control.

TABLE 6.1

Optimal Coefficient Values For The Pulse Amplitude and Pulse Width Models

Coefficient	Pulse Amplitude Model		Pulse Width Model	
	+Pulses	-Pulses	+Pulses	-Pulses
a_0	20.6	-16.7	0.897	0.774
a_1	-0.224	0.771	-0.001	-0.011
a_2	0.242	0.701	-0.33	0.012
a_3	0.037	-1.115	0.016	0.030
a_4	0.084	-0.535	0.017	-0.006
a_5	1.362	1.549	-0.039	-0.001
a_6	2.509	-1.066	-0.108	0.007
a_7	4.301	1.123	-0.030	-0.018
a_8	0.487	-1.854	0.062	0.002
a_9	-1.434	0.475	0.102	0.010
a_{10}	-4.812	-.3466	-0.119	0.070
a_{11}	-1.660	0.668	-0.072	-0.027
a_{12}	4.655	-2.308	-0.016	0.050
a_{13}	-1.403	0.030	0.096	-0.0901
a_{14}	1.486	-3.009	0.001	-0.007

In all four curves, there are minimums near the actual pulse initiation ($\tau=0$). If these minimums are selected rather than the ones occuring well after the pulse initiation a simpler model is obtained. These results are summarized in Table 6.2.

TABLE 6.2

	Polarity of Pulse	τ (sec)	θ min
Pulse Amplitude PDE	+	0.150	59
	-	-0.075	157
Pulse Width PDE	+	-0.075	155
	-	+0.050	111

The optimal PDE coefficient vectors are shown in Table 6. 1. The effectiveness of the models may be seen from the plats of model output versus the actual event magnitude, Figures 6. 15-6. 17. As in the previous chapter, the positive pulse amplitude model correlates better with the experimental data than does the negative pulse amplitude model. The criterion function had values of 59 and 157 for the positive and negative pulses respectively. It w-as hypothesized in section 5. 4. 1 that this asymmetry resulted from the use of separate muscle groups for the two directions of hand motion.

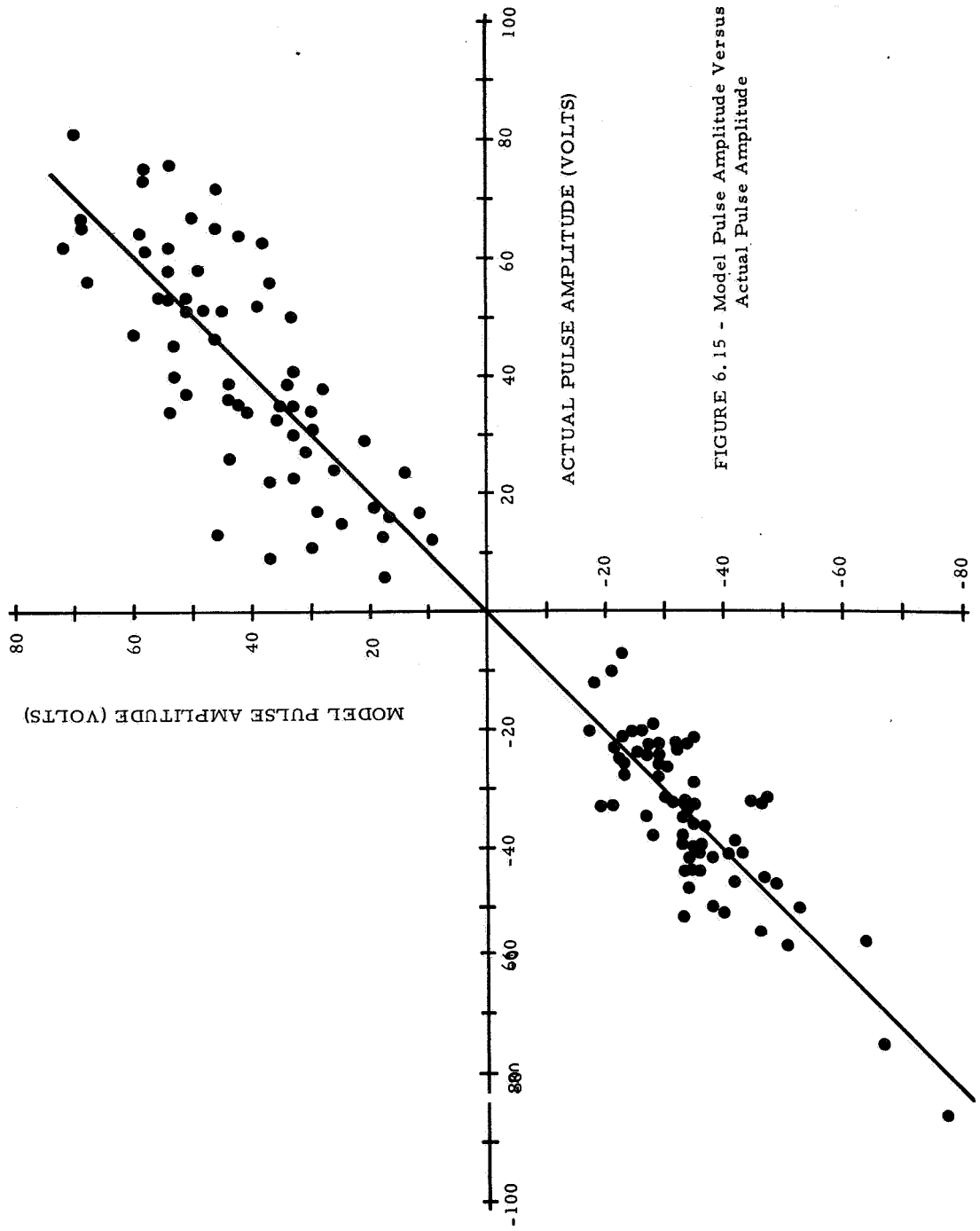

FIGURE 6.15 - Model Pulse Amplitude Versus Actual Pulse Amplitude

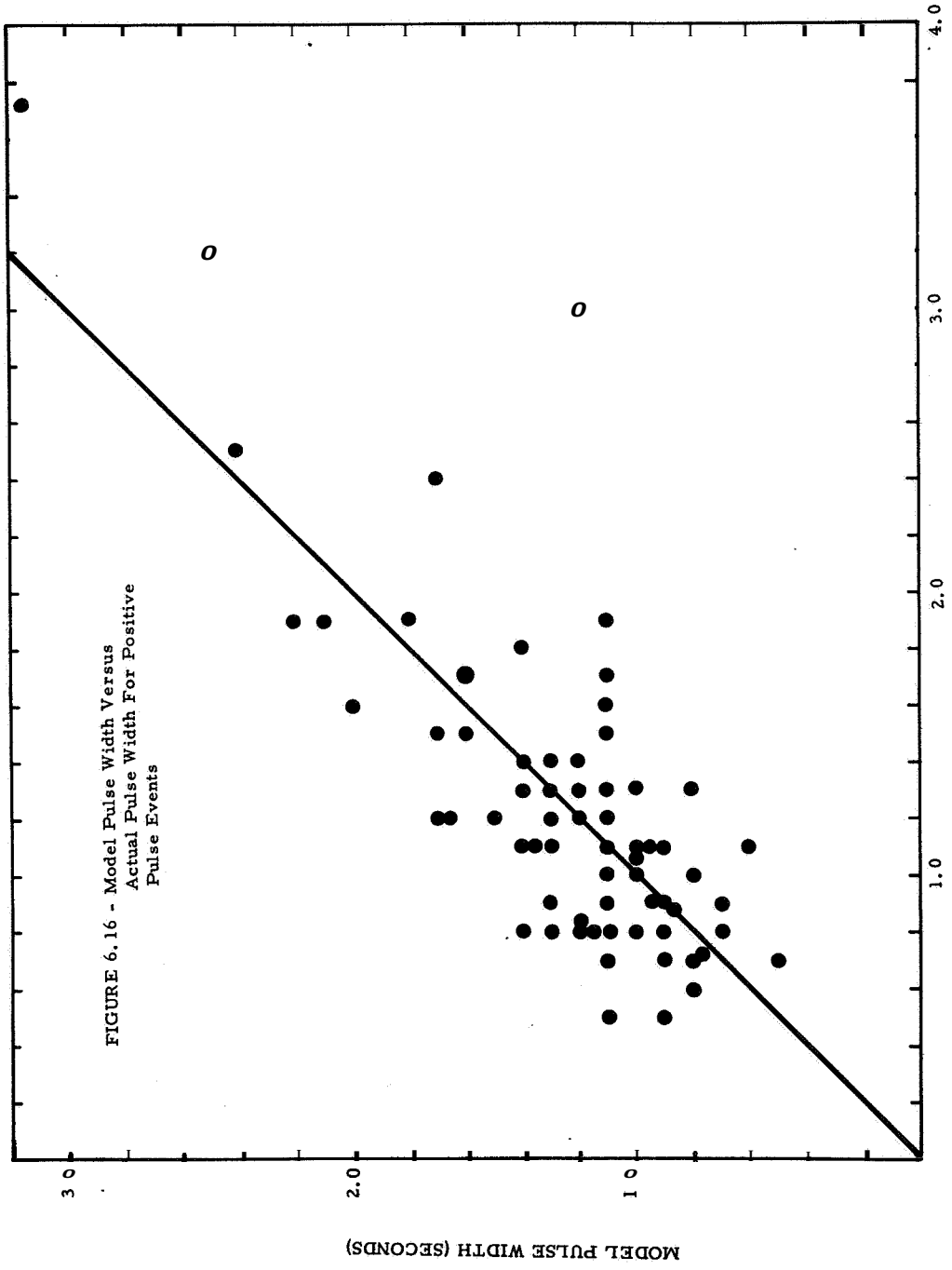

FIGURE 6.16 - Model Pulse Width Versus
Actual Pulse Width For Positive
Pulse Events

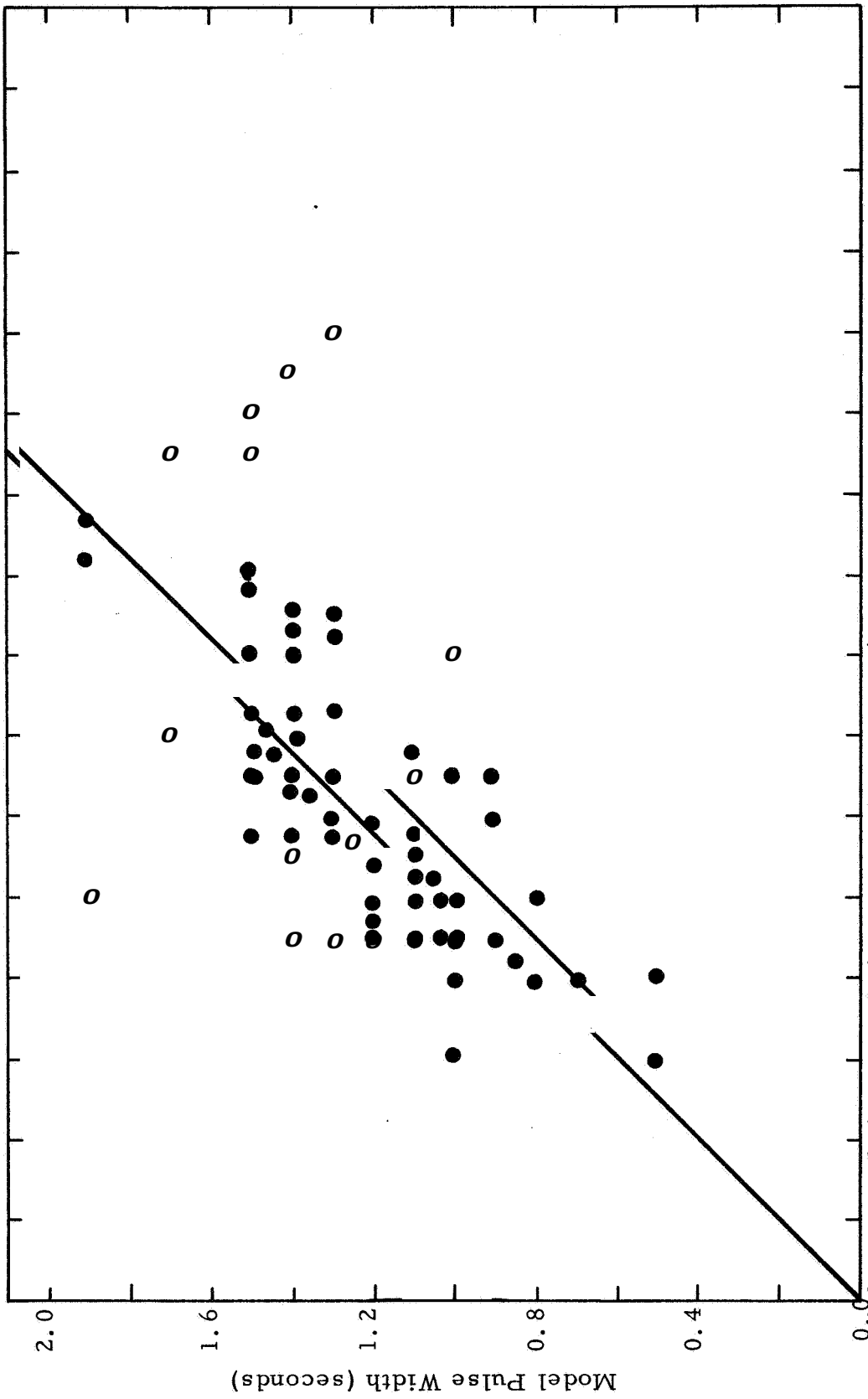

FIGURE 6.17 - Model Pulse Width Versus Actual Pulse Width For Negative Pulse Events

The pulse width scatter plots, Figures 6. 16 and 6. 17 are also asymmetric, the criterion function values are 157 and 111 for positive and negative pulse events respectively. This is just the reverse of the pulse amplitude model results. Further study is required to evaluate this phenomena.

The negative pulse amplitude PDE and the positive pulse width PDE sample the Operator Input 75 miiliseconds after the pulse is initiated.

This results in a more complex model than is desired here, as another set of decision elements must determine in what direction the control action is to be started. A compromise might be achieved by causing all of the PDE's to sample 50 milliseconds prior to the pulse initiation. Whether the compromise is necessary depends on the goals of the study. The goal here is to utilize decision elements to model discrete human operator behavior. Either type of model could be constructed.

6. 8 Pulse Initiation Model

It was hypothesized that the decision to initiate a pulse occured when the event trajectory crossed a decision surface in the space formed by e, $\dot{e}$, θ, $\dot{\theta}$. This is easily modeled by an MSDE.

In Chapter 5 an MSDE was used to model the decision to initiate a pulse, The structure of the MSDE and the selection of the components of the input vector w-ere based on an inspection of typical phase plane trajectories. The dimensionality of the task at hand precludes the use of graphical or intuitive methods for selecting the shape or even the approximate starting positions of the decision surfaces.

The MSDE must locate regions of the phase space w-hich are associated w-ith pulse initiations. The MSDE's input vector is derived from the Operator Input time history w-hich is generated by the scanning and signal processing system shown in Figure 6.9.

The MSDE actually makes two decisions. The first is the decision to initiate a pulsatile control action, the second is the selection of a pulse polarity. Two MSDE's can be used, one to initiate positive pulse events and the other to initiate negative pulse events. It is possible to add more decision elements to initiate preprogrammed pulse sequences.

The MSDE described below- w-as identified using the time history of the Operator Input prior to negative pulse events. A complete study w-ould require the identification of another MSDE for positive pulse events. Only one of the MSDE's is identified here, and it is assumed that the other could be identified by the same procedure

6. 8. 1 An MSDE Pulse Initiation Model

An MSDE containing three hyperplanes is shown in Figure 6. 18.

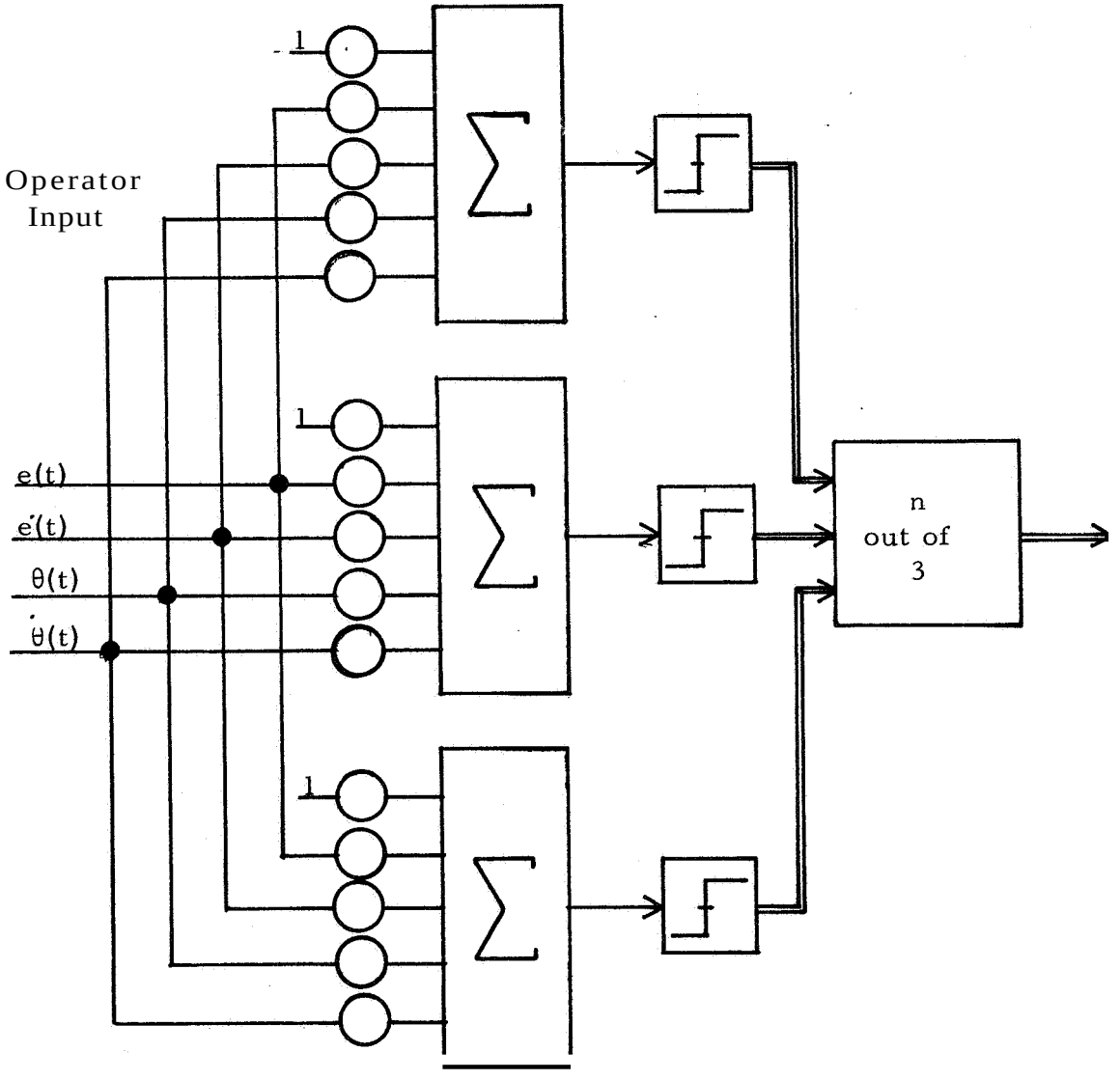

Figure 6. 18 Pulse Initiation MSDE

If the MSDE models the operator's covert decision, then its output should lead the actual time of initiation. The variation of the lead times should be a minimum. This formalized by defining

$$\tau_{AVE} = \frac{1}{N-M} \sum_{i=1}^{N-M} (t_i - t_{mi}) \qquad (6.5)$$

where t_i and t_{mi} are the times of the actual pulse initiation and the model output respectively, N is the total number of pulse events studied. If no output is produced before the actual pulse initiation is reached, the pulse has been missed and M is the total number of such pulses. The criterion function is:

$$\phi = K_1 \tau_{AVE} + \frac{K_2}{N-M} \sum_{i=1}^{N-M} (t_i - t_{mi})^2 + K_3 M \qquad (6.6)$$

The second term is the variance of the lead times. A numerical value of ϕ is obtained for particular values of the MSDE's coefficient vector, a, by applying the successive samples of the input vector to the MSDE until one of two things occurs. Either the MSDE generates an output, in w-hich case t_{mi} is recorded, or the time of the actual initiation is reached in which case M is incremented. The transient input vector is not scanned continuously. As soon as the MSDE generates an output, the scanning is stopped and resumed at the end of the pulse event being studied.

The procedure is summarized in Figure 6.19.

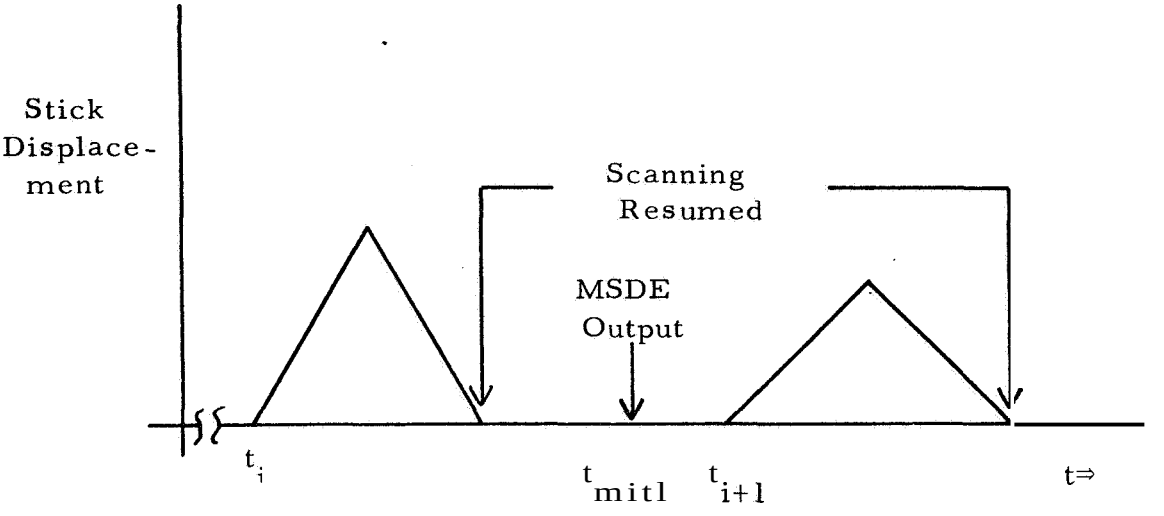

Figure 6. 19 Scanning Procedure For MSDE Identification

Approximately 20% of the pulses were separated by less than 200 milliseconds. In those cases scanning was begun 30 samples prior to the actual time of initiation. The results of the preceding chapter indicate that these pulses are probably part of pre-programmed sequences. A decision element which models both times of initiation and the number of pulses in the sequence is too complex to be considered here. The development of such models represents a necessary extension of this work.

6.8.2 On The Decoder

In Chapter 5, the structure of the pulse initiation MSDE, including the decoder, was determined from a priori knowledge which

w-as summarized in Figure 5. 15. Since this is not possible here, an n out of N binary element is used. It is not possible to determine the best value of n beforehand, consequently systematic search is used.

Some intuitive feel for the effect of n on the resultant decision space generated by the MSDE may be obtained by considering a two input, tw-o decision surface MSDE. In Figure 6. 20a, two decision surfaces are show-n, N=2. If n=l out of 2, the MSDE produces an output when the event trajectory is above either of the decision surfaces, as shown by the shaded area in Figure 6. 20b. If n=2 out of 2, the MSDE produces an output w-hen the event trajectory is above both surfaces, as shown by the shaded region in Figure 6. 20c.

The choice of the parameter n has a major effect on the resultant decision volumes mechanized by the MSDE.

6. 8. 3 Computational Results

Starting values for the coefficient vector, a, w-ere obtained by testing 1000 sets of 15 uniformly distributed random numbers between -1 and +1. Those yielding the lowest criterion function were used as starting values for the adjustment algorithm.

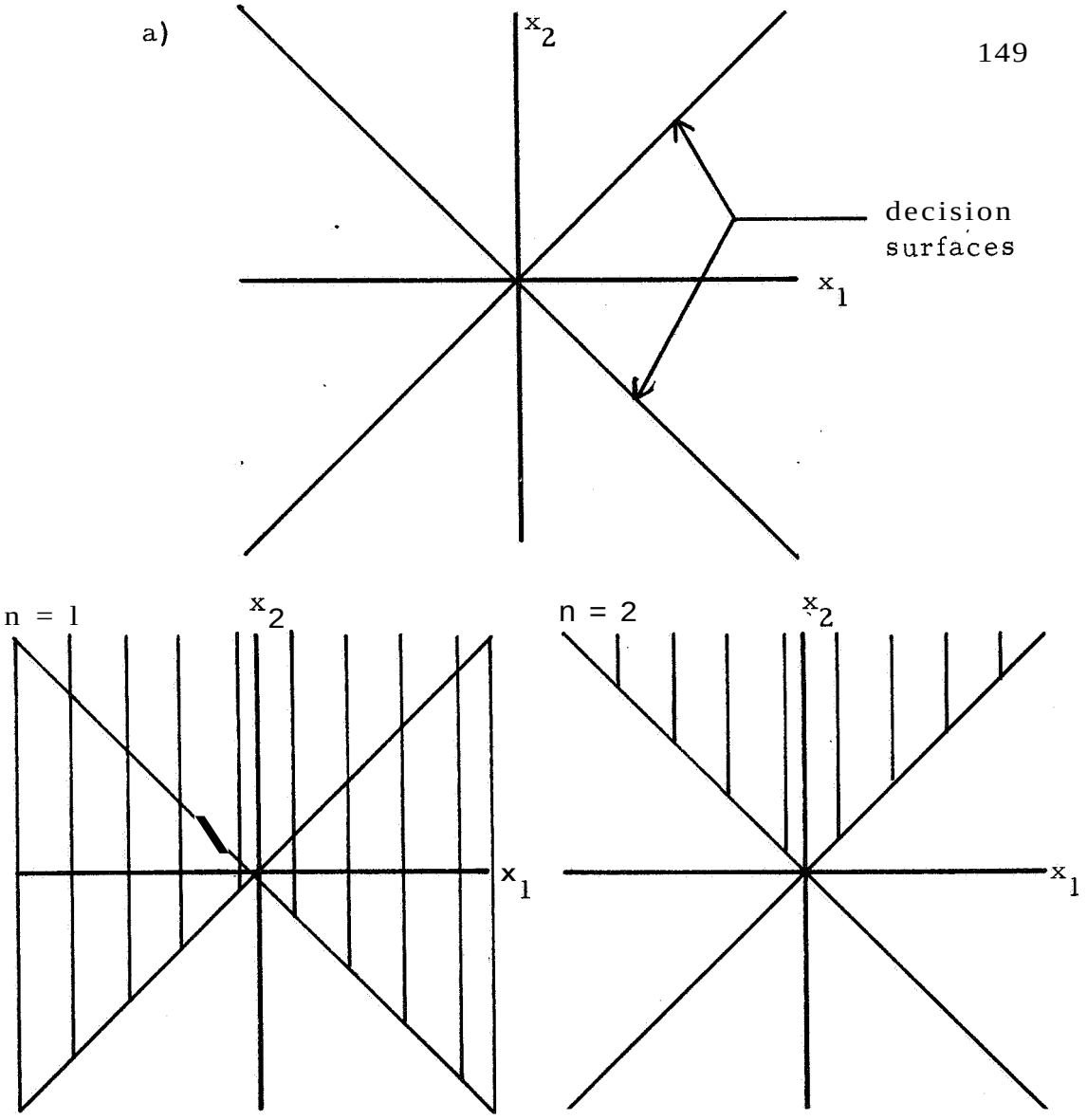

b) n t 1 (OR gate)

c) n = 2 (AND gate)

Figure 6.20 Effect Of The Decoder Parameter, n

The weighting factors, K_1, K_2 and K_3 appearing in the criterion function, equation 6.6, were selected such that all three terms contributed equally to its magnitude.

The computational results are summarized in Table 6. 3.

TABLE 6.3

n	Missed Events	τ (samples)	Variance of Lead Times
1	*	*	*
2	2	27	558
2	2	27	568
2	2	28	550
3	4	31	1295
3	4	28	1387
3	2	35	2314

* 1400 sets of random coefficients produced no acceptable starting conditions.

As seen in Table 6. 3, optimal results are obtained for n=2. Except for small differences in the lead time and variance, the results are almost identical. The lead time distribution functions are plotted in Figure 6.21. A large peak is observed in all three functions 30 samples prior to the actual pulse initiation. This results from artificially extending the Operator Input records of pulses spaced less than 200 milliseconds apart. The decision element produces an output as soon as scanning is resumed, on the first sample of these 30 sample sequences. This is a further

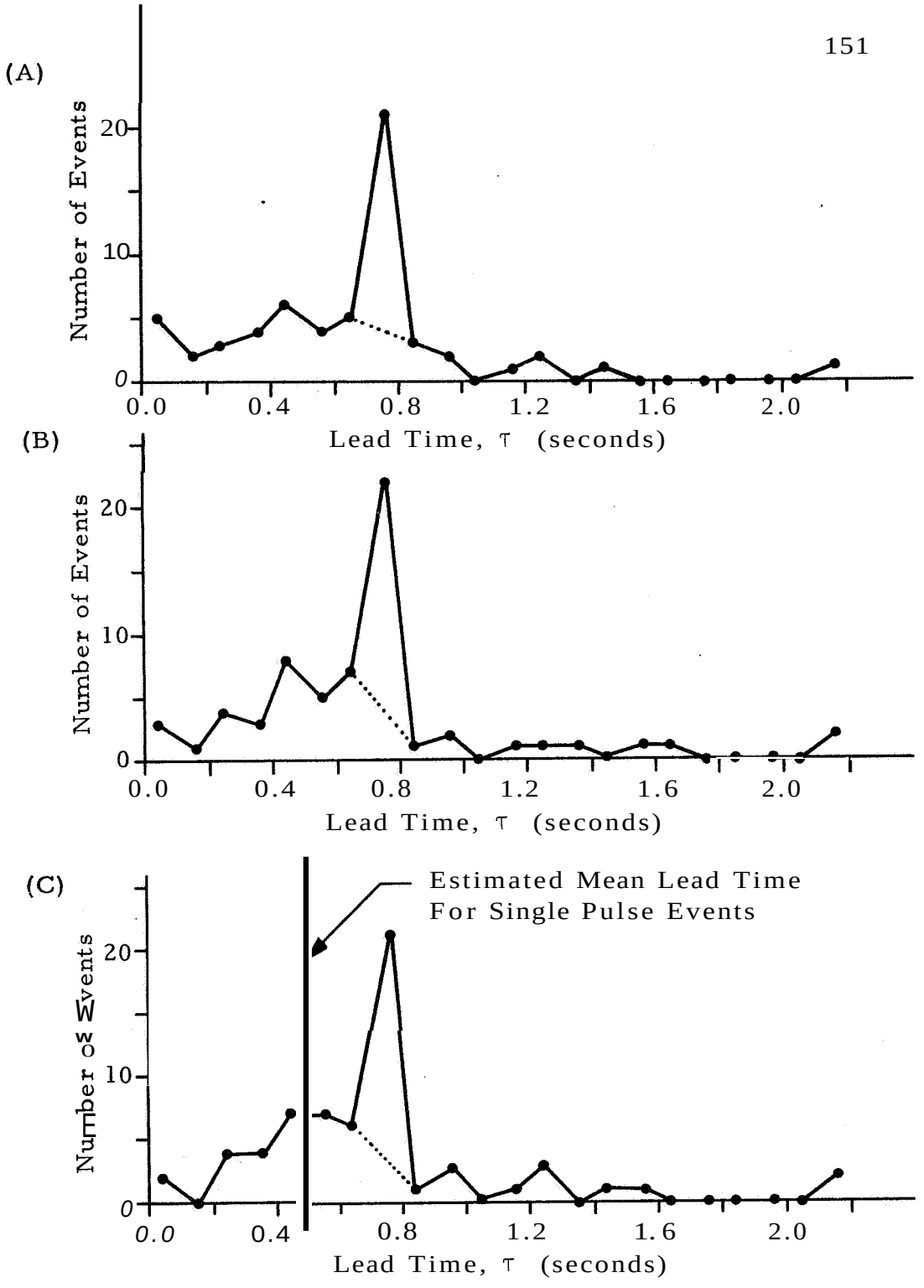

FIGURE 6.21 - Distribution Functions of Lead Times For Three MSDE's

argument that these pulses are part of preprogrammed pulse sequences. These pulses may be removed from consideration by interpolating between adjacent data points, as shown by the dotted lines in Figure 6.21. Although all three models exhibit similar criterion functions, the distribution function of Figure 6.21c best approximates a normal distribution about a mean lead time of 20 samples. The final model does not accurately represent closely spaced pulse events. Additional decision elements are required to represent these pulses.

The resultant negative pulse initiation MSDE leads the actual initiation of the pulse event by 500 milliseconds. This is substantially longer than the lead time found in the single display experiment of Chapter 5, of 200 milliseconds. This may result from the increased complexity of the control task or the need for scanning betw-een display devices.

Attempts w-ere made to add a fourth hyperplane to a partially identified MSDE. No improvement over the results described above were obtained.

6.8.4 A Logical Pulse Initiation Model

Although the results above are technically satisfying, they do not yield a great deal of insight into the operator's mentalprocesses.

It is difficult to obtain a geometric interpretation of six dimensional surfaces.

A more intuitive approach is based on the hypothesis that the operator makes separate decisions in the two dimensional spaces $(\theta, \dot{\theta})$ and $(e, \dot{e})$. An MSDE is easily constructed, as shown in Figure 6.22. The input vectors are formed from the Operator Input record.

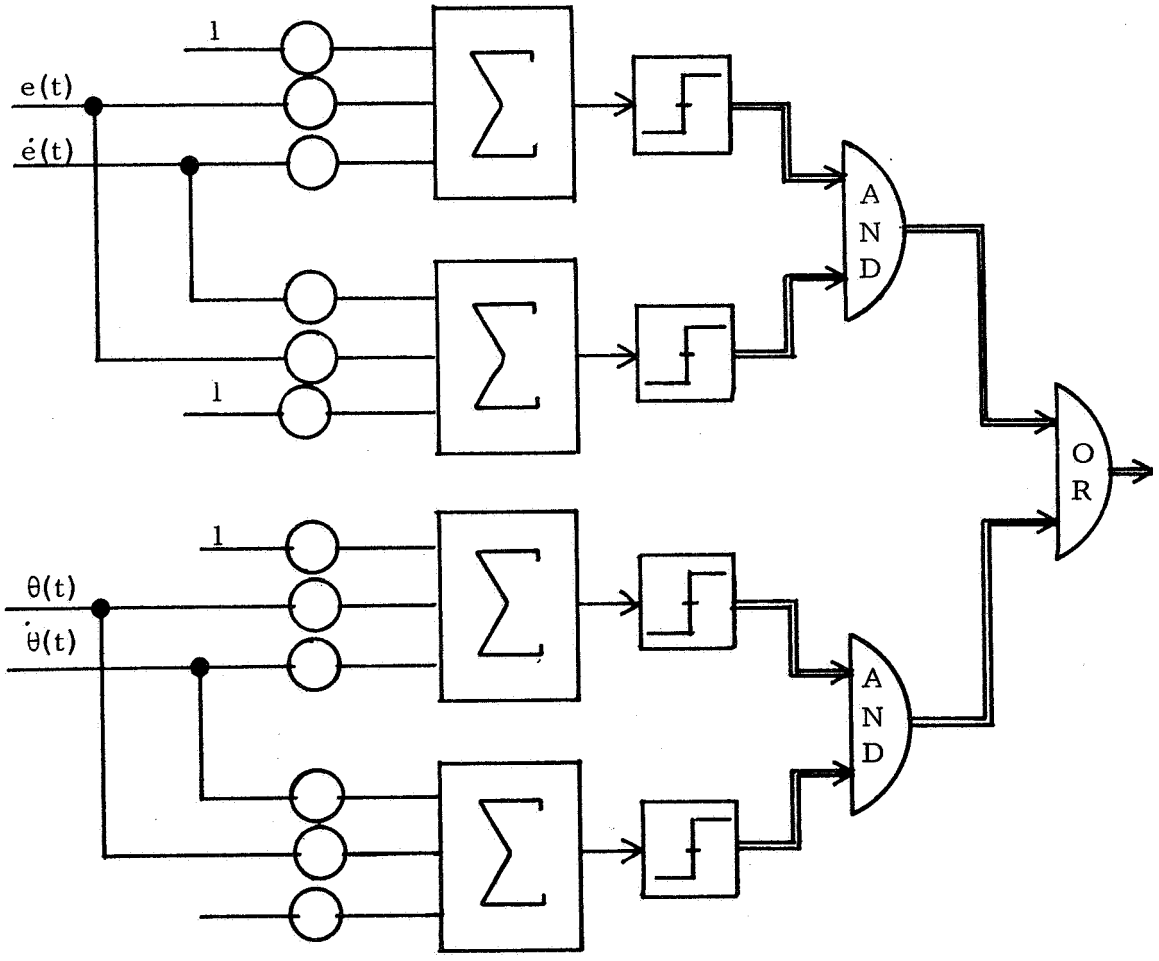

Figure 6.22 Logical MSDE

The advantage in this structure is that the decision surfaces become lines on a two dimensional phase plane.

Starting conditions for the adjustment algorithm were obtained by random search. The computational results are summarized in Table 6.4.

TABLE 6.4

Summary of Computation Results Using Logical MSDE Model

Number of Missed Pulses	Lead Time, τ (# of samples)	Variance of Lead Times
4	24	953
3	25	1208
2	28	1316
2	27	1437
4	26	1272
5	26	1334

The best set of coefficients are those obtained from the first case in Table 6. 4. Using the coefficients from this case, the equations for the decision surfaces can be written

$$
\begin{aligned}
y_1 &= 0.710 - 1.0\theta + 7.0 \\
y_2 &= 0.318 + 0.43\dot{\theta} \; t \; 11.0 \\
y_3 &= 0.41e \; t \; 0.376 + 20.5 \\
y_4 &= 0.08e \; t \; 0.92\dot{e} - 10.0
\end{aligned}
\tag{6.7}
$$

$$
T(y) = \begin{cases} 1 & \text{if } y \geq 0 \\ 0 & \text{if } y \leq 0 \end{cases}
\tag{6.8}
$$

The output of the MSDE is defined by

$$
\bar{h} = T(y_1) \cdot T(y_2) + T(y_3) \cdot T(y_4)
\tag{6.9}
$$

The decision surfaces are easily drawn from these equations, and are shown in Figure 6.23.

The comparison between the results obtained with the original MSDE and those obtained using the logical MSDE are shown in Table 6, 5.

TABLE 6.5

Comparison of Best MSDE Results

	Number Of Missed Pulses	τ (# of samples)	Variance
Original MSDE	2	27	558
Logical MSDE	4	24	953

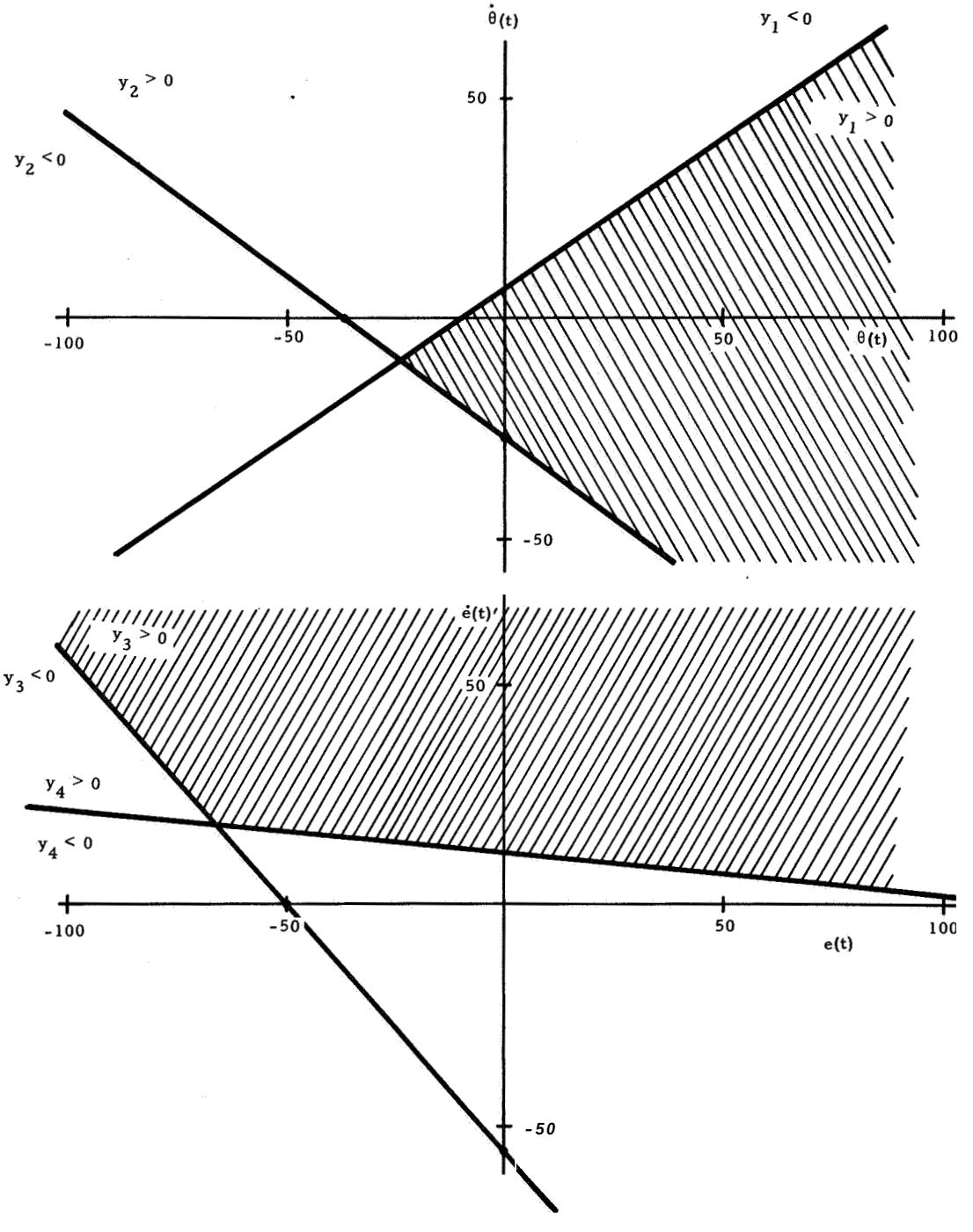

FIGURE 6.23 - Logical MSDE Decision Surfaces

The values of τ are not, in themselves, significant. The original MSDE missed 2 pulses less and produced a smaller variance about the lead time than did the logical MSDE.

The advantages of the Logical MSDE may overshadow- the differences in results. The original MSDE was constructed w-ithout using a priori knowledge, and required the identification of 15 parameters. The Logical MSDE contained only 12 parameters, while placing severe restraints on the class of decision surfaces that could be investigated. In this example, the results indicate that the restrictions do no significantly affect the modeling of the human operator's pulse initiation behavior. Further, know-ledge of human operator behavior allows the investigator to add dead zones to the phase planes and, in general, extend the models. The original MSDE is not easily extended.

6. 9 Eye Motion Decision Model

The control task selected was such that the operator required information from both displays in order to operate the control system Since the two displays w-ere w-ell separated the operated commutated between them.

The commutation consisted of rapid motion betw-een and fixations on the displays. The eye motion time history may be broken

up into four phases:

1) view-ing left display

2) view-ing right display

3) moving from left to right

4) moving from right to left

The eye motion time history was examined and the time (relative to the start of the run) of the beginning of each phase was determined. In all, 216 eye motion cycles, from left to right and back again, w-ere recorded. The distribution functions of the lengths of the four phases are shown in Figure 6.24-6.26. From these figures it can be seen that the left fixation intervals and right fixation intervals have similar shapes, with means ofapproximately 600 milliseconds. The transition phases are quite similar, withmeans of approximately 125 milliseconds.

6.9. 1 **An** MSDE Model

The decision to initiate an eye transition is assumed to be based on deterministic measures of the input available to the operator. If the deterministic measures take the form of decision surfaces in the operator's input space, then an MSDE may be used to model the decision process. The techniques described above for identification of the pulse initiation model are also suitable for this situation.

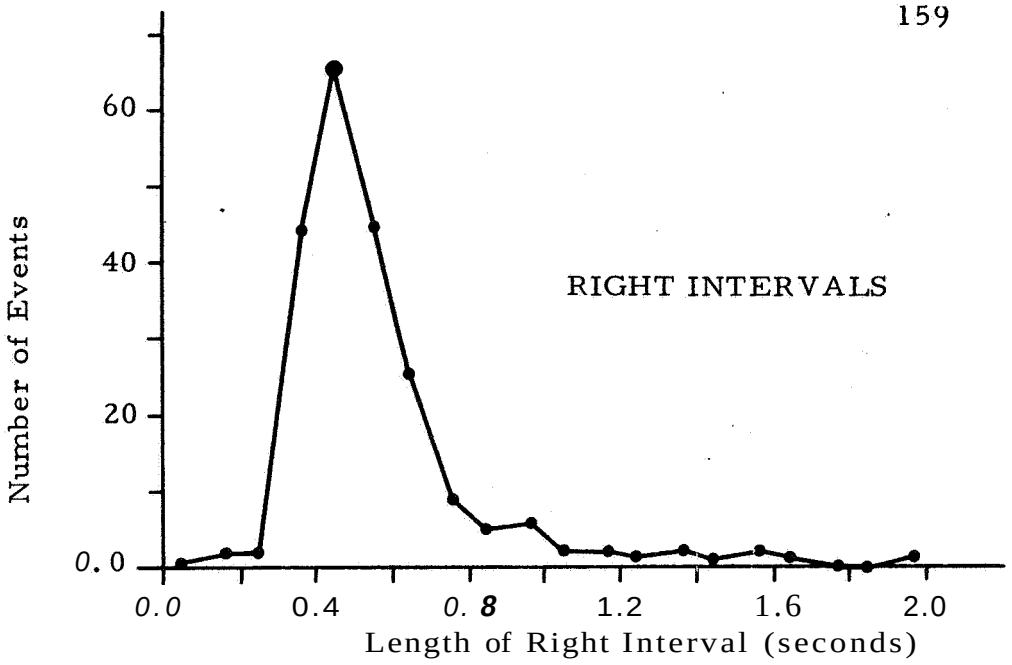

FIGURE 6.24 - Distribution Function Of Right Intervals

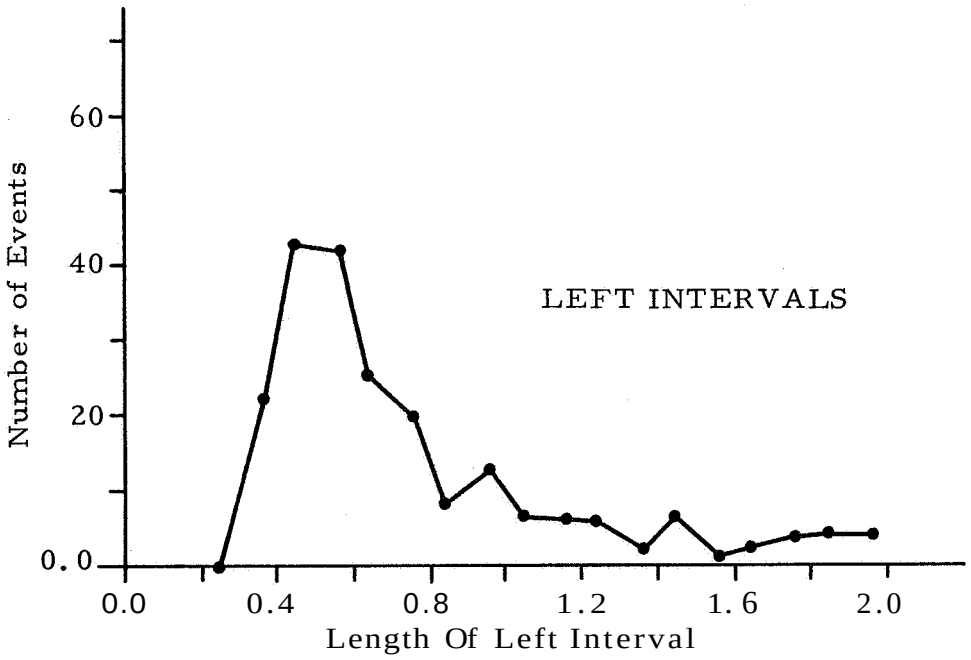

FIGURE 6.25 - Distribution Function of Left Eye Fixation Interval

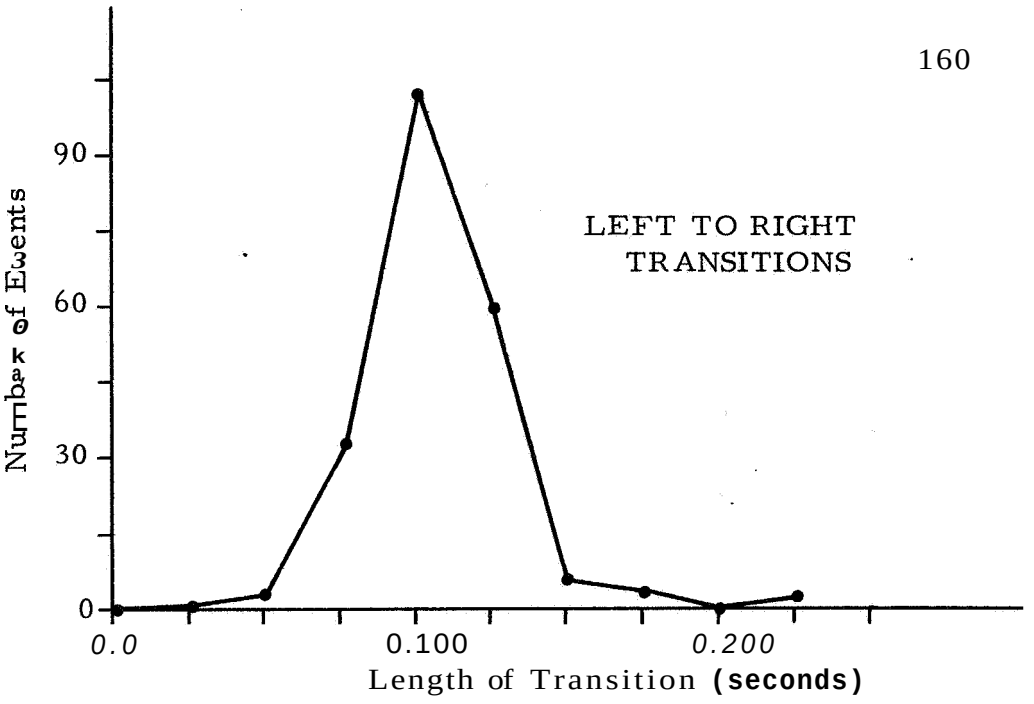

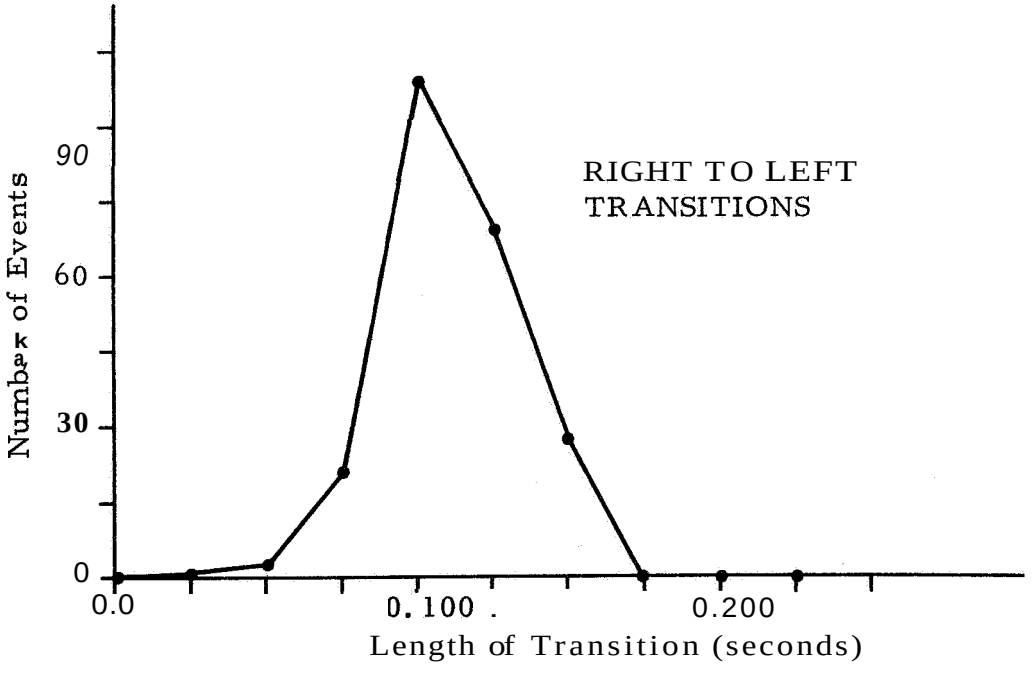

FIGURE 6.26 - Distribution Functions of Eye Motion Transitions

A thousand sets of 15 random coefficients were generated and tested in a three hyperplane MSDE. The twenty best sets were used as initial values in the adjustment algorithm.

In all cases, the resultant MSDE produced 80% or more of its outputs on the first sample after scanning was resumed. A typical MSDE produced no missed eye motion events, a mean lead time of 24 samples or 600 milliseconds, and a variance of 96. The small number of missed events and the small variance is of little consequence if all of the model outputs are produced on the first sample after scanning is resumed.

6.9.2 A PDE Model

The length of time the operator fixated on a display varied from a minimum of 100 milliseconds to more than three seconds. If the onerator computes the length of time to be spent viewing the next display, rathec than waiting until a decision surface is crossed, a PDE model may be constructed.

The PDE model assumed that once a transition is begun, the operator computes the fixation interval as eye motion towards the display is initiated. As soon as the time interval is exceeded, a transition is initiated and a new fixation interval computed. Samples of the operator's input were obtained starting midway in the eye

transition and proceeding for nine more samples. The PDE model takes the form:

$$f_i = a'x(t_i - \tau) \tag{6.10}$$

where f_i is the length of the ith eye fixation, t_i is the time at which the fixation began, a is a vector of unknown coefficients and τ is a time delay to be determined.

The first input vector corresponded to a four dimensional power series:

$$\begin{aligned}
x_0 &= 1.0 \\
x_1 &= \theta(t_i - \tau) \\
x_2 &= \theta(t_i - \tau) \\
x_3 &= e(t_i - \tau) \\
x_4 &= \dot{e}(t_i - \tau) \\
x_5 &= x_1^2 \cdot 0.01 \\
x_6 &= x_2^2 \cdot 0.01 \\
x_7 &= x_3^2 \cdot 0.01 \\
x_8 &= x_4^2 \cdot 0.01 \\
x_9 &= x_1 x_2 \cdot 0.01 \\
x_{10} &= x_1 x_3 \cdot 0.01 \\
x_{11} &= x_1 x_4 \cdot 0.01 \\
x_{12} &= x_2 x_3 \cdot 0.01 \\
x_{13} &= x_2 x_4 \cdot 0.01 \\
x_{14} &= x_3 x_4 \cdot 0.01
\end{aligned} \tag{6.11}$$

For fixed values of τ, the optimal coefficient vector, a, and the resultant value of the criterion function were computed by the procedure described above in Chapter 4. The results of this computation for RIGHT fixation intervals are presented in Table 6.6. The LEFT fixation intervals could be modeled in the same way.

TABLE 6.6

τ (samples)	ϕ
0	.082
1	.084
2	.084
3	.083
4	.083
5	.083
6	.081
7	.081
8	.082
9	.081

Varying τ does not affect the results significantly. Since $\tau = 0$ produces a simple model, this value was selected as the optimal value. A scatter plot of the model eye fixation lengths,

versus the actual eye fixation lengths is found in Figure 6.27. This plot shows rather good correlation between the model and the actual lengths for short fixations. When the actual fixation length is greater than 800 milliseconds the model generated intervals of approximately 800 milliseconds. Attempts to remedy this situation by including squares, cubes, and inverse terms in the input vector produced no significant improvements in the model responses.

The scatter plot shown in Figure 6.27 is clearly based by the large number of long fixation intervals, which the model is incapable of generating. In order to determine the effectiveness of the model on short fixation intervals, *a* computer run was made w-hich deleted all events with fixation intervals greater than 800 milliseconds. The scatter plot which resulted is shown in Figure 6. 28.

The criterion function, the variance of the model error, w-as reduced from 0. 082 to 0.008. This corresponds to a standard deviation of 90 milliseconds, The scatter plot exhibits good correlation between the model output and the actual fixation time.

6.9.3 Dual PDE-MSDE Model

As soon as an eye motion interval is over, the operator begins commutating towards the other display. Halfway between the two displays, or possibly before if peripheral vision is utilized,

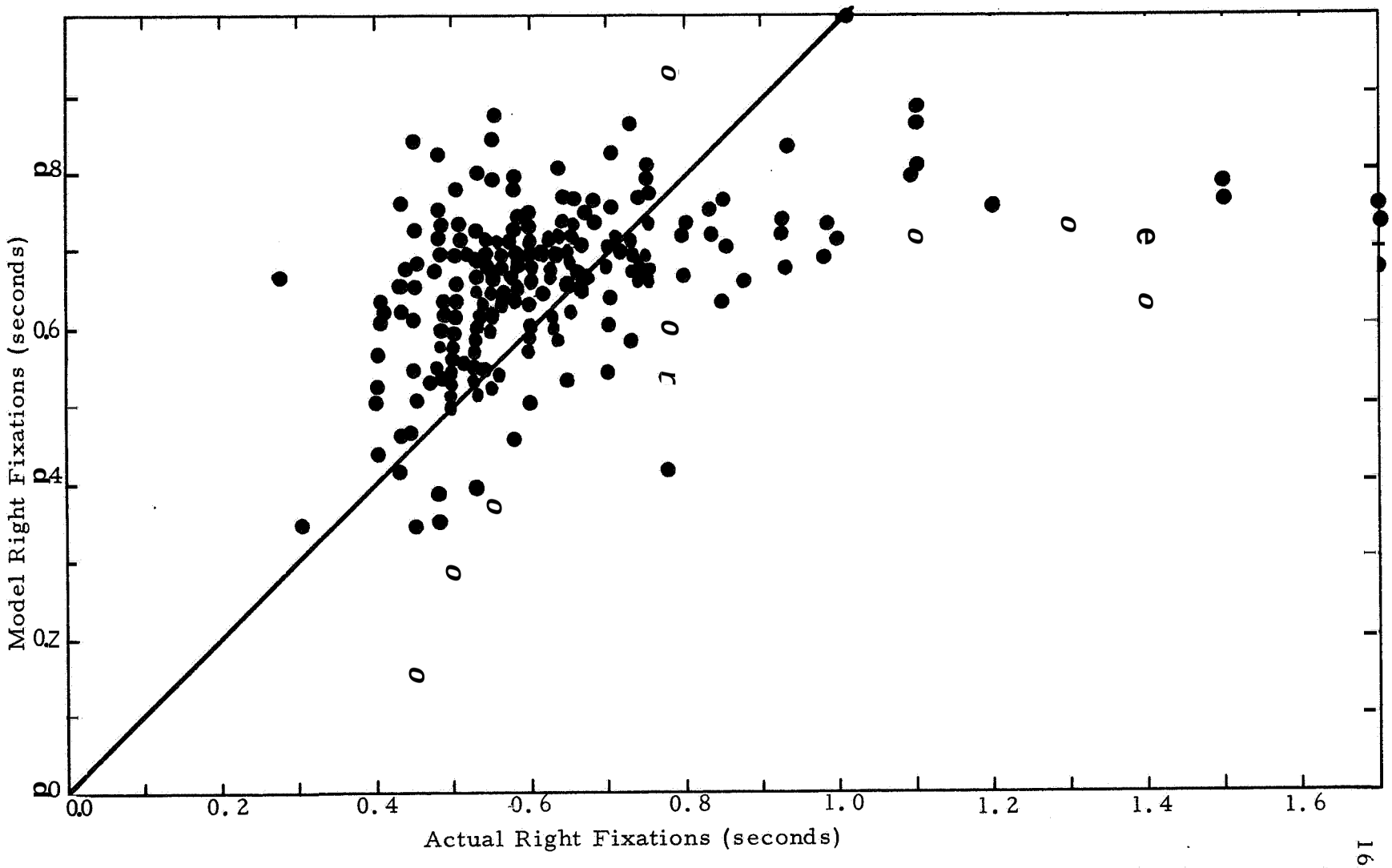

FIGURE 6.27 - Length of PDE Right Fixation Intervals Versus Actual Right Fixation Intervals

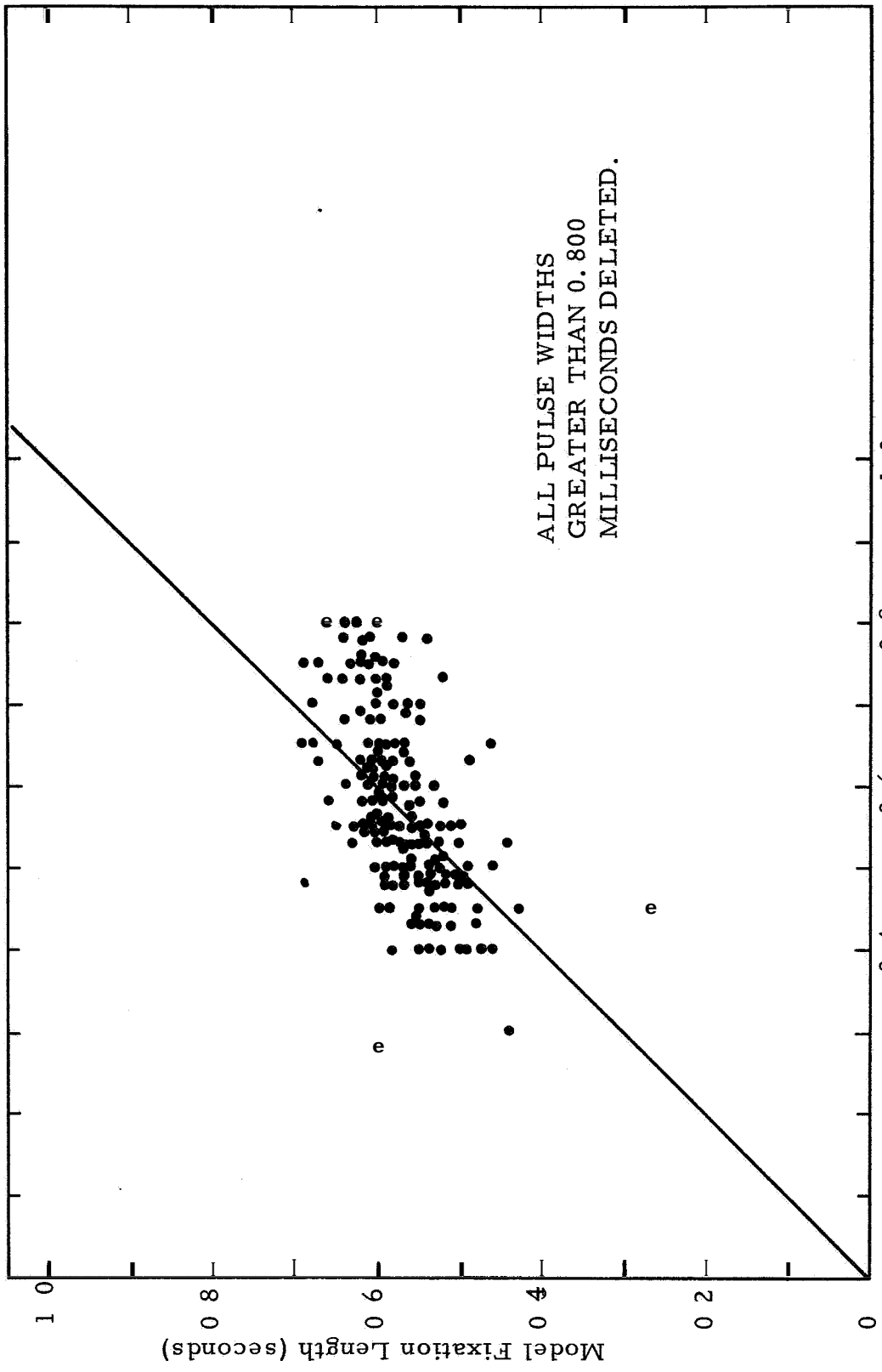

FIGURE 6 - Model Right Fixations Versus Actual Fixations

both display variables and their rates are available to the operator. Based on the available signals the operator determines how much time to allocate to the new display. At the end of this time the process is repeated, It seems apparent from the results described above that the decision concerning the amount of time to allocate to the new display is made by at least two processes. One decision process is used when rapid scanning is required and another decision process is used when more leisurely scanning will suffice. The resultant model structure is shown in Figure 6.29.

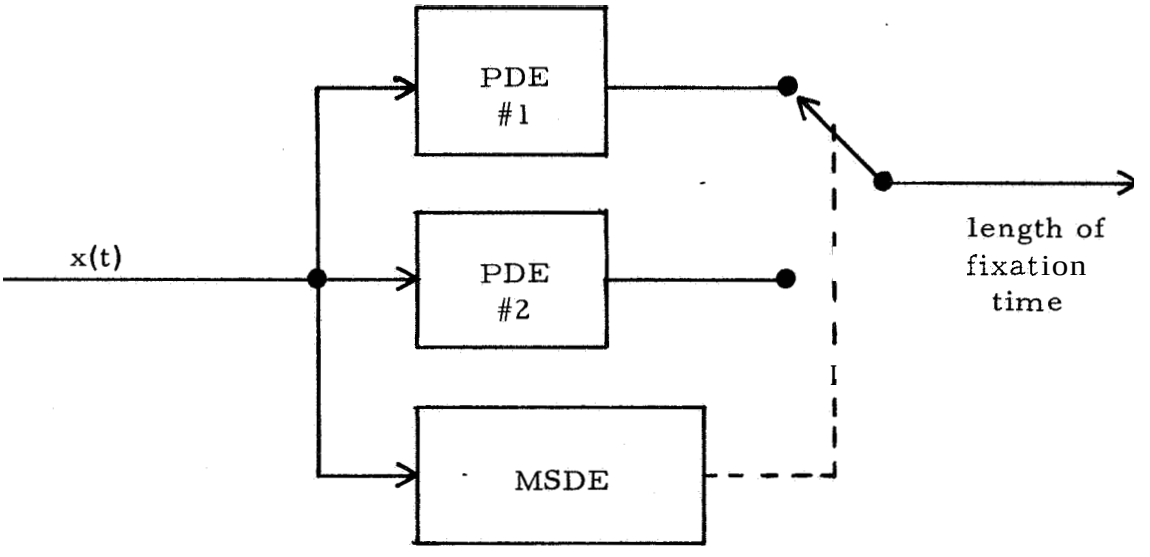

Figure 6.29 Dual PDE MSDE Eye Motion Model

An examination of the tracking record led to the hypothesis that "leisurely" tracking occurs in portions of the phase space where the generation of a pulse is unlikely. The results of the previous

chapter indicated that the operator did not initiate output pulses in the second fourth quadrants of the e, $\dot{e}$ phase plane. Further, where e, $\dot{e}$, θ and $\dot{\theta}$ are all sufficiently small, the operator does not initiate any pulsatile events. With this hypothesis in mind, the tracking records were examined. It was found that long fixation intervals occurred while the trajectory was inside the second and fourth quadrants if θ was large.

The MSDE used to determine whether the long or short fixation model was to be used is shown in Figure 6.30.

For fixed values of r_1 and r_2, the values of the inputs, θ, $\dot{\theta}$, e and $\dot{e}$ determine the output of the MSDE. This, in turn is used to determine which model the fixation interval is to be generated by. The two groups of fixation intervals are then modeled by a PDE.

This procedure yields two criterion functions and two scatter plots for each value of r_1 and r_2 selected. An overall criterion function may be defined as:

$$\phi = \frac{N_L \phi_L + N_S \phi_S}{N_L + N_S} \qquad (6.12)$$

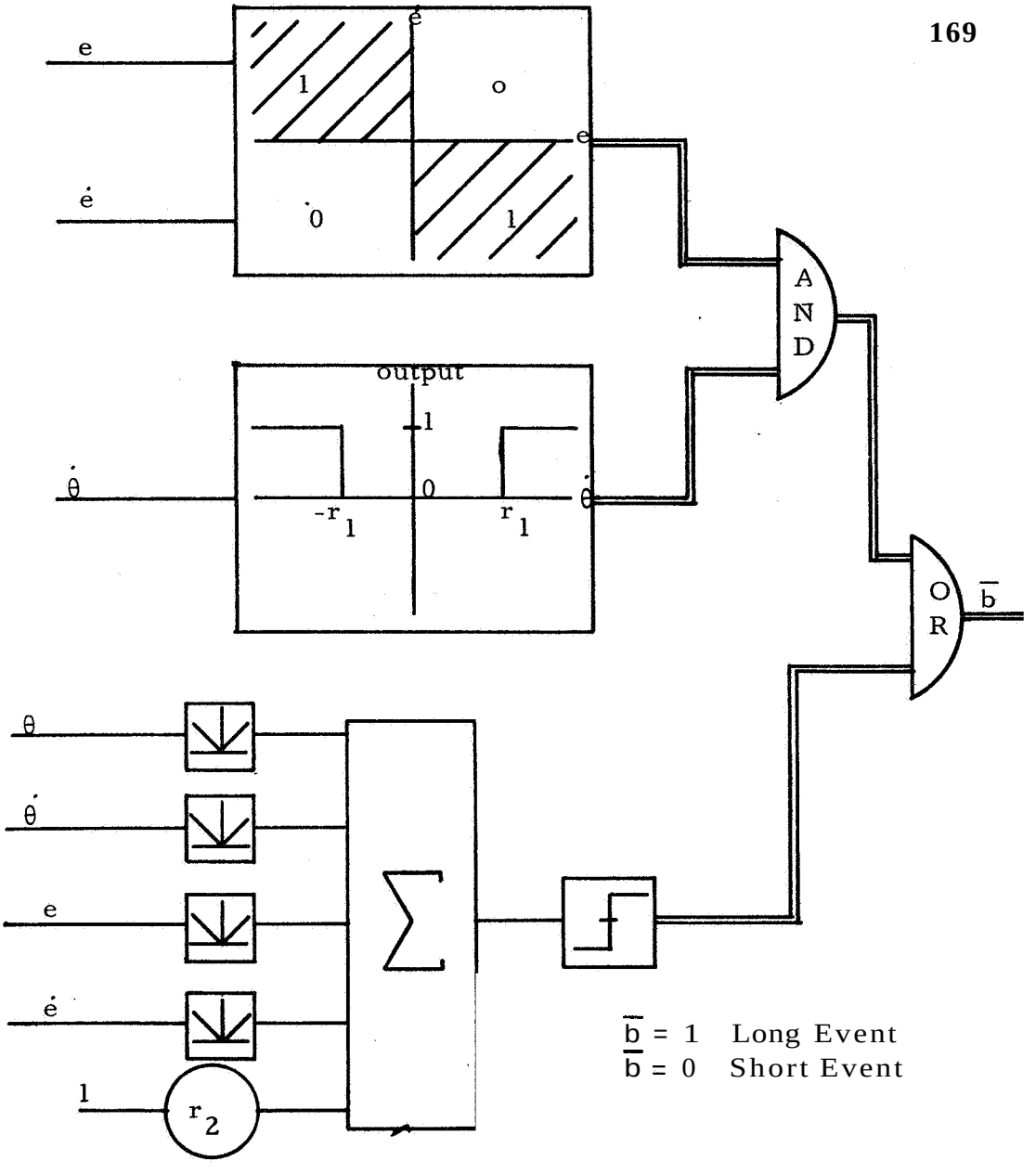

Figure 6.30 MSDE for Dual PDE, MSDE Eye Motion Model

where N_L and N_S are the number of events sorted into the long and short model groups, ϕ_L and ϕ_S are the criterion functions obtained for $\tau = 0$ for the long and short events respectively using the input vector defined in equation 6.4.

TABLE 6.7

$\Phi(r_1, r_2)$

r_2 \ r_1 ⇒	4	8	12	16	20
5	.077	.062	.066	.069	.070
10	.075	.060	.063	.067	.068
15	.074	.059	.062	.066	.067
20	.074	.059	.062	.066	.067
25	.074	.060	.062	.066	.067

Table 6. 7 summarizes the results obtained from a systematic study of r_1 and r_2. As can be seen from the table, the optimal parameter values are $r_1 = 8.0$ and $r_2 = 15.0$. Table 6.8 presents the optimum PDE coefficients.

The overall criterion function is 0. 059 which is considerably better than the criterion function of 0. 082 obtained using a single PDE. The separation of long fixation intervals from short ones is almost perfect, as seen from the scatter plots shown in Figure 6. 31 and 6. 32. There are 23 right fixation intervals lasting longer than 800 milliseconds, of these only 4 were generated by the short interval model.

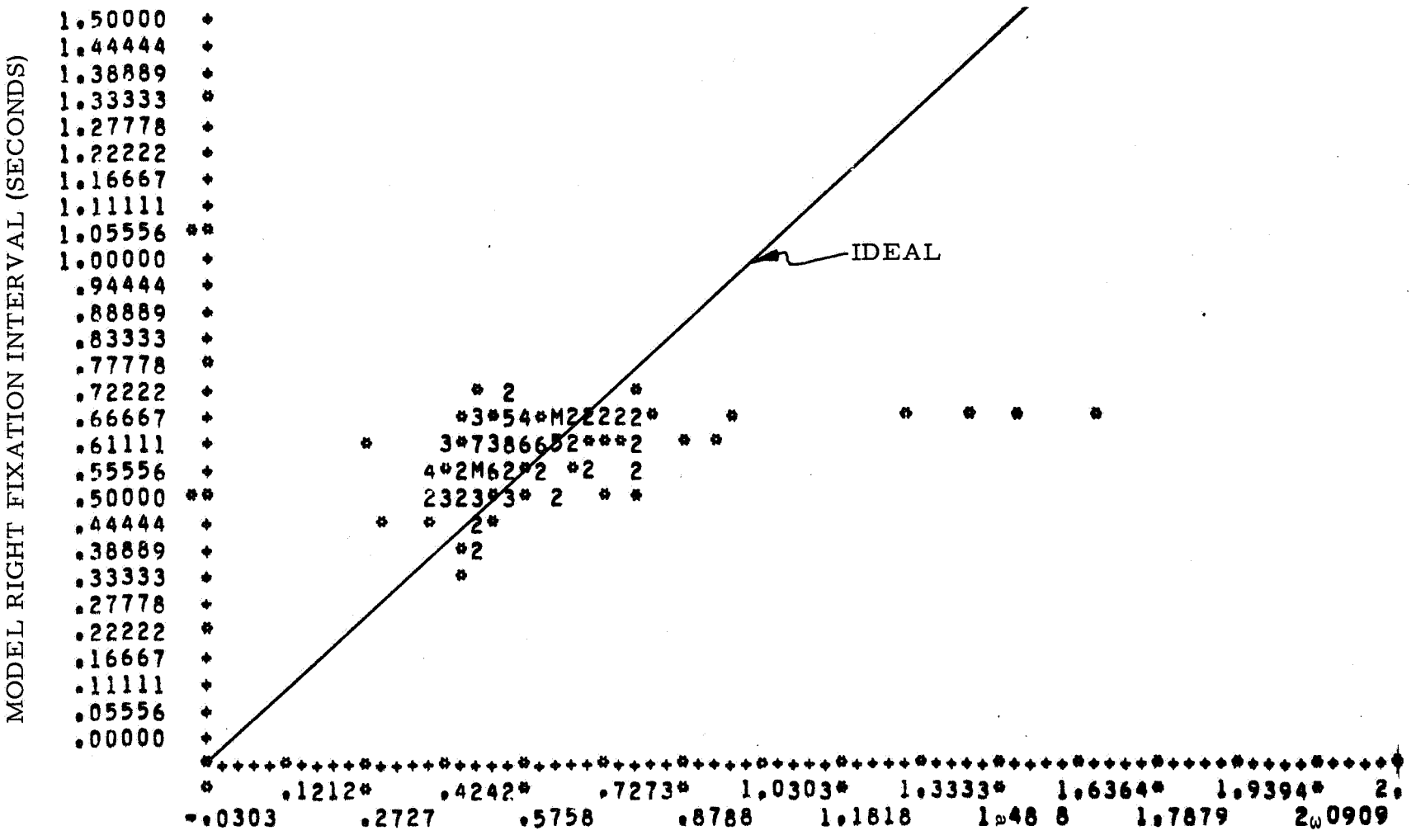

FIGURE 6.31-Model Fixation Length Versus Actual Fixation Length For RIGHT Display-SHORT PDE

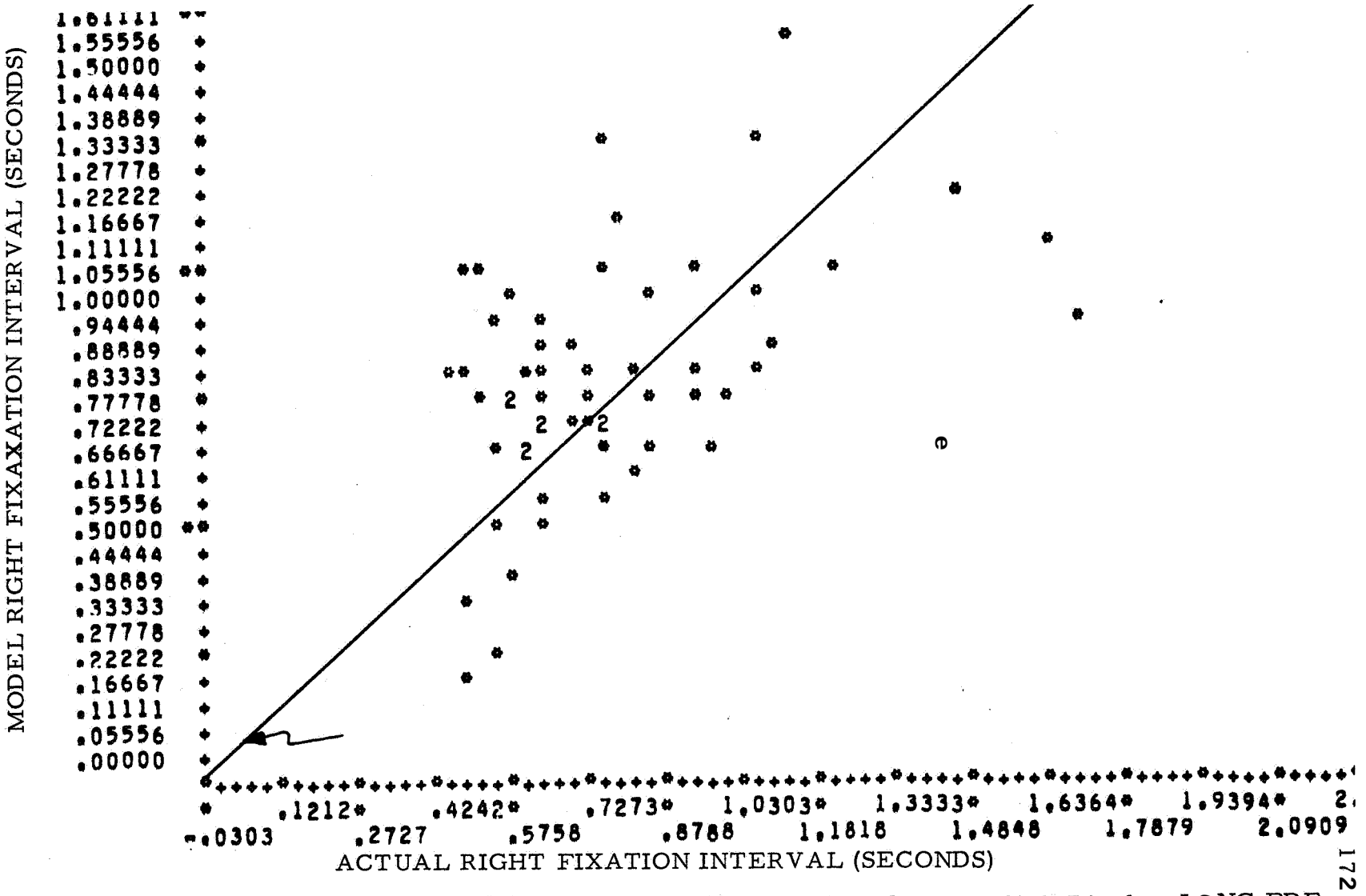

FIGURE 6 3Z-Model Fixation Length Versus Actual Fixation Length For RIGHT Display-LONG PDE

TABLE 6.8

Optimum PDE Coefficients

Input Components	Coefficient	
	Long Interval PDE	Short Interval PDE
1.0	-0.22	-0.011
θ	-0.037	-0.002
$\dot{\theta}$	0.009	0.001
e	-0.025	-0.001
$\dot{e}$	0.004	0.003
θ^2	0.281	-0.015
$\dot{\theta}^2$	-0.014	-0.002
e^2	-0.024	0.006
$\dot{e}^2$	0.429	-0.018
$\theta\ \dot{\theta}$	0.013	0.001
θ e	0.049	0.020
$\theta\ \dot{e}$	-0.247	0.011
$\dot{\theta}$ e	0.353	-0.010
$\dot{\theta}\ \dot{e}$	-0.050	-0.008
e $\dot{e}$	0.018	0.013

6.9.4 Summary Of Eye Commutation Model

The scatter plots for the RIGHT fixation intervals shown in Figure **6.31** and **6.32** indicate that the 2-PDE, MSDE model

outputs agree well w-ith the experimental data.

It is assumed that similar results may be obtained for LEFT fixation intervals.

The selection of the MSDE decison surfaces was based on intuition and an examination of the tracking records. This is an arbitrary procedure and there may be many surfaces which will yield better results. The purposes of this study are satisfied by finding one MSDE. The study of more complex decision surfaces is clearly a necessary extension of this work.

6. 10 The Complete Human Operator Model

The complete human operator model is obtained by combining the scanning and signal processing element of Figure 6. **9** with the models identified in sections 6. 7 and 6. 8. The basic structure is quite similar to the model developed in the previous chapter, Figure 5.20.

An MSDE continuously monitors the operator's input, when decision surfaces are crossed a pulse generation sequence is initiated. **A** delay occurs during which rapid eye motions may occur. At the appropriate times tw-o of the four PDE's sample and hold the amplitude and w-idth of the event to be generated, or being generated,

as some of the sampling operations may actually occur shortly after the initiation of the pulse. This timing sequence is summarized in Figure 6. 33.

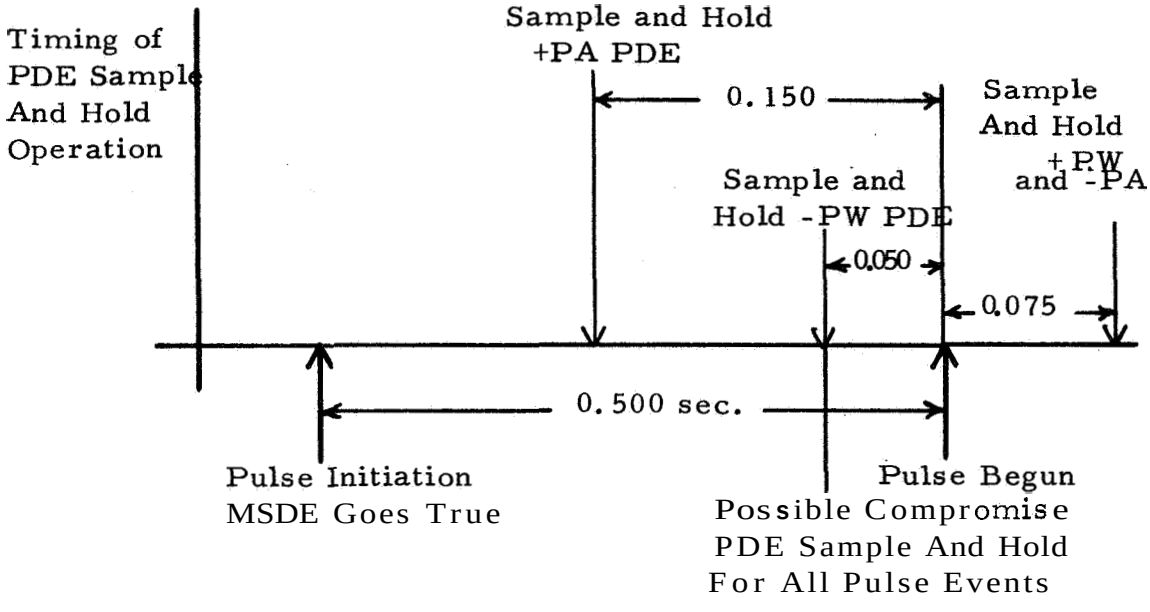

Figure 6. 33-Timing of PDE Control Signals

For simplicity, all of the sampling operations could be combined at 0. 050 seconds prior to the pulse initiation. This avoids the problem of deciding how- to generate a portion of the output event before the amplitude or w-idth has been selected. While this problem is not insoluble, a model which included this behavior would be unnecessarily complex. It remains for further studies to evaluate this aspect of the computational results.

The complete eye motion model is shown in Figure 6. 34.

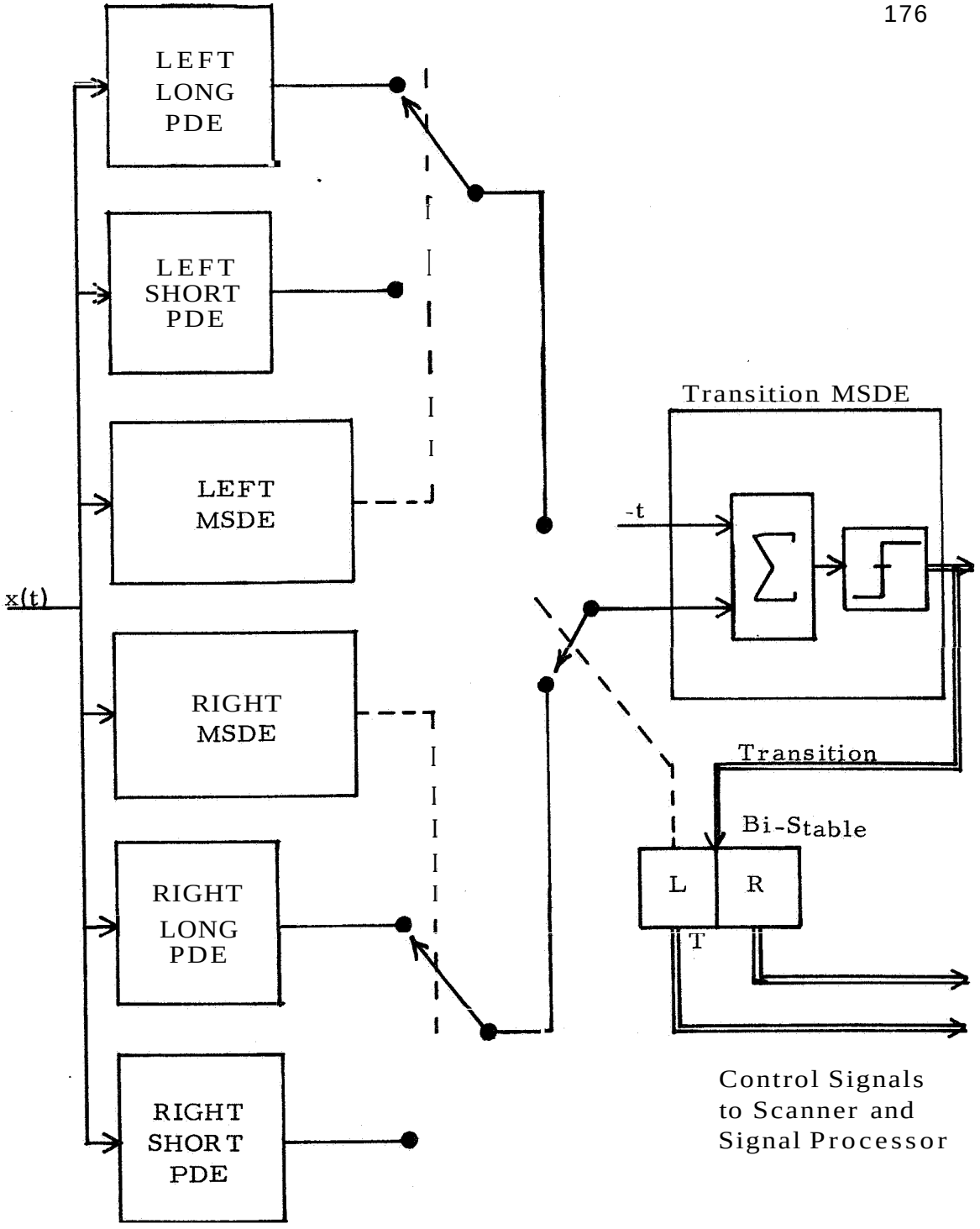

Figure 6. **34** Eye Motion Model

A bistable element is used to determine which display is being viewed and selects which input is to be used for timing. The timing signal, t, resets to zero when the flip-flop changes state and increases linearly with time. When the t input is equal to the output of the selected PDE the MSDE generates an output which initiates a transition. The transitions are assumed to be of constant duration, 100 milliseconds. The output of the flip-flop operates the scanner and signal processor of Figure 6. 9.

CHAPTER 7

CONCLUSIONS AND RECOMMENDATIONS FOR FUTURE WORK

7.1 Conclusions

The main objective of this dissertation has been the development of a class of discrete elements suitable for configuring models for the discrete control behavior exhibited by human operators. The Multi-State Decision Element (MSDE) and the Proportional Decision Element (PDE) were developed to meet this objective. That the two elements are general purpose was demonstrated by synthesizing and identifying two complete models for two different types of discrete control behavior. The model synthesized in Chapter 5 contains probably the first completely identified input dependent sampling model for a human operator performing manual control. Chapter 6 describes a deterministic model for the visual scanning behavior of human operators performing manual control with two coordinated displays.

Both models were based on results from a single, well-trained operator. Consequently, it is not possible to interpret particular numerical results; for example, the asymmetry of side arm

control motions observed in Chapters 5 and 6. The models do demonstrate the versatility and adaptability of the PDE and the MSDE and their associated identification algorithms.

7.2 Recommendations For Future Work

There are two separate areas in w-hich this dissertation is deficient. The first area is the modeling of pulsatile operator control actions w-hich are generated as part of preprogrammed pulse sequences. The second area is the application of the discrete elements to the identification of sampled data human operator models when the operator's output is not discrete.

Substantial evidence was found in Chapters 5 and 6 for the existence of preprogrammed pulse sequences. Both models were unable to generate closely spaced pulses and consequently failed to describe approximately 20% of the operator's control actions accurately. An asynchronous finte state machine containing threshold elements and memory elements (flip-flops) was utilized by Bekey and Angel [4] to study the generation of preprogrammed pulse sequences. Pattern recognition techniques were utilized by Gould [11] to generate two pulse sequences for certain controlled elements,

If the output of the model synthesized in Chapter 5 was assumed to be the force developed by an operator's muscles, then

a continuous filter (representing arm dynamics) could be added at the output of the model. The result could be used to investigate the internal discrete behavior of human operators in continuous output situations.

Another area of extension lies in the development of models for visual scanning behavior in more complex control tasks.

REFERENCES

REFERENCES

(1) Agarwal, G. C., Berman, B., Loehnberg, P., and Stark, L., "Peripheral Versus Central Adaptation: Some Preliminary Results," USC-NASA Working Conference on Manual Control, California, March 1967.

(2) Bekey, G. A., "The Human Operator as a Sampled Data System," IRE Transactions, Vol. HFE-3, No. 2, Sept. 1962.

(3) Bekey, G. A., "Sampled Data Models of the Human Operator in a Control System," Ph. D. dissertation, University of California at Los Angeles, 1962.

(4) Bekey, G. A., and Angel, E. S., "Asynchronous Finite State Models of Manual Control Systems," University of Southern California, Electronic Sciences Laboratory Report USCEE-160, 1966.

(5) Carbonell, Jaime R., "A Queueing Model of Many-Instrument Visual Sampling," IEEE Transactions on Human Factors In Electronics, Vol. HFE-7, No. 4, Dec. 1966.

(6) Chalk, C., "Flight Evaluation of Various Phugoid Dynamics For The Landing Approach Task," Cornel1 Aeronautical Laboratory Technical Report AFFDL-TR-66-2, Feb. 1966.

(7) Elkind, J. I., et al, "Evaluation of a Technique for Determining Time-Invariant and Time-Variant Dynamic Characteristics of Human Pilots," NASA Tech Note D-1897, May 1963.

(8) Elkind, J. I., Kelley, J. A., and Payne, R. A., "Adaptive Characteristics of the Human Controller in Systems Having Complex Dynamics," Proceedings of the Fifth National Symposium on Human Factors in Electronics, 1964.

(9) Elkind, J. I., and Miller, D. C., "On the Process of Adaptation By the Human Operator," MIT-NASA Working Conference on Manual Control, Cambridge, Massachusetts, Feb. 1966.

(10) Fu, K. S. and Knoop, D. C., "An Adaptive Model of the Human Operator in a Control System," Purdue University Report TREE 64-15, 1964.

(11) Fu, K. S., and Gould, E. E., "An Adaptive Pattern Recognizing Model of the Human Operator Engaged In A Time Varying Control Task," Purdue University, School of Electrical Engineering, TR-EE66-8, June 1966.

(12) Gefand, I. M., and Tsetlin, M. L., "Some Control Methods For Complex Systems," Translated by K. N. Tirirogoff, Aerospace Corporation, Aug. 1963.

(13) Hoff, M. E., "Learning In Networks of Adaptive Switching Circuits," Stanford Electronics Laboratory, Technical Report No. 1554-1, July 1962.

(14) Kelley, Charles R., "Design Applications of Adaptive (Self Adjusting) Simulators," Proceedings of NASA-MIT Working Conference on Manual Control, February 28-March 2, 1966.

(15) Kreifeldt, J. C., "A Sampled Data Pursuit Tracking Model," Ivlassachusetts Institute of Technology, Department of Mechanical Engineering Report DSR 9991-2, Jan. 1965.

(16) Kris, C. E., "A Technique For Electrical Recording Eye Position," WADC Technical Report 58-660, Dec. 1958.

(17) Lemay, L. F. and Westcott, J. H., "The Simulation of Human Operator Tracking Using An Intermittent Model," International Congress on Human Factors In Electronics, California, May 1962.

(18) Levison, W. H., "Two-Dimensional Manual Control Systems," MIT-NASA Working Conference on Manual Control, Massachusetts, Feb. 1966.

(19) Levison, W. H., and Elkind, J. I., "Two-Dimensional Manual Control Systems With Separated Displays," USC-MIT Working Conference on Manual Control, March 1967.

(20) Matney, R. M., and Harbourt, C. O., "Transistor Threshold Gates," University of Texas, College of Engineering Technical Report No. 23, Aug. 1966.

(21) McRuer, D. T., and Magdaleno, R. E., "Effects of Manipulator Restraints on Human Operator Performance," Systems Technology, Inc., Technical Report No. AFFDL-TR-66-72, Dec. 1966.

(22) McRuer, D. T., Wasicko, R. J., and Magdaleno, R. E., "Human Pilot Dynamic Response In Single Loop Systems With Compensatory And Pursuit Displays," Technical Report AFFDL-TR-66-137, Dec. 1966.

(23) McRuer, D. T., and Magdaleno, R. E., "Human Pilot Dynamics With Various Manipulators," Systems Technology Inc. Technical Report No. AFFDL-TR-66-138, Dec. 1966.

(24) McRuer, D. and Graham, D., "Pilot Models For Single and Multi-Loop Systems With Random Forcing Functions," Systems Technology, Inc. Report No. 134-1.

(25) McRuer, D. and Graham, D., "Human Pilot Dynamics in Compensatory Systems," Technical Report No. AFFDL-TR-65-15.

(26) Meissinger, H. F. and Bekery, G. A., "An Analysis of Continuous Parameter Identification Methods," Simulation, Feb. 1966.

(27) Miller, D. C., "The Effects of Performance Scoring Criteria on Compensatory Tracking Behavior," Transactions IEEE, Vol. HFE-6, No. 1, Sept. 1965.

(28) Morrison, Warren, "Adaptive Pattern Recognition," An unpublished Term Papaer submitted, University of Southern California, Department of Electrical Engineering, 1966.

(29) Pew, Richard W., "Temporal Organization in Skilled Performance," University of Michigan Technical Report 02814-11-T, 1963.

(30) Pew-, Richard W., "Performance of Human Operators in a Three State Relay Control System w-ith Velocity-Augmented Displays," IEEE Transactions on Human Factors in Electronics, Vol. 7 No. 2, June 1966.

(31) Pew, R. W., Duffendock, J. C., Fensch, L. K., "On the Relation Betw-een Discrete and Continuous Performance," 7th IEEE Symposium on Human Factors In Electronics, May 1966.

(32) Ridgeway, W. C., "An Adaptive Logic System With Generalizing Properties," Stanford Electronics Laboratories Technical Report No. 1556-1, April 1962.

(33) Rosen, Charles A., "Pattern Classification By Adaptive Machines," Science, Vol. 156, No. 3771, April 7, 1967.

(34) Senders, J. W., "Tracking With Intermittently Illuminated Stimuli," Aero Medical Laboratory, Wright Air Development Center Air Research and Development Command, Technical Report No. 55-378, Oct. 1955.

(35) Senders, J. W., "The Human Operator as a Monitor and Controller of Multi-Degree of Freedom Systems," 4th National Symposium on Human Factors in Electronics, Washington, D. C., May, 1963.

(36) Senders, J. W., Stevens, K. W., "A Re-Analysis of the Pilot Eye Movement Data," Bolt, Beranek and New-man, Inc. Report No. 1136, Job. No. 11154, May 1964.

(37) Senders, J. W., Elkind, J. I., Smallwood, R., "An Investigation of the Visual Sampling Behavior of Human Observers," Bolt, Beranek, and Newman, Inc., Report No. 124.6, Job No. 11154, May 1965.

(38) Smith, H. J., "Human Describing Functions Measured In Flight and on Simulators," MIT NASA Working Conference on Manual Control, Massachusetts, Feb. 1966.

(39) Smith, J. R., and Harbourt, C. O., "An Adaptive Threshold Logic Gate Using Capacitive Analog Weights," University of Texas, Department of Electrical Engineering Technical Report No. 22, Aug. 1966.

(40) Thomas, R. E., Tou, J. T., "Human Decision-Making In Manual Control Systems," MIT-NASA Working Conference on Manual Control, Massachusetts, 1966.

(41) Todosiev, E. P., Rose, R. E., Bekey, G. A., and Williams, H. L., "Human Tracking Performance in Uncoupled and Coupled Two Axis Systems," TRW Systems Report 2380-6003-R0000, 1965.

(42) Tomovic, R. and McGhee, R. B., "A Finite State Approach to the Synthesis of Bioengineering Systems," IEEE Transactions on Human Factors in Engineering, Vol. 7 No. 2, June 1966.

(43) Weir, D. H. and Phatak, A. V., "Model Human Operator Response To Step Transitions In Controlled Element Dynamics," MIT-NASA Working Conference, Massachusetts, Feb. 1966.

(44) Widrow, B., Hoff, M. E., "Adaptive Switching Circuits," Stanford Electronics Laboratories Technical Report No. 1533-1, June 1960.

(45) Wierwille, W. W., "A Theory for Optimal Deterministic Characterization of Time Varying Human Operator Dynamics," Cybernetics, Human Factors, IEEE Convention Record, Part 6, 1965.

(46) Wierw-ille, W. W. and Gagne, G. A., "Nonlinear and Time-Varying Dynamical Models of Human Operators In Manual Control Systems," Human Factors, April 1966.

(47) Wierwille, W. W., Gagne, G. A., and Knight, J. R., "An Experimental Study of Optimal Human Operator Models and Closed Loop Analysis Methods For High Speed Automobile Driving," Cornel1 Aeronautical Laboratory, advance copy, 1967

(48) Young, L. R., Stark, L., "Variable Feedback Experiments Testing A Sampled Data Model For Eye Tracking Movements, " IEEE Transactions on Human Factors In Electronics, Sept. 1963.

(49) Young, L. R., Green, D, M., Elkind, J. I., and Killey, J. A. "The Adaptive Dynamic Response Characteristics of the Human Operator In Simple Manual Control, " NASA Technical Note TN D-2255, April 1964.

(50) Young, L. R. and Meiry, J. L., "Manual Control of an Unstable System with Visual and Motion Cues, " IEEE Convention Record, Part 6, 1965.

(51) Young, L. R. and Stark, L., "Biological Control Systems - A Critical Review and Evaluation, " NASA Contractor Report CR-190, 1965.

(52) Young, L. R., "Methods of Oculography, " Department of Aeronautics and Astronautics, Massachusetts Institute of Technology, Massachusetts.

(53) Tustin, A. "The Nature of the Operator's Response in Manual Control and its Implications For Controller Design", Journal Institution Elec. Engrs. (London) 94(IIA): 190-202,1947.

(54) Ragazzini, J. R., "Engineering Aspects of the Human Being as a Servomechanism", Unpublished Paper, presented at the American Psychological Association Meeting, 1948.

(55) Schott, E., "Uber die Registrierung des Nystagmus und anderer Augenbewegungen vermittels des Saitengalvanometers Deutsches Arch. Klin. Med. Vol. 140, 1922.

(56) Mowrer, O. H., Ruch, .R. C., and Miller, N, E., "The Corneo-Retinal Potential Difference as the Basis of the Galvanometric Method of Recording Eye Movements", American Journal Physiology, Vol. 114,1936.

(57) Biddle, J., Jacobsen, A., and Bekey, G. A., "The Effect of Random Sampling Intervals on Sampled Data Models of the Human Operator", An informal presentation at the USC - NASA Working Conference On Manual Control, .California, 1967.